EXPERIMENTAL STUDY OF GEOMETRIC EFFECTS AND CONDUCTION LOSS ON FORCED AIR-COOLING OF REGULAR IN-LINE ARRAY OF ELECTRONIC COMPONENTS

By

MASOUD ARABZADEH

Bachelor of Science
Iran University of Science and Technology
Tehran, Iran
1976

Master of Science
University of Tulsa
Tulsa, Oklahoma
1979

Submitted to the Faculty of the
Graduate College of the
Oklahoma State University
in partial fulfillment of
the requirements for
the Degree of
DOCTOR OF PHILOSOPHY
December, 1993

EXPERIMENTAL STUDY OF GEOMETRIC EFFECTS AND CONDUCTION LOSS ON FORCED AIR-COOLING OF REGULAR IN-LINE ARRAY OF ELECTRONIC COMPONENTS

Thesis Approved:

A. J. Ghajar

Thesis Adviser

Ronald L. Dougherty

Bennett Basore

Thomas C. Collins

Dean of the Graduate College

ACKNOWLEDGMENTS

I wish to express my sincere appreciation to my major adviser, Professor Afshin J. Ghajar, for his invaluable assistance and guidance at all stages of this research. Appreciation is also extended to my Advisory Committee which consisted of Professors Ronald L. Dougherty, Frank W. Chambers, and Bennett L. Basore, for their very helpful criticism and suggestions.

I would like to thank the School of Mechanical and Aerospace Engineering, and the School of General Engineering of Oklahoma State University for providing me teaching and research assistantship during the course of my study. I also thank the Iran Ministry of Science and Higher Education for awarding me their scholarship during the course of my doctoral program.

I am grateful to Dr. Carl D. Latino, and Dr. Chriswell G. Hutchens, Professors at the School of Electrical and Computer Engineering, and Mr. Robert Taylor, laboratory technician of the School of Mechanical and Aerospace Engineering for their assistance in the fabrication of some of the minor equipment needed for the completion of the experimental phase of the research program. Special thanks go to my fellow graduate students, Mr. Yang Wang, Mr. Mahesh Rajagopalan, Mr. Eric Ogden, and Mr. Wen C. Tang for their valuable contribution during the course of my study. I also thank Ms. Leah Kinnaird and Ms. LeEtta Kitterman for their professional typing of this work.

On a more personal note, I thank all of my family; especially my late father, Dr. Mahmood Arabzadeh who deserves my deepest appreciation. God bless him who encouraged me from early stage of my elementary education, to pursue my study and serve the Scientific Society. I also thank my wife Fereshteh and my daughter Pardis for their patience and emotional support during the course of this study.

TABLE OF CONTENTS

Chapter Page

LIST OF TABLES

LIST OF FIGURES

Figure Page

Figure Page

NOMENCLATURE

A_c	Component Surface Area Exposed to Convection and Radiation
A_{ch}	Rectangular Channel Cross Sectional Area
A_d	Circular Duct Cross Sectional Area
A_f	Frontal Surface Area of the Heated Component
A_k	The Heated Component Contact Surface Area With the Channel Floor
A_t	Total Wetted Area of the Heated Component
b	Diameter of the Circular Duct
C	Overall Velocity Correction Factor
C_{ch}	Channel Velocity Correction Factor
C_d	Duct Velocity Correction Factor
C_f	Circumference of the Heated Component Frontal Surface
Cg	Geometric Coefficient
D	Height of the Rectangular Channel
h	The Heated Component Convective Heat Transfer Coefficient
h_a	Actual Convection Heat Transfer Coefficient of the Heated Component
h_c	Calculated Convection Heat Transfer Coefficient of the Heated Component
H	Height of Flow Passage Between the Component and Opposite Wall of the Channel
k	Thermal Conductivity of Air at T_∞
k_1	Thermal Conductivity of Commercial Plexiglas
k_2	Thermal Conductivity of NEMA-G11 Fiberglass
l	Characteristic Length
L	Component Planform Dimension

n	Exponent of the Reynolds Number (Re_L)
N	Total Number of Rows in the Test Section
Nu_{cal}	Predicted Nusselt Number of the Heated Component, Based on L
Nu_{exp}	Experimental Nusselt Number of the Heated Component, Based on L
Nu_L	Nusselt Number of the Heated Component Based on L, $Nu_L = hL/K$
P	Pressure
P_{atm}	Barometric Pressure of Air
Q_c	Rate of Convective Heat Transfer for Heated Component
Q_k	Loss of Heat Due to Conduction Heat Transfer Through the Test Section Floor
Q_L	Total Loss of Heat Due to Conduction and Radiation
Q_r	Thermal Radiation Heat Transfer of the Heated Component to the Surroundings
Q_t	Input Power to the Heated Component
r	Heated Component Row Number
R	Parameter which shows the Effect of Heated Component Row Number in the Correlation
Re_D	Reynolds number based on D, $Re_D = \overline{V}_{ch}D/\nu$
Re_L	Reynolds number based on L, $Re_L = \overline{V}_{ch}L/\nu$
R_w	Thermal Resistance of the Test Section Floor
S	Intercomponent Spacing
SBR	Surface Blocking Ratio
t	Height of Component
t_1	Thickness of Plexiglas
t_2	Thickness of Fiberglass
T	Temperature
T_c	Surface Temperature of the Heated Component
T_∞	Temperature of Approach Air Upstream of the Test Section
V	Local Velocity

V_{ch} Channel Center Velocity

$\overline{V}_{ch}$ Channel Average Velocity

$V_{ch,c}$ Calculated Local Velocity at the Center of Rectangular Channel

$V_{ch,m}$ Measured Local Velocity at the Center of Rectangular Channel

$\overline{V}_{ch,c}$ Calculated Average Velocity at the Rectangular Channel

$\overline{V}_{ch,m}$ Measured Average Velocity at the Rectangular Channel

V_d Duct Center Velocity

$\overline{V}_d$ Duct Average Velocity

V_{max} Maximum Velocity

W Width of the Rectangular Channel

y Normal Spatial Coordinate

Greek Letters

δ Designates Uncertainty Interval When Used as Prefix

Δ Designates Difference When Used as Prefix

ε Emissivity of Polished Aluminum

ν Kinematic Viscosity of Air at T_∞

ρ_d Duct Air Density

ρ_{ch} Channel Air Density

σ Stefan-Boltzman Constant

CHAPTER I

INTRODUCTION

Electronic computers and electronic systems are rapidly shrinking in size, while their complexity and capabilities continue to grow at an amazing rate. Lower costs and the desire for smaller system sizes have resulted in large scale component integration. High speed processing requires short transmission lengths and, consequently, close component packaging (propagation delay is proportional to length). These factors have produced a dramatic increase in the power density, resulting in rapidly rising temperatures and a large increase in the number of failures. Consequently, the thermal management of electronic systems has become an increasingly challenging task for electronic package designers for the past decade. The operating temperatures must be controlled on every component in order to ensure a reliable electronic system.

Removal of dissipated heat from electronic packages is an economically significant problem. When thermal effects go undetected and unchecked, the failure rate of electronic components and assemblies doubles for every increase of 10 to 20°C in component temperature. The costs resulting from these failures can be substantial. In a study of 200 aircraft, the U.S. Department of Defense estimated that $10 million in annual maintenance and repair expenditures could be saved for each drop by 5°C in coolant air temperature of electronic equipment in the aircraft (Weiss et al. 1989).

Figure 1.1 shows the four levels of the structure of an electronic computer; the chip, the package, the printed wiring board (PWB), and the system. The chip is a rectangular slice of single crystal silicon where microscopic patterns of electronic circuits

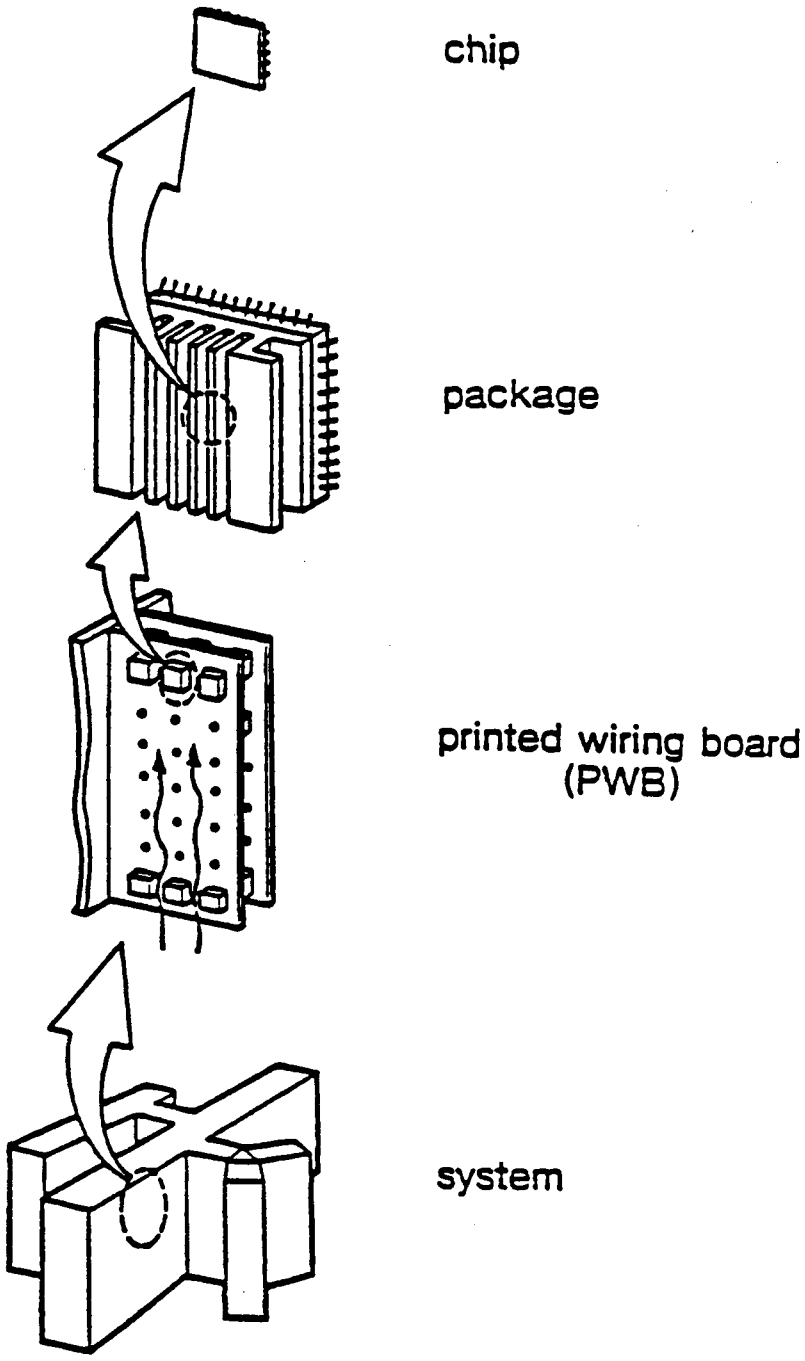

Figure 1.1. Structural Levels of an Electronic Computer (Nakayama, 1986)

are provided through a number of thermal, chemical, mass transfer, optical, and mechanical processes. Several chips are housed in a package, whose primary function is to seal from the atmosphere. The package contains the electrical leads for the pulsed signals to be transmitted in and out of the package. Packages are mounted on the PWB, where layers of conductor networks are fabricated to connect the different packages electrically. The system is composed of PWBs, mutually connected by wiring, the power supply, and the coolant moving device (a fan or pump). More complex gas or liquid cooling arrangements may be required for the larger, more powerful classes of computers. However, for smaller computers, direct forced air-convection cooling remains an appealing technique because of its mechanical simplicity, high reliability, ready availability, and attractively low cost (Incropera, 1986 and 1987).

The Printed Wiring Board (PWB) is a representative subsystem with chip-carrying packages which is usually simulated as an array of rectangular components. The term "component" will be used hereafter instead of similitude "package" in PWB. Component arrangement may be semi-regular (in geometry), as for example, Very Large Scale Integrated (VLSI) chip carriers, Dual-In-Line Packages (DIPs), and Single-In-Line Packages (SIPs), or they may be irregularly shaped components, such as resistors and capacitors. The distribution of components on a board is application-dependent, but frequently components are mounted "in-line" in the direction of flow. When multiple PWBs are utilized, they are usually mounted back-to-back in horizontal racks, and if space is a consideration, PWBs may be mounted vertically in the system cabinet or rack.

Figure 1.2 shows a typical regular in-line array of rectangular components. The present study is mainly concerned with this particular type of configuration. For forced convective heat transfer of a single heated component in such an array, the relevant geometric parameters are: L, the component plan length; t, the component height; S, the component streamwise and spanwise spacing; and D, the channel height, as illustrated in Fig. 1.3. These parameters can be non-dimensionalized and specified in terms of D/t,

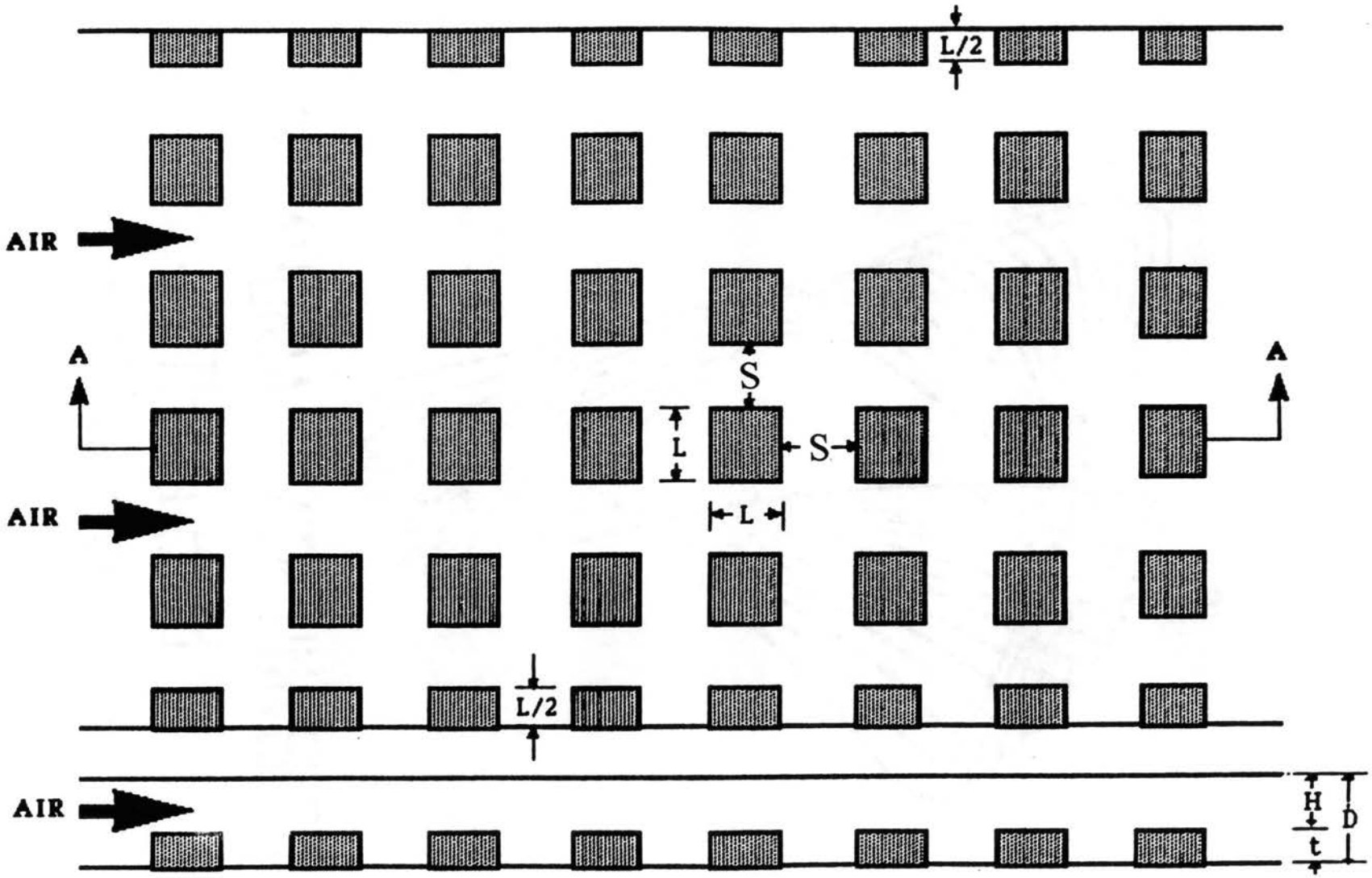

Figure 1.2. Typical Regular In-Line Array of Rectangular Components

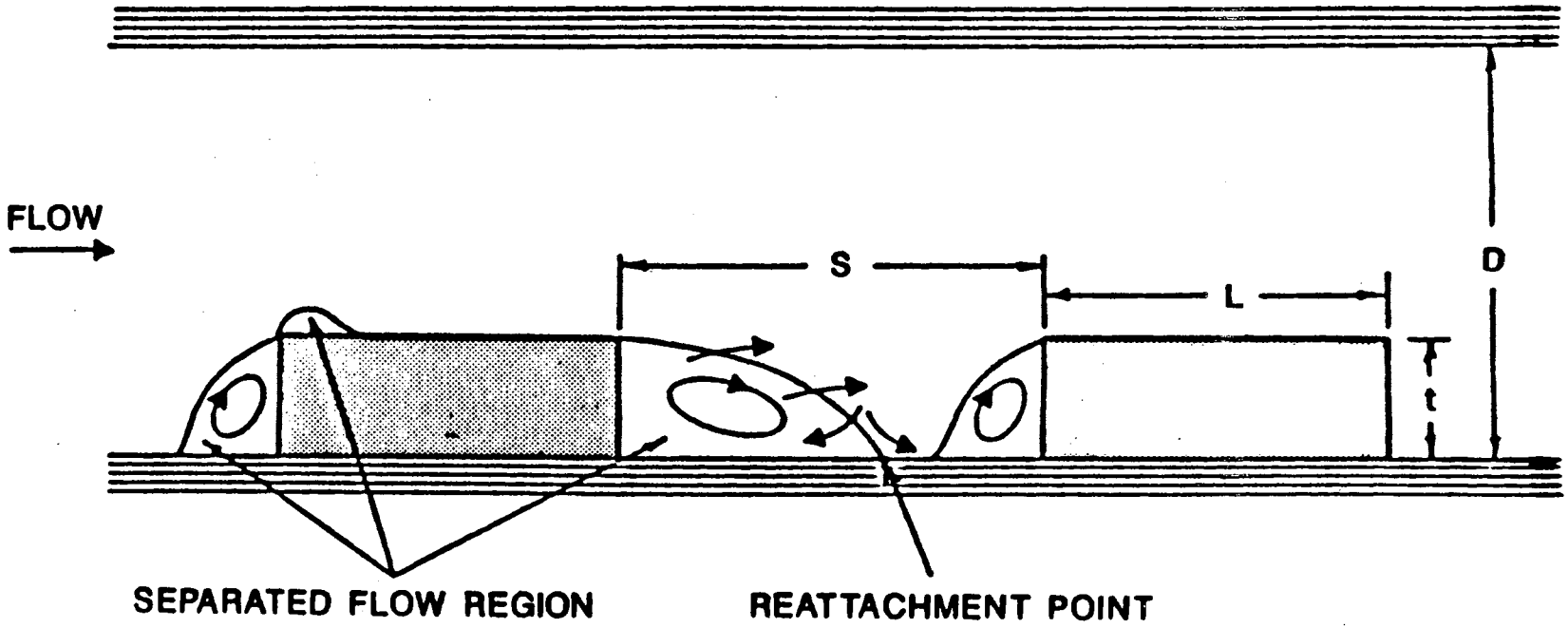

Figure 1.3. Relevant Geometric Parameters for Channel Airflow Over Surface Mounted Components

S/L, and t/L. The first parameter, D/t, indicates the fraction of the total flow that passes over the top of the components. Since most of the heat transfer takes place from the top of the component, the ratio D/t is an important parameter. The second parameter, S/L, expresses the flow disturbance due to interaction of outer flow and cavity flow formed by two neighboring components. The third parameter, t/L is associated with the total wetted surface area of the component exposed to the air flow. Furthermore, the location of a heated component (row number, r) in such an array can be considered as the fourth effective geometric parameter, since the upstream components have hydrodynamic effects on the heat dissipation rate of the downstream heated components.

Before any attempt can be made on the components' heat transfer enhancement, the thermal engineer of electronic packages needs to be provided with a tool to predict the operating temperature of each component, given the above mentioned geometric parameters and the air flow rate. To accomplish this task, there is a need in the joint design of experimental and numerical research in the area of electronic cooling. It is important that the numerical methods are applied with appropriate consideration of the experimental instrumentation and procedures which are used.

In recent years, Computational Fluid Dynamics (CFD) codes have been extensively used for predicting flow and the associated heat transfer for cooling problems in electronic packaging. However, before CFD can become widely accepted in electronic cooling design, benchmark problems must be posed and solved to establish the validity and applicability of CFD. A CFD benchmark problem should consist of a clear and complete specification of the problem in terms of the above mentioned geometric parameters, material properties, and flow conditions, which are representative of the electronic cooling situations. Several investigators (for example see Choudhury, 1993; Linton and Agonafer, 1993; Patankar, 1993) have shown that a set of reliable experimental data is required for a benchmark problem, in order to judge the adequacy of the mathematical model used. Thus the user of a CFD code can decide whether the model incorporated in the code is

satisfactory for the conditions covered by this benchmark problem. For the developer of mathematical model, such a benchmark represents a valuable resource that can be systematically used to identify the shortcomings of available models and to construct improved models. As a result, benchmark problems can make a valuable contribution, only if accurate and reliable experimental heat transfer data are provided.

At this point the necessity of providing a set of reliable experimental heat transfer data for a range of different geometric parameters and flow rates becomes evident. This is the main purpose of the present research. In the absence of such data, the design tends to evolve on a trial-and-error basis, which is extremely time consuming and hence, costly.

Experiments were conducted for a range of different geometric parameters (D/t, t/L, and r), air flow rates, and input power to the heated component placed in a regular in-line array of rectangular components. The results of these experiments were used to develop an emprical correlation that expresses the *local convective heat transfer coefficient of any single heated component placed in a regular in-line array of rectangular unheated components.*

Temperature rise of any component may be expressed as the sum of two parts; its *self-heating temperature rise* due to its own internal heating, and its *temperature rise due to thermal wake effects of upstream components.* The self-heating temperature rise is a function of the above mentioned geometric parameters, as well as the flow rate, and can be predicted with our proposed correlation. The thermal wake of upstream heated components can constitute a significant percentage of the total temperature rise of the heated component, especially if it is located far downstream of the entrance, and if all of the components upstream of it have a significant level of heat dissipation. This temperature rise due to thermal wakes can be predicted using the available correlations in the literature (Arvizu, 1981; Arvizu and Moffat, 1982; Anderson and Moffat, 1990; etc.). These correlations, together with our proposed correlation, will enable the prediction of the operating temperature of any component in a regular in-line array of rectangular components, for any

combination of geometric parameters, flow rates, and heat dissipation levels. This is a significant step towards solving the electronic cooling problem.

In most practical applications of convective cooling in air, there will be some heat lost due to conduction. The amount of conduction losses can greatly affect the component operating temperature and therefore the system as a whole. Experiments were conducted to examine the effects of varying Reynolds number, component placement, and board conductivity on the conduction heat transfer to the board. More information about details of these experiments can be found in Arabzadeh, et al. (1993).

In the next chapter, a brief review of the experimental work published in the open literature in the area of electronic cooling will be presented. Both studies, which are directly or indirectly related to the proposed research will be considered. The work of those investigators who recognized the effect of any geometric parameter (D/t, S/L, t/L, and r), are considered as directly related work, while the studies of those who performed their experiments without taking the effects of these parameters into account are regarded as indirectly related work.

CHAPTER II

LITERATURE REVIEW, RESEARCH NEEDS, OBJECTIVES, AND PRACTICAL IMPACT OF THE PROPOSED RESEARCH

In this chapter, a brief review of experimental work published in open literature on forced convective electronic cooling in arrays of rectangular components is presented. Papers related to conduction heat transfer through the board are presented in section 4.2.1. Studies which are directly related to the present work show lack of development of a comprehensive heat transfer correlation which takes into account the effects of all relevant geometric parameters (D/t, S/L, t/L, and r). This comprehensive correlation should have sufficient generality in order to be "transportable" to any regular in-line array of rectangular components having arbitrary geometry. Indirectly related papers refer to those experimental studies who did not investigate the effect of any geometric parameters, but used different techniques or arrangements in order to enhance the convective heat transfer of their special tested arrays. These studies are reported at the end of this chapter, along with the objectives and practical impact of the proposed research.

2.1 Present State-of-the-Art

Several experimental investigations related to forced convective heat transfer in air-cooled electronic equipment have been conducted over the past decade. These experimental studies (both directly and indirectly related to the proposed work) have been summarized in Table I. This table outlines specifics about the experimental setup used in each study, the parameters and techniques used by each investigator, and the variables measured. A brief review of some of the directly related work listed in Table I will be presented first.

TABLE I

Summary of Previous Experimental Studies With Ranges of Tested Parameters and Relevant Geometries

STUDY	COMPONENT'S INFORMATION:									
	SIZE:					MATERIAL	HEAT DISSIPATION		ARRANGEMENT	
	L (cm)	W/L	t/L	S_t/L	S_p/L		ohm/component	watts/component (q_n)	rows	columns
Anderson and Moffat, 1988	1.27	1.	1.	1. & 2.	1.& 2.	aluminium	100.	3. for low v 5. for high v	10	8
Sparrow, et al 1982-4	2.667	1.	3/8	1/4	1/4	brass & naphthalene	use of naphthalene sublimation		17	4
Santos, and Mendes, 1986	2.667	1.	3/8	1/4	1/4	brass & naphthalene	use of naphthalene sublimation		17	4
Arvizu, 1981	1.27	1.	1.	1. to 14	1 & 2.	aluminium mounted on plexiglas plate	100.	0.5	10	5
Arvizu, and Moffat, 1982	1.3	1.	1.	1. 2. 14.	1. & 2.	aluminium	100.	NR	10	5
Buller, and Kilburn, 1981	2.4 2.8 3..6	1. 1. 1.	0.196 0.168 0.133	N/A	N/A	aluminium	NR	NR	5	2
Ashiwake, et al 1983	2.2 2.0	1. 1.	0.364 0.25	0.72 0.5	1.18 1.5	acrylic	NR	3.	2	5
Wirtz, and Dykshoorn, 1984	2.54	1.	0.25	1.	1.	aluminium	NR	1. to 5.	8	5
Wirtz, et al 1985	2.54	1.	0.25	1.	1.	aluminium	60	1. to 5.	8	5
Lehmann, and Wirtz, 1985	5.	1.	0.25	0. to 1.	N/A	aluminium	only 11th element was fixed and heated		12	1
Moffat, et al 1985	1.27	1.	1.	1. & 2.	1. & 2.	aluminium mounted on plexiglas plate	100.	NR	8	14
Chou, and Lee 1987	3.	1.	1.	0.5 & 1.	N/A	aluminium	upstream module was heated with 25. volts		2	1
Ratts, et al 1987	1.9	1.	0.334	0.526	0.526	copper	66.8	varied only modules on 3rd column & 5th row heated	4	6
Chang, et al 1987	6.	1.	0.334	0.167 to 3.834	N/A	copper	140.	14.5	2	1
Lehmann 1985	5.08	1.	0.25	0. to 1.	N/A	aluminium	only 11th element was fixed and heated		12	1
Ortega, and Moffat, 1986	1.27	1.	1.	2.	2.	aluminium	100.	0.1 to 0.8	10	8
Biber, and Sammakia, 1986	2.4 2.8 3.6	1. 1. 1.	NR	NR	NR	NR	single module heated with 2. watts		5. 4 4.	7. 6. 5.
Hollworth, and Fuller, 1987	2.5	1.	0.25	1.	1.	aluminium	60.	0. to 30. VDC regulated power supply	8	4.5
Moffat, and Anderson, 1990	1.27	1.	1.	1. & 2.	1. & 2.	aluminium	100.	3. for low v 5. for high v	10	8
Copeland, 1988	2.54	1.	0.25	0.3 to 1.05	0.3 to 1.05	aluminium	NR	5.	9.	11
Torikoshi, et al, 1988	2.	1.	0.25 0.375 0.5	0.25	0.25	aluminium	NR	NR	16	7
Anderson and Moffat, 1990	4.65	0.806	0.204	0.273	0.273	aluminium	100.	3. for low v 5. for high v	8	6
Garimella ,and Eibeck, 1990	2.54	1.	0.4	0.2 to 2.6	0.2 to 2.6	copper	7.	90.	6	5

Note: Symbols and nomenclature used in this table are described at the end of the table

TABLE I (CONTINUED)

STUDY	TEST SECTION INFORMATION:								CHANNEL INFORMATION:				
	SIZE:			FLOW		MATERIAL	CON	MODE	SIZE:				MATERIAL
	LT (cm)	WT (cm)	D/L	V (m/s)	Re_D				LI (cm)	LO (cm)	LC (cm)	WC (cm)	
Anderson, and Moffat, 1988	35.56 (test plate)	45.7	2.25	3. & 6.2	6000 to 25000	0.95 balsa wood plank epoxied on .44cm plexiglas	VT	SU	10.16	NR	240.	45.7	NR
Sparrow, et al 1982-4	56.	13.34	1.	1.07 1.98 3.75	2000 3700 7000	0.95 cm of aluminium plate	H	SU	165.	48.	269.	13.34	The same as test section
Santos, and Mendes, 1986	56.	13.34	1.	1.07 1.98 3.75	2000 3700 7000	0.95 cm of aluminium plate	H	SU	165.	48.	269.	13.34	The same as test section
Arvizu, 1981	35.56	10.2	1. to 5.	1. to 10.	900 to 45000	1.27cm lexan	VT	SU	NR	NR	266.7	35.56	aluminium steel & lexan
Arvizu, and Moffat, 1982	35.56	10.2	1. to 4.6	1. to 9.	1800 to 37000	1.27cm lexan	VT	SU	NR	NR	266.7	35.56	aluminium steel & lexan
Buller, and Kilburn, 1981	10 flow tests of 3. cm by 4.6cm cross section each contained a single component			5. to 3.8	346 to 2720	ceramic substrate	H	SU	NR	NR	75.	NR	NR
Ashiwake, et al 1983	19.	11.7	0.564 & 0.62	1. to 10.	870. to 8700	NR	VT	SU	NR	NR	NR	NR	NR
Wirtz, and Dykshoorn, 1984	38.1	25.4	0.375 to 1.15	1. to 10.	650 to 6500.	1.6mm layer of balsa wood overlying 12.5mm plexiglas	H	SU	75	52	50.8	25.4	plexiglas
Wirtz, et al 1985	38.1	25.4	0.5	1.5 to 9..	2500 to 15000.	1.6mm layer of balsa wood overlying 12.5mm plexiglas	H	SU	75	52	50.8	25.4	plexiglas
Lehmann, and Wirtz, 1985	60. to 115.	5.	0.5 0.75 1.0	NR	1000. 3750.	plexiglas	VT	SU	45. to 100.	5.	165.	5.	plexiglas
Moffat, et al 1985	test plate		1. 2.25 4.62	1.5 to 9.	13300 to 55000	1.27cm lexan	VT	SU	NR	NR	266.7	35.56	aluminium steel & lexan
Chou, and Lee 1987	test plate		NR	NR	3560 * 7120 10680	absestos	H	SU	NR	NR	NR	NR	NR
Ratts, et al 1987	16.4	12.6	1.53	1.8 to 5.2	3680. to 10770	clear plexiglas	H	DI	21.7	4.	42.1	12.6	clear plexiglas
Chang, et al 1987	N/A	20.	0.5 to 1.	1.5 to 10.	2700 * to 19000.	acrylic plate	H	SU	N/A	N/A	244.	20.	acrylic plate
Lehmann 1985	50.8 test plate	25.4	0.5 0.75 1.0	NR	1000. to 3750.	plexiglas	VT	SU	45. to 100.	5.	165.	5.	plexiglas
Ortega, and Moffat, 1986	35.56 test plate	45.7	1.0 to 4.0	0.01 to 1.5	10. to 1000.	.95cm balsa wood plank epoxied on 0.44cm plexiglas	VT	SU	8.865	6.375	240.	45.7	aluminium, steel & lexan
Biber, and Sammakia, 1986	set of twenty circuit carts			NR	2000. to 10000	fiberglass epoxied on resin	VT	SU	NR	NR	NR	NR	NR
Hollworth, and Fuller, 1987	38.1	22.9	0.5 0.75	1.5 to 15.	1310. to 19670.	3.2mm balsa wood sematzed to a backing of 12.7mm plexiglas	VT	SU	7.6	7.6	53.3	22.9	12.7mm plexiglas plate
Moffat, and Anderson, 1988	35.56	45.7	1. 2.25 4.6	3.4 to 6.2	2000. to 25000	.95cm balsa wood plank epoxied on 0.44cm plexiglas	VT	SU	10.16	NR	240.	45.7	NR
Copeland, 1988	38	42.	0.5 to 1.25	0.5 to 5.5	500 to 13750	1mm thick epoxy glass	H	SU	61.	23.	122.	42.	NR
Torikoshi, et al 1988	50.	20.	1.25	2.5 to 8.5	2500 5000 8500	1.6 mm thick fiberglass	VT	SU	NR	NR	NR	20.	Transparent acrylic plate
Anderson and Moffat, 1990	38.9	35.6	0.3to 0.94	1.5 to 8.	1350 to 22100	1.5mm polycarbonate epoxied on 1.27 cm balsa wood	VT	SU	8.	53.	100.	35.6	1.27 cm thick lexan
Garimella and Eibeck, 1990	180.3	36.6	0.47 to 1.41	NR	150 to 5150	1.9 cm thick plexiglas	H	DI	NR	NR	180.3	36.6	Plexiglas

TABLE I (CONTINUED)

STUDY	CONSIDERATION OF FOUR EFFECTIVE KEY PARAMETERS				CORRELATIONS OBTAINED:	COMMENTS:
	D/t	S/L	t/L	r		
Anderson and Moffat, 1988					figures only	installed scoops increased thermal mixing & reduced adiabatic temperature by 10-50%
Sparrow, et al 1982-4				X	X	use of analogy between mass transfer and heat transfer
Santos, and Mendes, 1986					figures only	use of analogy between mass transfer and heat transfer
Arvizu, 1981	X	X		X	X	He wrote a computer code which predicted the operating temperature of each element , in a fully populated in line for various V, D/L S_t /L
Arvizu, and Moffat, 1982	X	X			figures only	use of superposition method to predict the operating temperature and compare it with measured temperature.
Buller, and Kilburn, 1981			X		X	use of colburn J factor to predict the operating temperature.
Ashiwake, et al 1983					X	the local temperature rise of air reduced by as much as 70% of conventional in line by using staggered arrangement.
Wirtz, and Dykshoorn,1984	X			X	X	correlations were obtained for contribution to the temperature rise of components down stream of a given heat dissipating component.
Wirtz, et al 1985					figures only	infrared thermographic study: its advantage and disadvantage
Lehmann, and Wirtz, 1985	X				X	an overall correlation is reported which includes the effect of component Reynolds no. channel height, & module stream-wise spacing
Moffat, et al 1985	X	X		X	X	heat transfer coefficients and thermal wake functions are reported for fully populated in-line arrays for several combinations of channel height and approach velocity.
Chou, and Lee 1987					figures only	finding the optimum size of vortex generator to reduce the surface temperature and nonuniformity.
Ratts, et al 1987					figures only	cooling enhancement by vortex shedding cylinders in cross-flow (maximum of 62 %).
Chang, et al 1987	X				X	correlations obtained by using colburn J factor
Lehmann, 1985	X	X			X	the average convective resistance (R_{c-a}) was related to L and average velocity by: $R_{c-a} = (UL)^{-0.65}$
Ortega, and Moffat, 1986		X			X	temperatures of individual elements in in-line array can be predicted given the heat dissipation from each element.
Biber, and Sammakia,1986					X	investigation of the applicabilityof published correlations shows that effects of enterance losses,exit gains and conduction are significant
Hollworth, and Fuller, 1987					figures only	enhancement of 50 % in h for staggered arrangement compared to in-line arrangement
Moffat, and Anderson, 1988	X	X			X	applying their previous obtained data in order to analyse superposition method.
Copeland,1988	X	X		X	X	Their offered correlation does not include different ranges of components' heights and input power to the heated component
Torikoshi,et al 1988			X		X	Only effects of components' height on heat transfer coefficient of heated component were investigated
Anderson and Moffat, 1990	X			X	X	Applying superposition method to obtained data for different channel heights and row numbers
Garimella and Eibeck, 1990	X	X			X	They performed their experiments in water channel

SYMBOLS AND NOMENCLATURE USED IN TABLE I

*	Reynolds number is based on length of component, adequate information is not available to convert it to Re_D
CON	configuration of the test section
D	height of channel
DI	blower in discharge mode
H	horizontal test section
L	length of each component
LC	total length of channel
LI	length of inlet section
LO	length of outlet section
LT	length of test section
MODE	mode of blower (suction or discharge)
N/A	not applicable
NR	not reported
q_e	power dissipation of each component
r	heated component row number
Re_D	Reynolds number based on the height of channel (D)
S	intercomponent spacing
S_p	spanwise spacing between components
S_t	streamwise spacing between components
SU	blower in suction mode
t	height of each component
v	voltage input to the heated component
V	channel inlet velocity
VT	vertical test section
W	width of each component
WC	width of channel
WT	width of test section

Sparrow et al. (1982) reported heat transfer data for a regular in-line array of "flatpacks". They used the naphthalene sublimation technique, with the heat transfer Nusselt number deduced from the measured Sherwood number by invoking the mass-transfer analogy. They reported row-independent (fully developed) heat transfer coefficients for fifth and all subsequent rows. None of the important geometric parameters appear in their suggested correlation. Furthermore, since they used the analogy between mass and heat transfer, the accuracy of their results should be verified by actual temperature measurements.

Arvizu (1981); Arvizu and Moffat (1982); and Anderson and Moffat (1990), reported a superposition method to calculate the temperature rise of a rectangular component due to the effects of thermal wakes of its upstream heated components. It should be noted that during our data collection, the temperature rise of components upstream of the heated component were also measured and recorded in order to compare with their data for the superposition method. This comparison revealed and verified that their suggested superposition correlation is accurate enough (within our experimental uncertainty) for only prediction of the temperature rise of any component due to the thermal wakes of its upstream heated components, in a regular in-line array of rectangular components. However, another comprehensive correlation is needed to predict the self-heating temperature rise of the component due to its internal heating, which is a function of all relevant geometric parameters. This can be the proposed correlation of this study. As mentioned in Chapter I, summation of these two temperature rises gives the total temperature rise of the component. Their suggested correlation for prediction of self-heating temperature rise is only limited to their tested array, since the effects of important parameters such as components' height (t), and heated component row number (r) were not included.

Buller and Kilburn (1981) obtained heat transfer data for a single heated rectangular component placed in the test section, and successfully correlated the data using a hybrid

characteristic length based on features of both the flow and component geometries. They had only one component in their test section, therefore, their suggested correlation can not be applied to fully populated arrays. Hydrodynamic effects of upstream components (heated component row number, r) and effects of components' spacing can not be investigated when there is only one component in the test section.

Wirtz and Dykshoorn (1984), and Wirtz et al. (1985), reported heat transfer studies for an in-line array of "flatpacks". The components were arranged in a square array in both the streamwise and the spanwise directions. In these tests, the components were electrically heated, and the heat transfer coefficient was deduced from an energy balance. Using conventional temperature measurement and infrared thermographic techniques, the experimental results showed that the thermal wakes from heat dissipating components have significant influence on heat transfer of downstream components. However, the effects of the hydrodynamic wake and components' height were not investigated separately. It was found by Lehmann and Wirtz (1985) that the convection from the component surface increased when component spacing was increased.

Moffat et al .(1985) with an experimental setup similar to that used by Arvizu and Moffat (1982), presented heat transfer coefficients and thermal wake functions for in-line arrays of cubical components mounted on one wall of a parallel planar channel for several combinations of channel height (plate spacing) and approach velocity. It was found that the change in channel height can result in different flow patterns and hence, large variations in the heat transfer coefficient. However, they did not investigate effect of components' height and heated component row number, on convective heat transfer coefficient of the heated component.

Chang et al. (1987) investigated the influence of the hydrodynamic wake from one unheated component on the heat transfer of a downstream heated component. Only two components were used in their experiments. It was found that the hydrodynamic wake from the upstream component can cause a large variation in heat transfer on the heated

component, depending on the spacing between the two components. They also showed that the average heat transfer coefficient from the heated component can be expressed by the Colburn j-factor, which is a function of the Reynolds number and the ratio of channel height to component height. Since their test section was composed of only two rectangular components, effects of components' spanwise spacing, as well as components' height were not included in their offered correlation. Their results can not be used for fully populated arrays.

Copeland (1992) performed a series of experiments to study the effects of channel height, components' spacing, and heated component row number on forced convection of a regular in-line array of "flatpacks". Their suggested correlations are only limited to their tested arrays, since effects of input power to the heated component and components' height were not taken into account.

Torikoshi et al. (1988) suggested a set of correlations based on their experimental data for regular in-line arrays of flatpacks. They included the effect of components' height in their offered correlations, while effects of other important parameters such as channel height, components' spacing and heated component row number were neglected.

More recently, Garimella and Eibeck (1990) conducted an experimental study for water cooling of a regular in-line array of rectangular components. The Nusselt numbers of the heated components were correlated in terms of array Reynolds number, channel height, and components' spanwise and streamwise spacing. However, the effects of components' height and heated component row number were not included in their suggested correlations. Furthermore, as mentioned in their paper, water cooling is more applicable to the mainframe computers, rather than portable electronic equipment.

Heat transfer enhancements have been reported by other investigators by using several different techniques and arrangements, such as pin-mounted components, regular in-line array with a missing component, or a component with different height (odd size component), implanted fence-like barriers, and staggered arrangement of the rectangular

components. These studies are not directly related to the proposed work, however, a brief review of some of these work listed in Table I will be presented here.

Anderson and Moffat (1988) reported that installed scoops (turbulators) increased thermal mixing and reduced the temperature rise of the component due to the thermal wake by 10-50%. Chou and Lee (1987) found the optimum size of the vortex generator installed on the leading edge of the component in order to reduce the component surface temperature and nonuniformity. Ratts et al. (1987) reported the cooling enhancement of the components up to 82%, by placing cylinders periodically above the back edge of each row of components.

Experiments with a "missing component", a component with a different height (odd-size component), and implantation of fence-like barriers in a regular in-line array of rectangular components, were performed by Sparrow et al. (1982-1984), and Santos and Mendes (1986). They reported that all of these techniques enhanced the heat transfer, however, since they deduced the heat transfer Nusselt number from the measured Sherwood number by invoking the mass transfer analogy, the accuracy of their results should be verified by actual temperature measurements.

Ashiwake et al. (1983), Hollworth and Fuller (1987), and Garimella and Eibeck (1990), reported a notable advantage by placing the components in a staggered arrangement on a card. Staggered arrangement of the components on a card reduces both the thermal resistance and the local temperature rise of the air by as much as 70% of the conventional regular in-line arrangement. One of the focuses of their work was on reducing the non-uniformity in the temperature rise of the cooling air. For different channel heights tested, their flow visualization showed little or no mixing from the recirculating regions behind each component into the flow in the lanes for an in-line array, while a staggered arrangement had better mixing in these regions.

Mounting the components in a staggered configuration may enhance the convective heat transfer, but it will increase both the pressure drop in the channel and the total

interconnect length and/or bus-line length. An increase in the total length of bus-lines potentially causes a reduction in computer speed (speed being inversely proportional to the total length of bus-lines). In spite of having a considerable heat transfer enhancement by placing the components in a staggered arrangement, the trade-off between this advantage and its effect on the pressure drop in the channel and reduction of computer speed has not been assessed.

2.2 Areas of Research Needs

Undoubtedly, the work discussed in the foregoing and the results summarized in Table I represent major steps forward. However, there are several shortcomings and needed research in certain areas associated with the work available in the literature. These shortcomings can be classified in two different categories; shortcomings of the studies which are directly related to our proposed work, and shortcomings of the studies which are not directly related to our study. For directly related work, a detailed discussion will be presented, while for indirectly related work, a brief discussion of the needed research will be outlined.

2.2.1 Shortcomings and Research Needed for Directly Related Studies

For forced convective heat transfer of a heated component in a regular in-line array of rectangular components, the relevant geometric parameters are D/t, S/L, t/L, and heated component row number (r). Influence of these important geometric parameters on heat transfer coefficient of the heated component was outlined in Chapter I (see Figure 1.3). In addition to these parameters, the influence of channel approach velocity and input power to the heated component should also be considered in these studies.

None of the experimenters who investigated the convective heat transfer in a regular in-line array of rectangular components took the effects of all of the above important parameters into account. The heat transfer results of these studies have not sufficient generality to be transportable to another setup, since they don't cover the effects of all relevant parameters. The urge to combine the reported correlations and deduce the appropriate correlation(s) which cover the effects of all of the above mentioned parameters is also impossible. Consequently, the available correlations for forced convection of a regular in-line array of rectangular components have many gaps, and the accuracy of the reported results is not well established.

The purpose of this study was to address most of the above mentioned shortcomings by conducting a full scale "systematic" experiment in a regular in-line array of rectangular components. It is believed that a significant contribution is made by expanding the existing experimental database and developing the proposed correlation, for the local convective heat transfer response to *any heated component placed in a regular in-line array of unheated rectangular components.* This correlation includes the effects of most of the important relevant geometric parameters (D/t, t/L, and r), as well as approach channel velocity, for different range of input power to the heated component. Such information is required to accurately predict the operating temperature of a heated component in any arbitrary regular in-line array of rectangular components.

It should be noted that the experiments with different S/L ratios are underway (Kim, 1993). The results of these experiments will complement the database developed in this study and could be easily incorporated into the proposed heat transfer correlation. In order to conduct these experiments, two different boards for S/L ratios of 0.429 and 2.333 were designed and constructed.

2.2.2 Shortcomings and Research Needed for Indirectly Related Studies

Investigators who conducted their experiments with pin mounted components, vortex generators, missing components, components with different height (odd size component), implantation of fence-like barriers, and staggered arrangement of rectangular components, all reported the increase of convective heat transfer for their special tested array. Few of them obtained correlations for the heat transfer enhancement. Undoubtedly, these correlations work for their tested array have special geometries. Once the components and array geometries change, *the rate of increase of heat transfer* will be changed. The rate of these heat transfer enhancements should be correlated in terms of the involved effective parameters in order to have sufficient generality to be transportable to arrays having different geometries. Consequently, before any attempt can be made on heat transfer enhancement, a general correlation which expresses the heat transfer coefficient of a heated component in a regular array of rectangular components in terms of relevant parameters is needed. This was the main purpose of the proposed research. Based on our proposed correlation, research for the above mentioned different techniques can be continued to find a general correlation for each case. Furthermore, as mentioned in the previous section, the trade-off between the advantage of heat transfer enhancement by mounting the components in a staggered arrangement, and the disadvantage of increased pressure drop, as well as reduced computer speed, has not been investigated.

2.3 Objectives

The main purpose of this study was to take a step forward in the direction of the overall objectives in the area of forced air-cooled electronic cooling: to develop the techniques and the databases needed to be able to predict the operating temperature of any

rectangular component in an arbitrary array of arbitrarily different rectangular components mounted on a circuit board and contained in a forced-air-cooled cabinet.

The specific objectives of the proposed research were:

1. Design and construction of a versatile experimental setup which is capable of performing experiments with different channel heights, component heights, spanwise and streamwise spacings, component arrangements (in-line and staggered), as well as test section orientations (vertical or horizontal). The setup should also be capable of accurate control and measurement of the channel average velocity, heated component temperature, and input power to the selected component(s).
2. Systematic expansion of the experimental heat transfer database applied to forced convective air-cooling of regular in-line array of rectangular components. Detailed and systematic experiments were performed with different channel heights, components' heights, heated component row numbers, channel approach velocities, and input power to the heated component.
3. Development of a general heat transfer correlation in terms of most of the effective parameters, using the experimental data. This systematic approach will permit the use of the proposed correlation for regular in-line arrays of rectangular components with any arbitrary geometry, channel approach velocity, and input power to the heated component.
4. Investigation of the effects of board conductivity and conduction losses of the heated component, on the convective heat transfer coefficient and consequently on the operating temperature of the heated component. Experiments were performed to examine the effects of varying Reynolds number, component placement, and board conductivity on the conduction heat transfer to the board.

2.4 Practical Impact of This Research

The results of this study and the available correlations in the literature (Arvizu, 1981; Arvizu and Moffat, 1982; Anderson and Moffat, 1990) for thermal wakes of upstream components can be combined in order to predict the operating temperature of *any component in an arbitrary regular in-line array of arbitrarily heated rectangular components.* This serves as the primary significant step towards solving the electronic cooling problem. Consequently, the practical benefits emanating from this investigation are enormous:

1. Allow heat transfer behavior to be predicted for a wide range of arrays with only a minimal amount of testing required for the array in question.
2. In the initial stages of the design effort, predictions of component failure rates and corresponding equipment reliability could be made based on the accurately predicted temperatures. This improved prediction ability would allow the designer to assess the various trade-offs between component types (material, size, weight, etc.) and failure rates before the optimized design is established.
3. Provide a set of accurate and reliable experimental heat transfer data as the input for CFD benchmark problems. Such benchamrk problems that are bundled with experimental data are very useful in judging the satisfactoriness and adequacy of the mathematical models used.
4. Ultimately, the improved temperature predictions that could be performed in the design stage will lead to more efficient, more reliable equipment.

Collectively, these benefits would markedly speed up the entire thermal design process, and reduce the overall production cost, while providing improved reliability.

In the next chapter, details of different parts of the experimental setup will be presented. Efforts have been made to design and construct different parts of the experimental setup, in order to be able to perform a series of systematic experiments which include variations of all effective involved parameters.

CHAPTER III

EXPERIMENTAL SETUP, DATA ACQUISITION SYSTEMS, AND PROCEDURES

Lack of systematic approach is one of the main shortcomings of the work available in the literature, as mentioned in Chapter II. Efforts have been made to design and construct different parts of the experimental setup, as well as development of data acquisition systems and establishment of a well-defined velocity profile in order to accomplish this task. This allowed us to perform a series of systematic experiments which was needed to fill in the gaps in the database and provided preliminary heat transfer results that can be directly compared to previous work. It is the objective of this chapter to explain the experimental setup, data acquisition systems and facilities, procedures, and data reduction. These are presented in detail in the subsequent sections.

3.1 Experimental Setup

In this section, different parts of the experimental setup will be presented. These parts are the contraction, rectangular host channel, test section, components, plenum, circular duct, and blower. A schematic diagram of the setup, which illustrates these parts is shown in Fig. 3.1.

3.1.1 Contraction

The large entrance contraction is made of wood and has a movable bottom part that can move along with the entire channel floor in order to adjust to the desired channel height

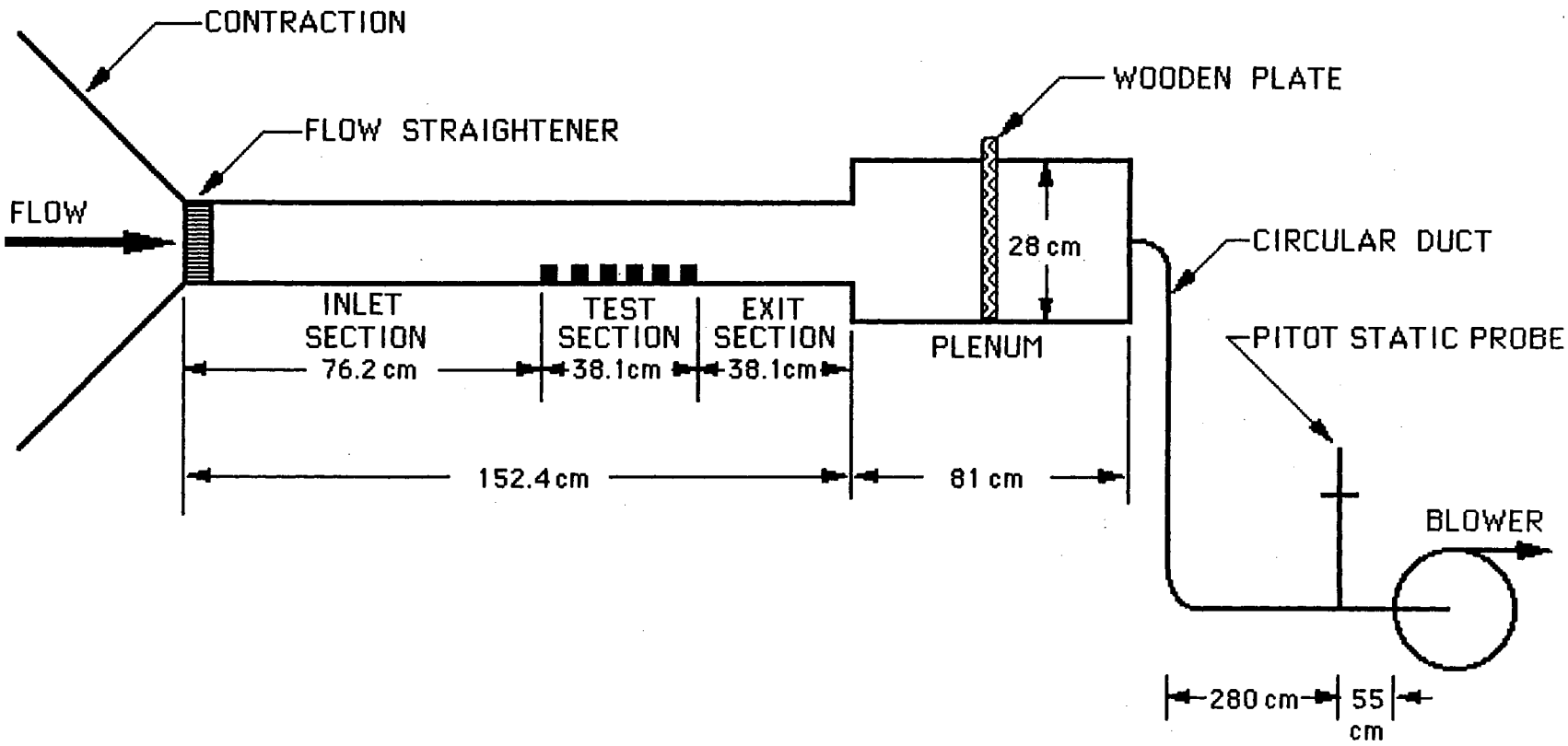

Figure 3.1. Schematic of Experimental Apparatus

(1.27 to 7.62 cm). A perspective view of the contraction with this movement arrangement is shown in Fig. 3.2. The contraction's inlet to outlet area (contraction ratio) varies from 14.5 to 82, depending on the channel height. The start of the channel floor rests on a wooden flap, which is attached to the movable part of the contraction. The surface of this wooden flap is at the same level as the bottom surface of the channel floor and has a maximum elevation of 137 cm above the laboratory floor for the minimum channel height. The start of each adjacent side wall of the channel rests on another wooden flap attached to a wooden strip. These strips are screwed to the fixed side walls of contraction and rest on a stand, which is made of light angle iron and secured to the laboratory floor. A small hydraulic jack is positioned under the bottom of the movable part in order to move and adjust it smoothly for the desired channel height.

3.1.2 Rectangular Host Channel

Ambient air passing through the contraction enters a 152.4 cm long rectangular channel. The entire channel was made of 1.27 cm commercial-grade plexiglass with a fixed 25.4 cm width and a height that is easily adjustable from 1.27 to 7.62 cm.

Flow straighteners for different channel heights are made of tightly packed soda straws (0.55 cm inside diameter, 12 cm length, 0.901 open area ratio), sandwiched between galvanized steel mesh screens (wire diameter 0.044 cm, mesh width 0.32 cm, open area ratio 0.773). For any desired channel height, the appropriate flow straightener can be positioned at the start of entrance to the rectangular channel as shown in Fig. 3.1. This provides a uniform flow at the entrance to the rectangular channel.

The entire channel floor is covered with a 1.6 mm layer of epoxy resin plate mixed with fiberglass (NEMA-G-11 manufactured by Polypenco, Inc.), which is close to what is commonly used in the actual computer board.

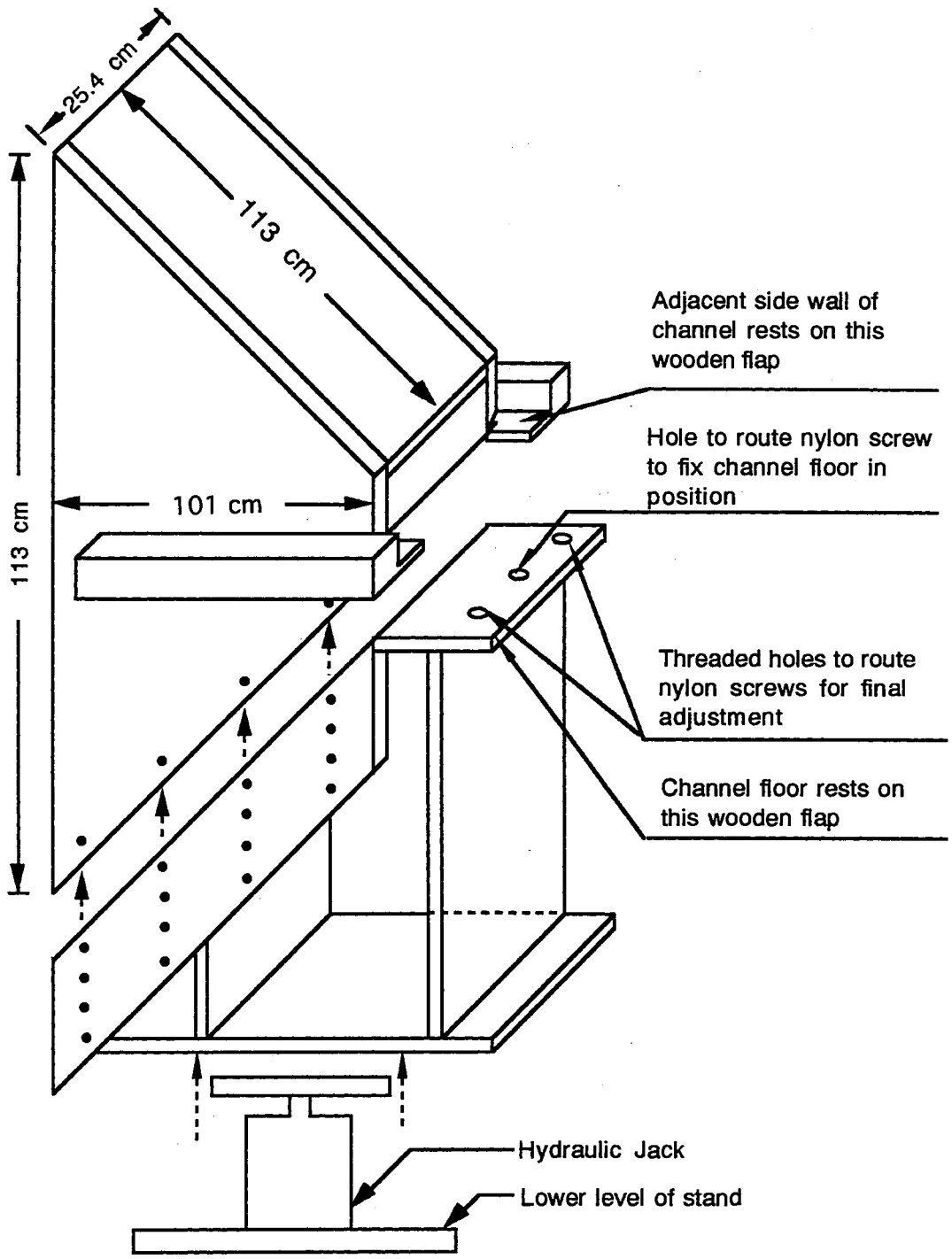

Figure 3.2. Perspective View of Contraction With the Movement Arrangement of Its Bottom Part

To accommodate variation in the height of the channel, the setup is constructed such that the bottom part of the contraction with the entire channel floor, along with the plexiglass flap attached to the inlet part of the plenum, can all be moved together and adjusted for the desired channel height. This design will prevent flow disturbance caused by the sharp leading edges of splitters or adjustable flap used by other investigators to adjust the channel height by moving the test section floor only.

The two adjacent side walls of the channel are connected from the bottom with two pieces of 25.4 x 16 cm rectangular plexiglass, which are fixed in place with nylon screws (see Fig. 3.3). These fixed pieces allow to place spacers under the channel floor for a desired channel height in order to support the weight and avoid buckling. Two threaded holes are made through each of the support pieces, and two through the wooden flap of contraction, in order to place the nylon screws. Final adjustment of a desired channel height can be achieved with an accuracy of 0.025 cm by adjusting these six nylon screws with two other screws placed under the plexiglass flap attached to the inlet part of the plenum. The contraction wooden flap, spacers, and each piece of plexiglass support have a hole at the center to route a threaded nylon rod. One side of each of these three rods is fixed in a threaded hole under the channel floor and the other side is connected to a nylon nut. After final adjustment, these three nuts allow to fix the entire channel floor in place and avoid any movement caused by high air velocity drawn through the channel.

The top portion of channel consists of three pieces. The contraction side (68.6 x 28 cm) and plenum side (30.5 x 28 cm) are fixed in place with nylon screws. The upper wall of the test section (53.3 x 28 cm) can be removed and reset in place in a matter of seconds, thus enabling rapid access to the array of components.

The rectangular channel, as shown in Fig. 3.1, consists of three sections: inlet, test, and exit sections. Attention now will be focused on the test section, which is the most important part of the experimental setup.

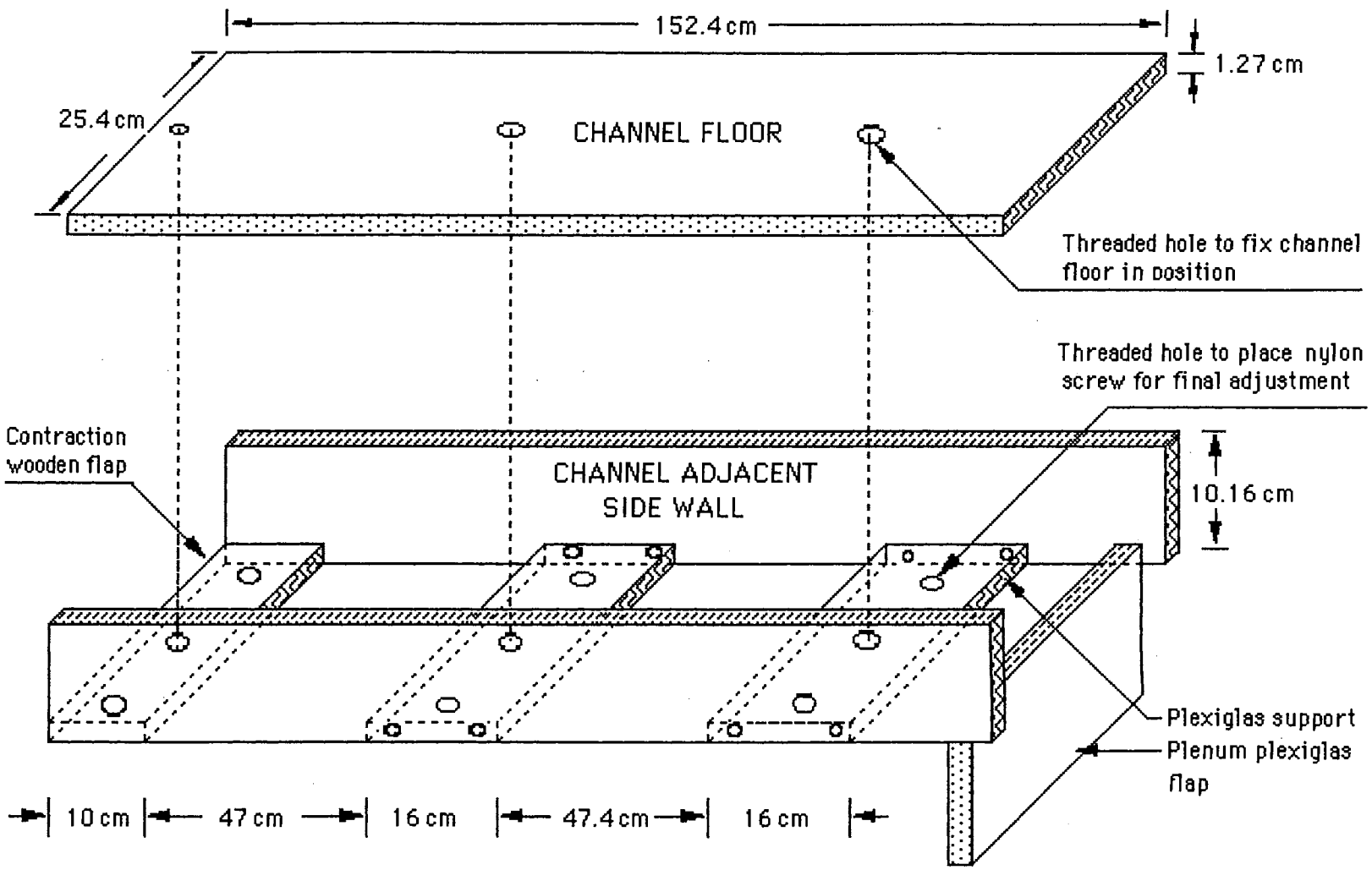

Figure 3.3. Perspective View of Arrangements for Final Adjustment and Positioning of Channel Floor

3.1.3 Test Section

The start of the test component array is positioned 76 cm from the entrance to the channel and extends for 38.1 cm. The dimensions of test section, the range of test parameters, and the dimensions of components were carefully chosen and constructed in order to be able to perform experiments with different arrangements and configurations, similar to some of the experimental studies summarized in Table I, see for example, Wirtz and Dykshoorn (1984), and Hollworth and Fuller (1987). This allowed comparison and cross-check of our experimental data with their results (see Chapter IV for the details of these comparisons). The good agreement between our results and those of other investigators allowed the experiments for more complex geometries to be performed with more confidence.

The test section, as illustrated in Fig. 3.4, encompasses eight rows of components with four columns of full-size components flanked on both ends by half components. Each half component mounts on the adjacent side wall of the host rectangular channel. The idea underlying the use of the half components is to more closely model an infinitely wide array. Figure 3.5 shows a staggered arrangement of the components in the test section. This configuration is achieved by shifting every other row of the in-line arrangement shown in Fig. 3.4 by the component planform dimension L in the span-wise direction.

To accommodate variation for different arrangements of the components, the fiberglass layer on the channel floor is made of three pieces, a piece of 74.93 cm length for the inlet section, a piece of 36.83 cm length for the exit section, and a piece of 40.64 cm length for the test section. The piece which covers the test section floor can easily be removed, reset, and aligned with the edges of the other two pieces. This allows placement of the fiberglass sheet with the appropriate holes under the components for a desired arrangement of the test component arrays.

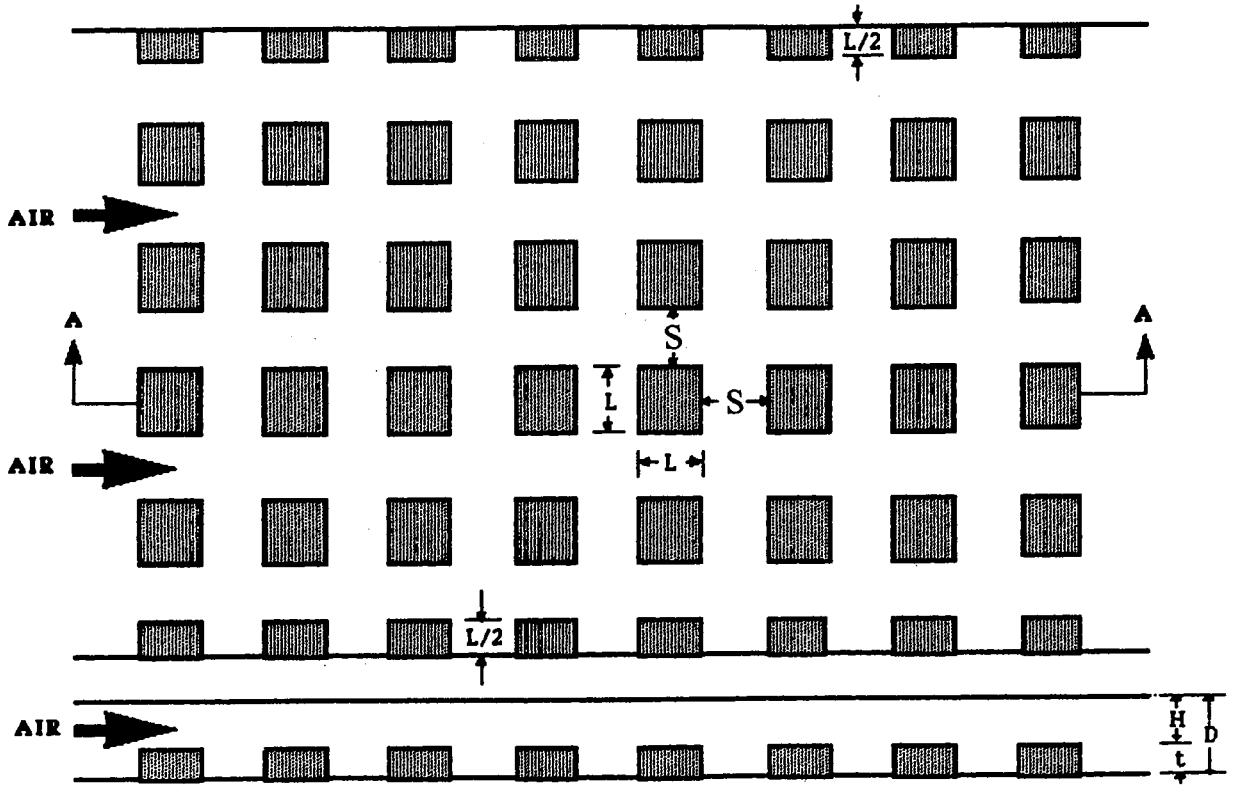

Figure 3.4. In-Line Arrangement of the Components in the Test Section

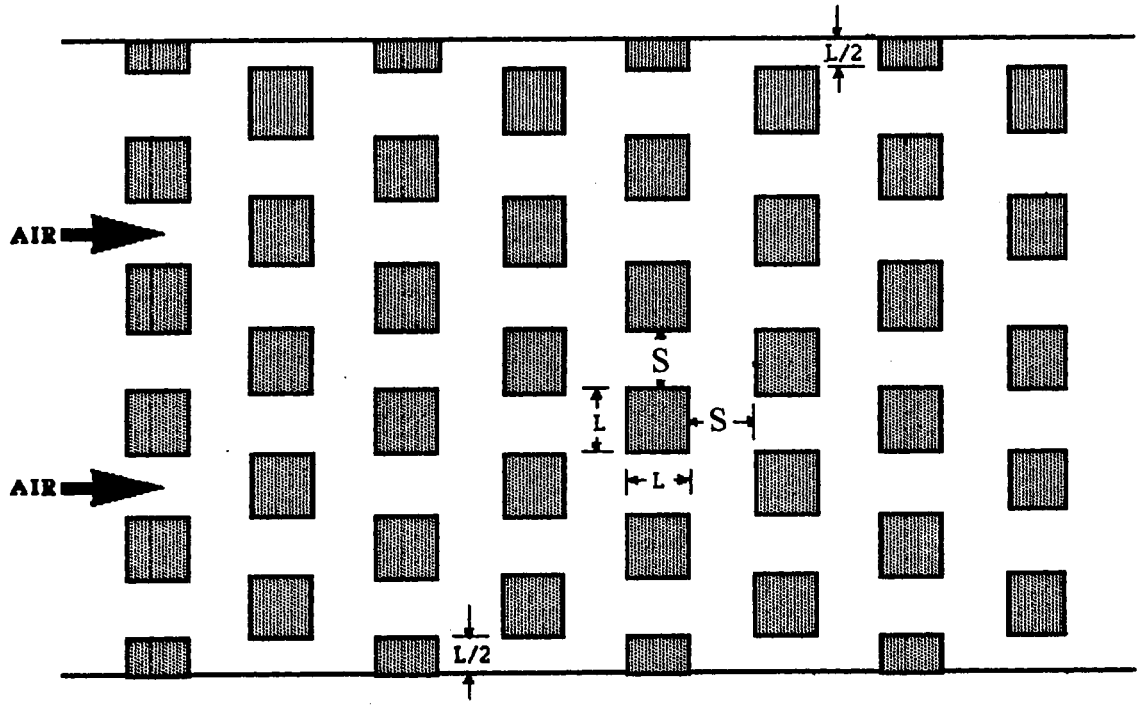

Figure 3.5. Staggered Arrangement of the Components in the Test Section

3.1.4 Components

Cubic shaped aluminum blocks with heights varying from 1.27 to 5.08 cm were used to simulate various electronic components. As shown in Fig. 3.4, all components have the same square plan-view. Furthermore, the transverse and longitudinal intercomponent gaps are identical. However, for a desired arrangement, it is possible to remove some components and arrange the appropriate transverse and longitudinal gaps. There are four length dimensions which define the geometrical characteristics of the array and its relationship to the flow passage. These include the component planform dimension L, the component height t, the intercomponent gap S, and the height H of the flow passage between the component and the opposite wall of the channel. Although there is a tendency to deal with dimensional quantities in connection with electronic equipment cooling, the use of dimensionless parameters is preferable because they accord greater generality to the results. The range of dimensionless ratios defining the array and its related flow passage are:

$$t/L = 0.5 \text{ and } 1,\ S/L = 1,\ (H + t)/L = 1.5 \text{ to } 3$$

where $H + t = D$ is the channel height.

These dimensionless ratios were chosen to closely correspond to a practical configuration. Thus far, only dimensionless ratios have been specified. With the above equations, all test section dimensions can be deduced when only one dimension is specified. For example, with L = 2.54 cm and t/L = 0.5, each component dimension is 2.54 x 2.54 x 1.27 cm.

A detailed schematic diagram of each component is illustrated in Fig. 3.6. As shown in this figure, each component was hollowed out from the back side and a small (0.9 x 0.35 cm) ceramic resistor (RN60D-NA60, manufactured by Mini-system, Inc.) having 475 Ohm resistance was embedded exactly at the center of the aluminum block. The component surfaces were also polished to reduce thermal radiation effects. To

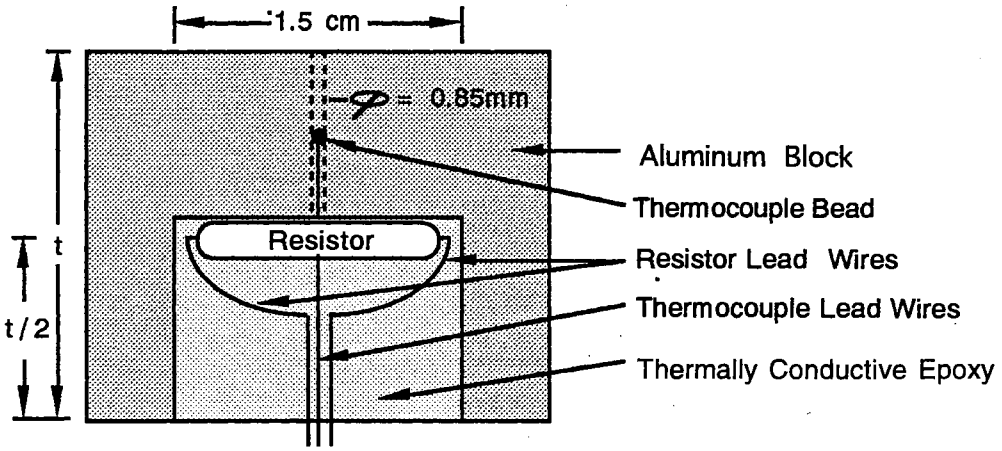

Figure 3.6. Detail of an Active Aluminum Block

measure surface temperature of each component, a 36 AWG Type-T copper/constant thermocouple (0.381 mm bead diameter, 0.127 mm wire diameter, 91.44 cm wire length with teflon insulation, manufactured by Omega Company) was used. The calibration of the thermocouples (using an oil bath) against a platinum resistance thermometer which was certified by the National Bureau of Standards, showed an accuracy of ± 0.5°C. The thermocouple for each component was bonded exactly at a position half-way between the top surface and the embedded resistor using OMEGABOND 100 epoxy, having a thermal conductivity of 1.038 W/m K and electrical insulation volume resistivity of 10^{12} ohm-cm. A small hole of 0.71 mm was drilled at the center of each component in order to route the thermocouple wire through it. The rest of the cavity of each component was filled with thermally-conducting epoxy (OMEGATHERM 201) having thermal conductivity of 2.304 W/m K and electrical insulation volume resistivity of 10^{14} ohm-cm. The electric leads of the resistor were covered with teflon tubing to avoid electrical contact with the aluminum, and then soldered to stranded 22 AWG wires. Thermocouple wires and electric leads of the resistor were routed through a threaded, hollowed nylon rod, which is used to hold the component to the test section floor with a nylon fastener nut.

Heat flow sensors equipped with built-in T-type thermocouples (RdF Corporation, model 20453-3) were used for direct measurement of heat flux and temperature on all five exposed surfaces of the heated component (inside the wind tunnel) and the back of the board (outside of the wind tunnel). These sensors measure radiation as well as convection losses. Each heat flow sensor is individually calibrated at a base temperature of 21 degree celsius with output of 5.83×10^{-8} V m^2/W, thermal resistance of 2.11×10^{-3} °C m^2/W, heat capacity of 1022 J/m^2°C, and response time of 0.400 second. For monitoring the heat flux, the voltage signals from the heat flow sensors were passed through a high gain DC amplifier. An A/D conversion program called (READFLUX), written in C language, converts the output analog voltage of the amplifier to a digital voltage. Estimates of

uncertainty of the measured heat fluxes was determined to be ±5%. More information about heat flow sensors and program READFLUX can be found in Ogden (1992).

In order to ensure that the measured temperature by the inserted thermocouple inside the component represents the component surface temperature, a special component with a thermocouple inserted exactly half way between each surface and the cavity, was heated with three different input powers (2, 3, and 5 Watts). The temperature of each surface was also measured separately by a heat flow sensor. The average difference between the temperature measured by the inserted thermocouple, and the temperature measured by the heat flow sensor at different surfaces of the component were 0.33°C, 0.50°C, and 0.94°C for input powers of 2, 3, and 5 Watts, respectively. Low channel average velocity (2m/sec) was chosen for this test, in order to show maximum possible temperature difference. For velocities higher than 2 m/sec, this average temperature difference is less than 0.4°C, which is within our experimental error.

3.1.5 Plenum

Air exits the host rectangular channel and discharges in an acoustically absorbent relaxation plenum (81 cm long, 76 cm wide, and 28 cm high) made of wood. The plenum "relaxes" or reduces the speed of the air due to its larger area of cross-section compared to the rectangular channel. As illustrated in Fig. 3.1, a 30.48 x 28 x 1.9 cm rectangular wooden plate is inserted vertically at the center of the plenum to stop jet flow in the channel. The entire plenum rests on a stand which is made of light angle iron and secured to the laboratory floor.

It should be noted that the present horizontal test section has the versatility of being converted to a vertical test section, as was done by some investigators (see Table I in Chapter II). In order to do this, the contraction, rectangular channel, and plenum should be rotated 90°.

3.1.6 Circular Duct

A circular duct of 15.24 cm diameter and 335 cm length made of thin aluminum sheet connects the plenum to the blower. A pitot static probe is placed at the far end of the duct (55 cm from the blower). The pitot probe is connected to an MKS model 223BD differential pressure transducer which is, in turn, connected to the data acquisition system (see Section 3.2.3).

3.1.7 Blower

A New York Blower compact G.I Fan, size 106, capable of delivering 17 m^3/min with the driver motor of 2HP and 3600 rpm is used. To control excessive acoustic noise from the blower, an insulated wooden housing was constructed around it. The blower exhausts outside the building, allowing flow visualization experiments with smoke to be performed (Wang and Ghajar, 1991). A single vane damper mounted by the factory on the exit duct of the blower can be used for adjusting the blower. Due to the limitations of this damper, very low velocities can not be reached. Hence, an arrangement consisting of a movable wooden damper, along with the necessary parts, was designed for accurate control of velocities. The details of the arrangement are explained in Section 3.2.3.2.

3.2 Data Acquisition Systems and Facilities

In order to accurately measure and control the velocity, temperature, and power given to the components, the experimental setup is equipped with a microcomputer driven data acquisition system. This fully automated system is programmed to control and monitor the air velocity through the test section, to scan temperature readings across the component array, and to store the readings on hard disc. The system also automatically

gives the required heat to the selected component(s) to be heated. A block diagram of the automated component test plate is shown in Fig. 3.7. This consists of a thermal regulator board, a thermocouple datalogger for temperature measurement, and an air flow control signal. These different parts are explained in detail as follows.

3.2.1 Thermal Regulator Board

This unit, which was developed through the Oklahoma State University's School of Electrical and Computer Engineering, provides precise open loop control of individual component power dissipation. It is interfaced with an IBM/PC compatible, and a desired power ranging from 0 to 5 watts with the increments of 0.1 watts can be simultaneously supplied to each component by the keyboard. Preliminary tests for this unit providing different power for each component has been performed while monitoring supplied powers with an accurate oscilloscope. The tests showed that the thermal regulator board works with an accuracy of ± 1%.

3.2.2 Thermocouple Datalogger

A programmable forty channel datalogger ECD-5100 (manufactured by Electronics Controls Design Corporation) was used to monitor the temperature reading of T-type thermocouples. The different features of ECD-5100 include a built-in 24 column thermal printer, an alphanumerical keyboard, a 16-digit vacuum fluorescent display, a real time clock, and an RS-232 port. It also includes a "data cache memory feature", which provides temporary storage of logged data for reviewing before printing or unloading to a computer or a printer. The data logger was initially calibrated and monitors the temperatures with a reading accuracy of ± 0.05°C.

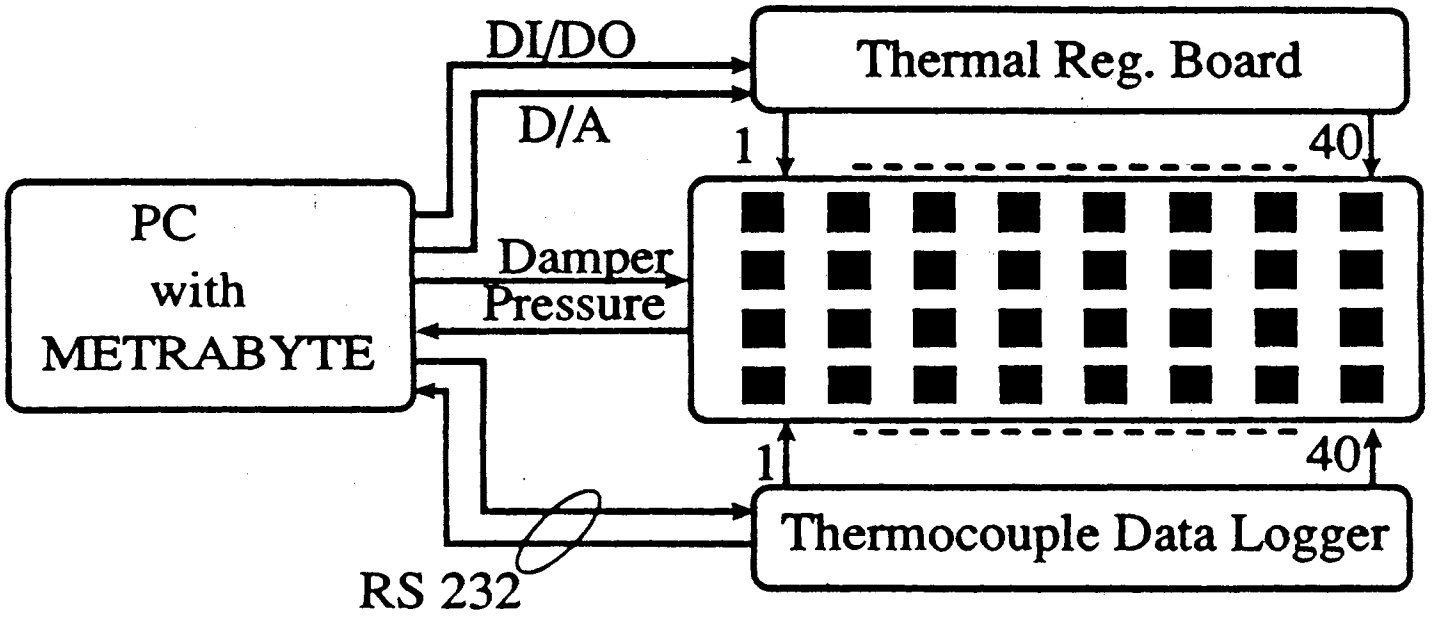

Figure 3.7. Block Diagram of Automated Component Test Plate

The output of datalogger can be transferred to a personal computer through a datalogger-computer interface software called PC-TALK (program by Freeware Corporation). An interactive data acquisition and data reduction computer program, called RED40, reads data from the file created by the datalogger and PC-TALK. The program, which is written in FORTRAN 77, outputs average, maximum, and minimum temperatures of the desired number of channels for a given number of data sets over a certain period of time. A sample input/output of this program is shown in Appendix A. More information about RED40 program can be found in Rajagopalan (1991).

3.2.3 Air Flow Measurement and Control

Accurate velocity measurement, control of the desired velocity, and documentation of the approach velocity profile upstream of the component arrays are three important key factors in order to achieve the more precise heat transfer results. These are explained in detail, along with necessary parts and the data acquisition programs in the following sections.

3.2.3.1 Velocity Measurement The voltage signal from the differential pressure transducer was digitized and averaged on the personal computer equipped with a Metrabyte-DAS-8 analog-to-digital data translation board. This convertor board has 8 A/D channels with 12 bit resolution, 7 bits of digital I/O (4 outputs, 3 inputs) and other features.

An MKS model 223 BD differential pressure transducer, which was connected to a pitot static probe, was used to measure the velocity. The differential pressure transducer can read a maximum differential pressure of 0.5 inches of water, which corresponds to 14.5 m/sec velocity in the 15.24 cm circular duct. The range of its voltage output is -5 to +5 volts. It has an accuracy of 0.3% of reading and can be powered by a -12 to +12 volts power supply.

An A/D conversion program written in C-language converts the analog voltage measured by the pressure transducer to a digital output displayed on the monitor. The pressure transducer was calibrated against an inclined manometer and the calibration curve is illustrated in Fig. 3.8. This figure shows the monitored digital voltage versus the pressure measured by an inclined manometer. The obtained linear curve fit equation shown in Fig. 3.8 relates the output voltage signal of the pressure transducer to the differential pressure of the pitot static probe. The velocity then can be found using the differential pressure and other physical properties.

3.2.3.2 Velocity Control Arrangement Manually changing the position of the built-in single vane damper on the exit duct of the blower to reach the desired velocity was found to be a tedious operation. It was also not a very accurate method of changing the velocity. Furthermore, low velocities could not be reached by this method of operation. Hence, it was decided to automate the control of velocity in the wind tunnel. To accomplish this task, the arrangement shown in Fig. 3.9 was designed and assembled on the blower wooden housing.

A movable wooden damper, along with an aluminum sprocket of 1.25" pitch diameter, three aluminum pulleys of 1.25" pitch diameter, and a plastic chain were used. A stepper motor manufactured by Superior Electric Company, model number SS50-1009, with 50 oz-in torque, 5.5 volts DC, 1.3 Amps, 60Hz, and 200 steps per revolution was connected to the aluminum sprocket to rotate it clockwise and counter-clockwise in order to move the wooden damper up and down. Movement of this damper changes the flow rate, and hence, the velocity in the wind tunnel. Sprocket, pulleys, and plastic chain were purchased from Berg Company.

3.2.3.3 Program VELAIR The A/D conversion program mentioned in Section 3.2.3.1 converts the output analog voltage of the pressure transducer to a digital voltage.

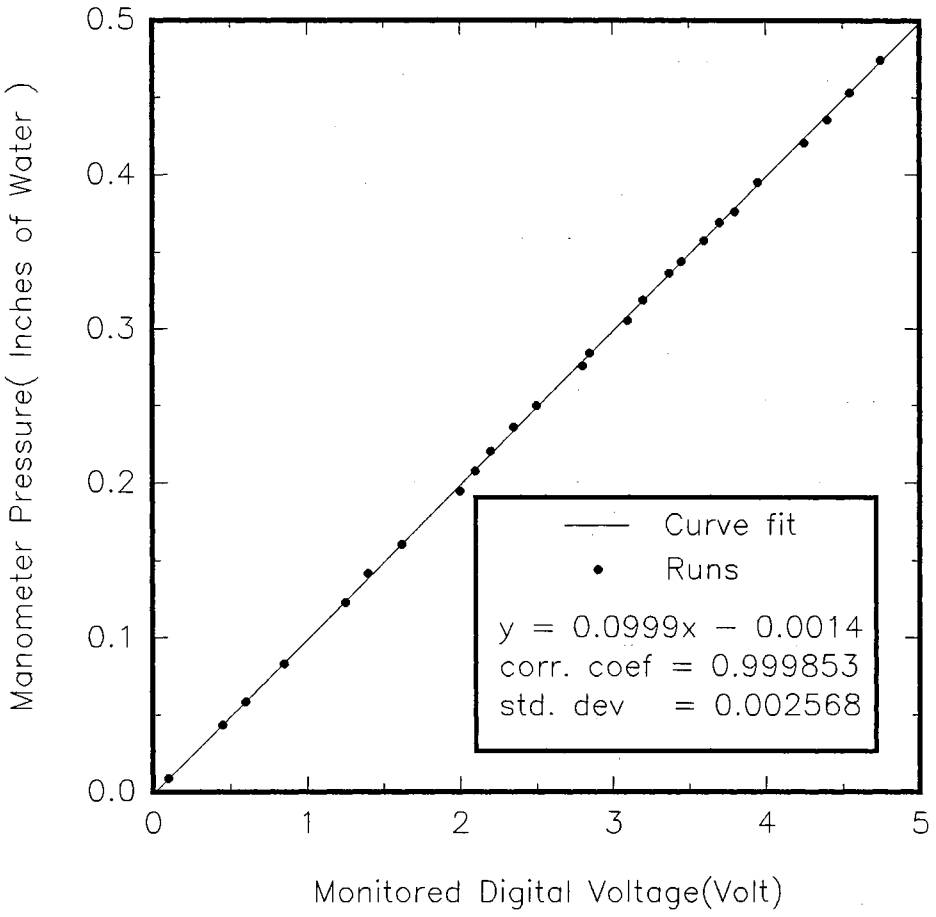

Figure 3.8. Manometer Pressure Versus Monitored Digital Voltage

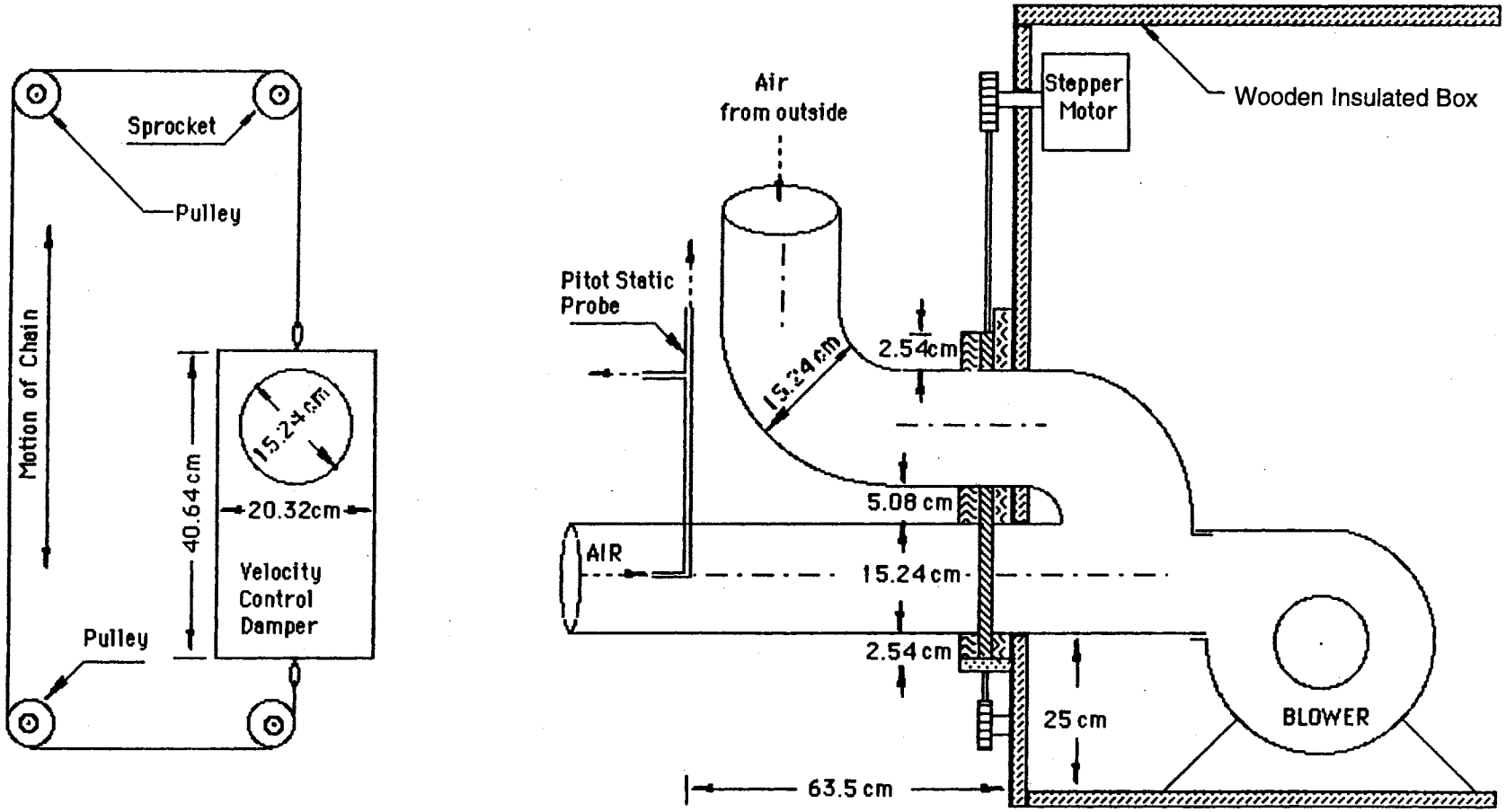

a. Front view of the damper movement.

b. Side view of the velocity control damper and stepper motor along with other facilities attached to the wooden box

Figure 3.9. Arrangement Used to Control the Air Velocity by Moving the Wooden Damper

The digital voltage is related to the differential pressure (measured by pitot static probe) through the calibration curve equation shown in Fig. 3.8. The differential pressure gives the duct velocity using appropriate physical properties. The velocity in the channel can be calculated from the duct velocity by mass flow rate equation depending on the channel height. By reversing the above procedure for a desired channel velocity, the output analog voltage of the pressure transducer can be found.

To accomplish all of these tasks, an interactive data acquisition program called VELAIR (see Appendix A), written in C-language, was developed. The A/D conversion program, calibration curve equation, relation between the differential pressure and duct velocity, fixed physical properties, relation between the duct velocity and channel velocity, and the digital I/O program for stepper motor were all incorporated into VELAIR program. Variable parameters such as channel height, barometric pressure, etc., can be input by the keyboard.

Figure 3.10 shows the setup for measurement and control of the velocity in the channel. Program VELAIR utilizes this setup in order to find channel velocity, using only the pressure transducer, and to change the position of the "velocity control damper", using the stepper motor and pressure transducer, until the desired channel velocity is reached. The program has also the option of back calculating the channel velocity for a given Reynolds number based on channel height. Block diagrams of these options are shown in Figs. 3.11 and 3.12.

3.2.3.4 Velocity Profile Accurate determination of the mean velocity upstream of the test section is needed for calculation of Reynolds number and obtainment of accurate heat transfer results. During each heat transfer experiment, it is possible to traverse the inlet section by a pitot static probe in several strategic locations, and the measured local velocities can be numerically integrated to render mean velocity in the channel. This is not an accurate and convenient method because of the following reasons:

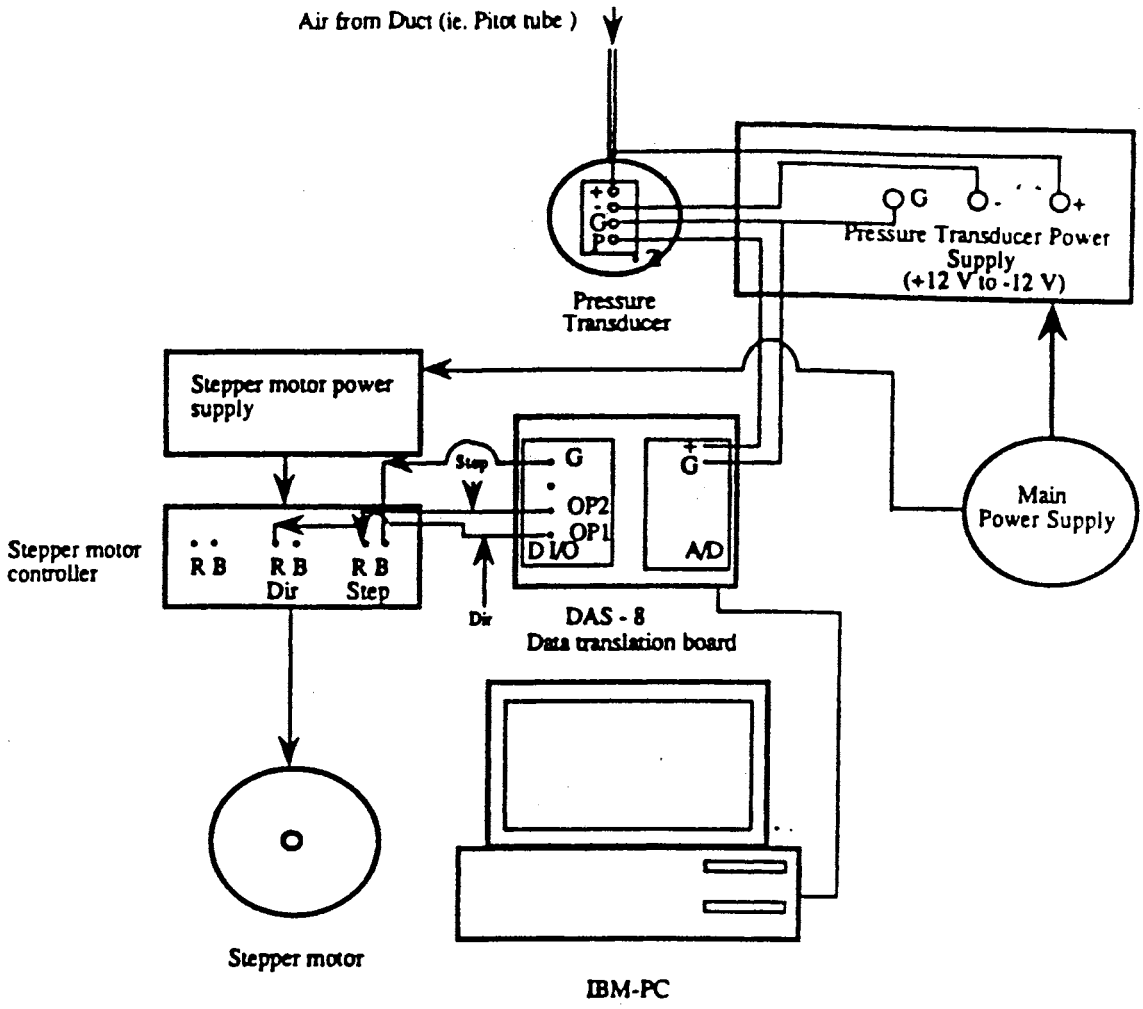

Figure 3.10. Setup for Measurement and Control of Velocity in the Rectangular Channel

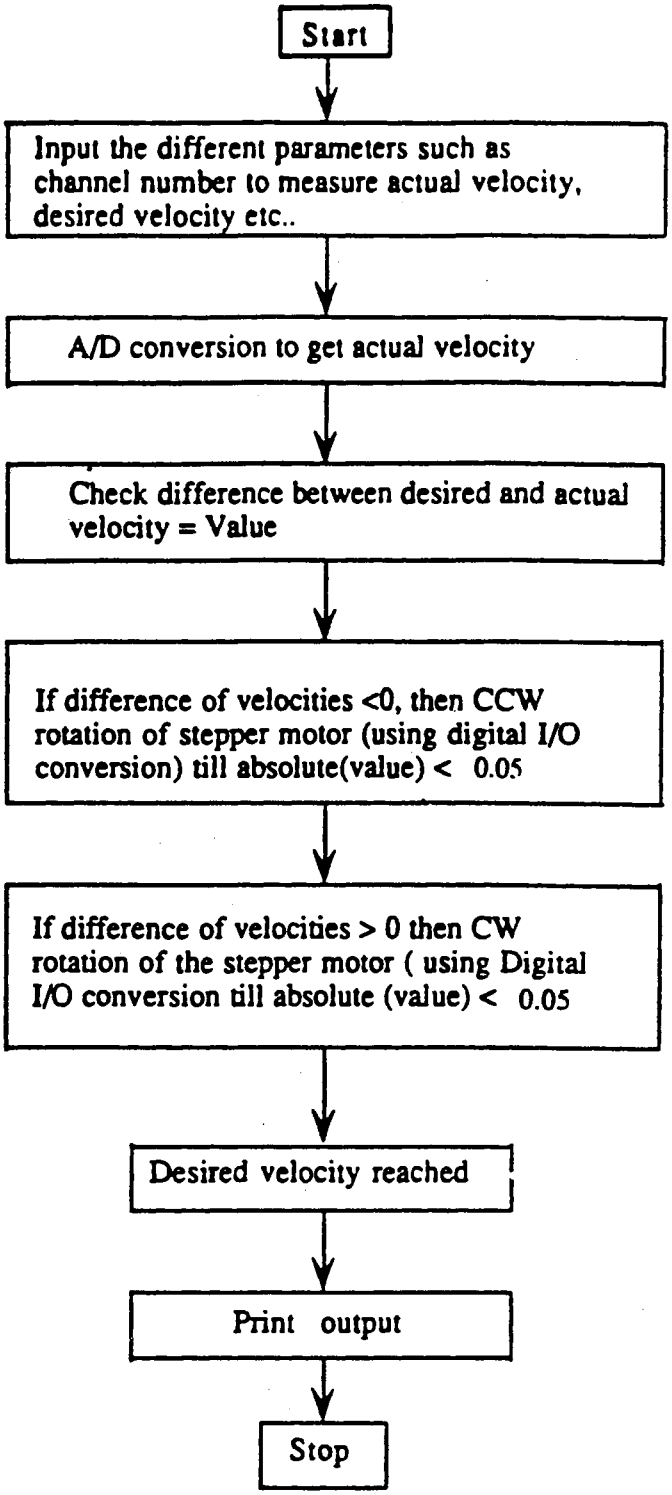

Figure 3.11. Block Diagram to Show Air Velocity Control in the Rectangular Channel

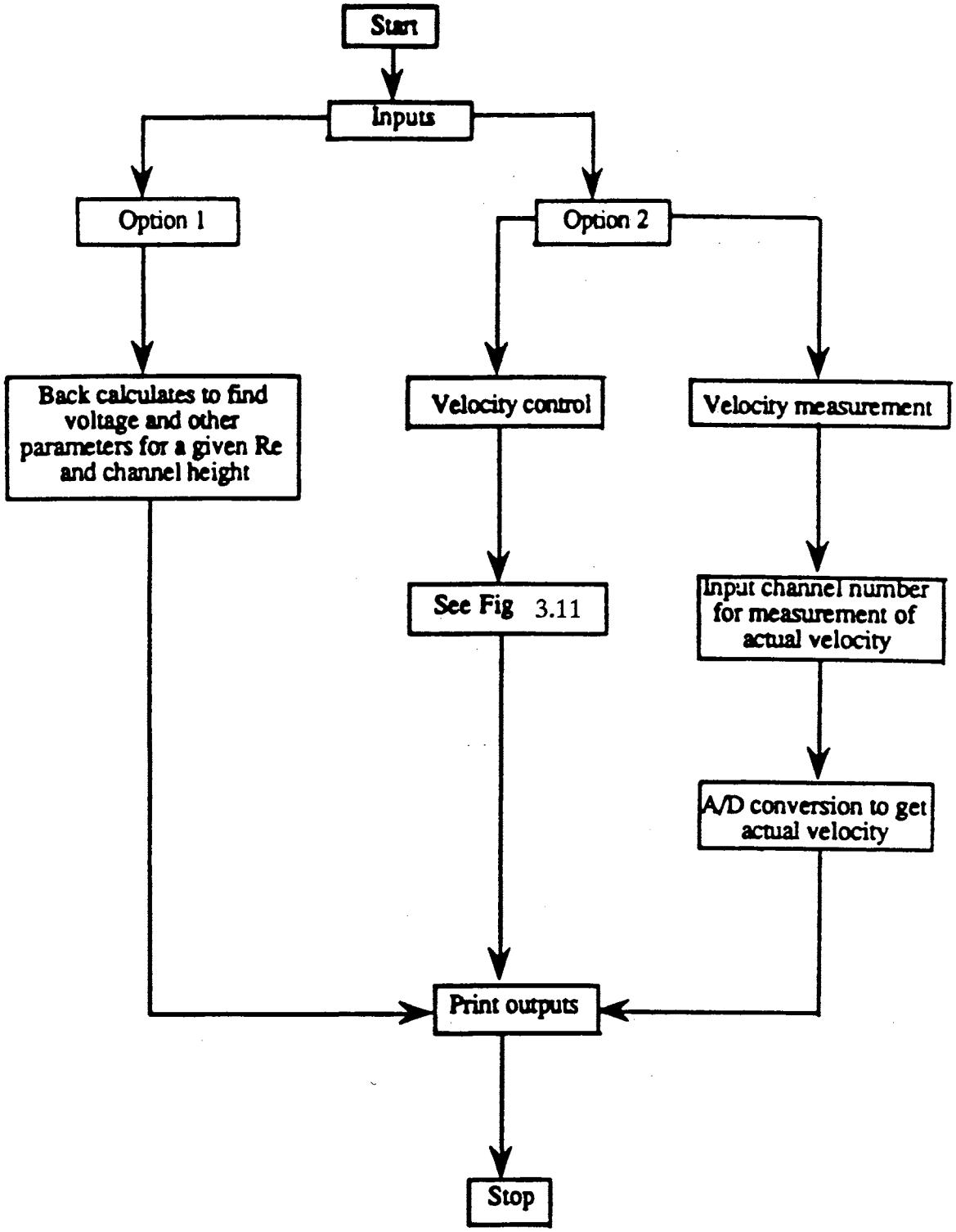

Figure 3.12. Block Diagram to Show the Working of VELAIR Program

1. Traversing the inlet section by the pitot static probe may disturb the flow, and consequently, affect the accuracy of heat transfer results.
2. It is a tedious and time consuming method to perform the above operation during each single heat transfer experiment.

Hence, it was necessary to find an alternative method for determination of the average velocity for different flow settings (low, medium, and high) in the channel. The alternative method measures the local velocity at the center of the duct for each heat transfer experiment, and then relates that to the approach mean velocity in the channel by an appropriate correction factor. To accomplish this task, the following extensive direct local velocity measurements at different locations of the circular duct and rectangular host channel were made.

3.2.3.4.1 Duct Velocity Profile Direct local velocity measurements were performed across the height of the circular duct at fifteen locations and different flow settings (low, medium, and high velocities). Figure 3.13 shows the dimensionless velocity profiles versus dimensionless height for these three settings. These local velocities were numerically integrated and three correction factors of 0.852, 0.864, and 0.896 were found for low (2 m/sec), medium (6 m/sec), and high (10 m/sec) velocities, respectively. Since these three values were very close to each other (a maximum difference of 5%) and their difference were within the range of the experimental error, they were averaged in order to present a single duct correction factor (C_d), which was 0.871. This correction factor relates the duct average velocity ($\overline{V}_d$) to the maximum duct local velocity (V_d), which was found to be at the center of the duct:

$$\overline{V}_d = 0.871\ V_d \tag{3.1}$$

For each flow setting, the wooden velocity damper was sealed and the corresponding direct local velocity measurements were made in the rectangular channel for the same setting.

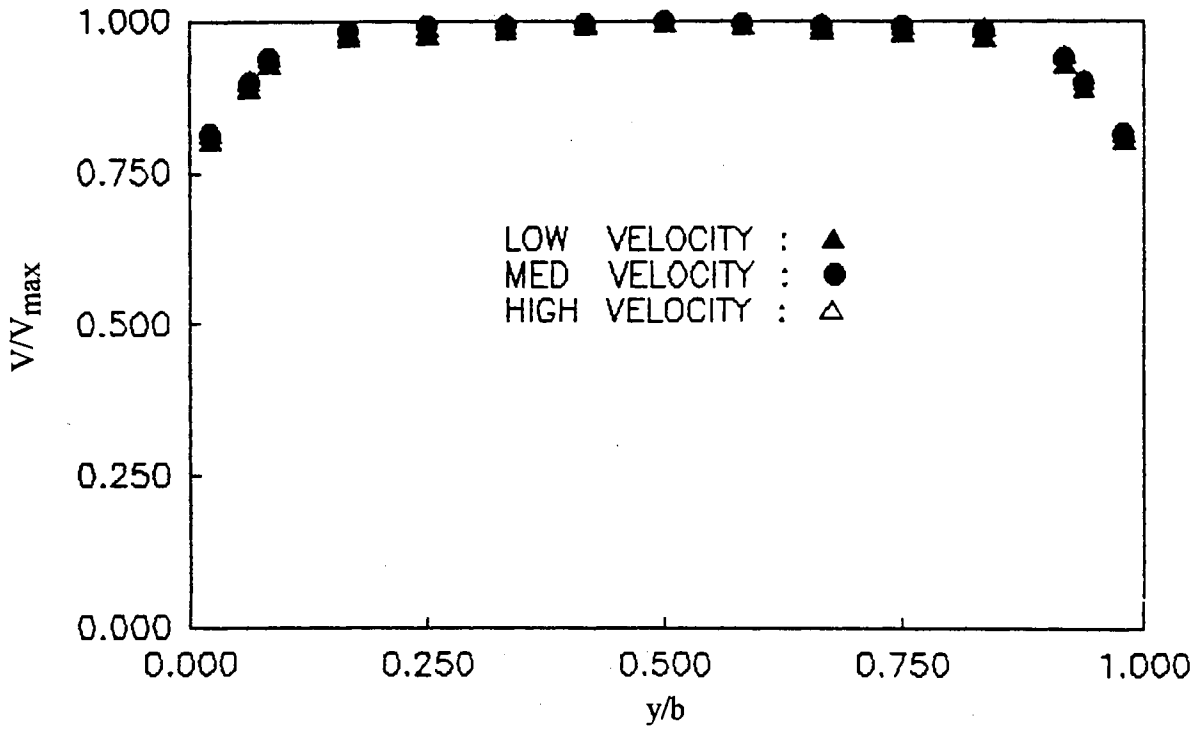

Figure 3.13. Dimensionless Duct Velocity Profiles for Three Different Velocities

3.2.3.4.2 Channel Velocity Profile Direct local velocity measurements were made upstream of the component test section (68.58 cm from the entrance of the rectangular channel) at three different locations across the width of the channel (at channel center line and about 6 cm from the wall on either side of the channel) and up to thirteen different locations (depending on the channel height) across the height of the channel. The flow settings were the same as mentioned for "Duct Velocity Profile", since the wooden velocity damper was sealed during each flow setting measurement. Figures 3.14 to 3.16 show the dimensionless velocity profiles for low, medium, and high velocities, respectively. The dimensionless velocity profiles at left, center, and right of the channel are shown in Figs. 3.17 to 3.19, respectively. The velocity profiles for each individual flow setting and location are depicted in Appendix B.

The local velocities in the channel were numerically integrated and three correction factors of 0.803, 0.808, and 0.814 for low, medium, and high velocities were found. Since these three values were very close to each other (a maximum difference of less than 1.4%) and their difference was within the range of the experimental error, they were averaged in order to present a single channel correction factor (C_{ch}), which was 0.808. This correction factor relates the channel average velocity ($\overline{V}_{ch}$) to the maximum channel local velocity (V_{ch}), which was found to be at the center of the channel:

$$\left(\overline{V}_{ch}\right) = 0.808\ V_{ch} \tag{3.2}$$

A relationship between the channel average velocity ($\overline{V}_{ch}$) and the measured duct center-line velocity (V_d) can be obtained by equating the mass flow rate between the circular duct and the rectangular channel:

$$\rho_d \overline{V}_d A_d = \rho_{ch} \overline{V}_{ch} A_{ch}$$

Substituting Equation (3.1) in the above equation and rearranging:

$$\overline{V}_{ch} = \frac{1}{D}\left(\frac{1}{W}\frac{\rho_d}{\rho_{ch}} A_d C_d\right) V_d$$

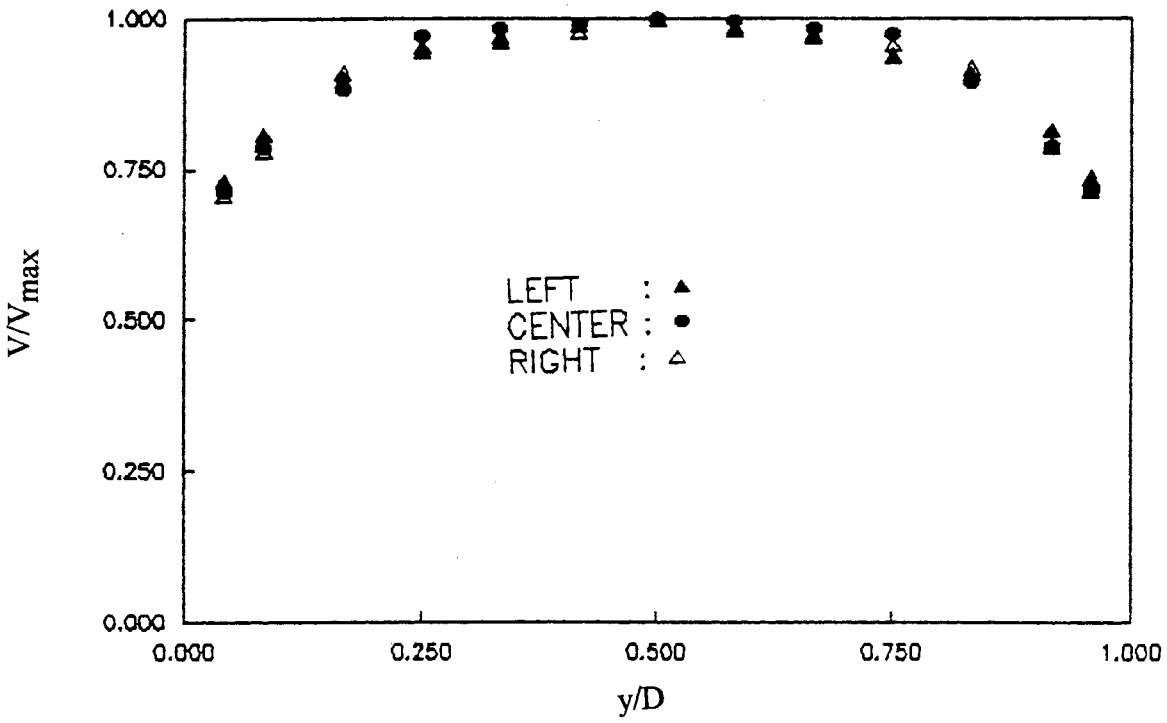

Figure 3.14. Dimensionless Low Velocity Profiles at the Channel for Three Different Locations

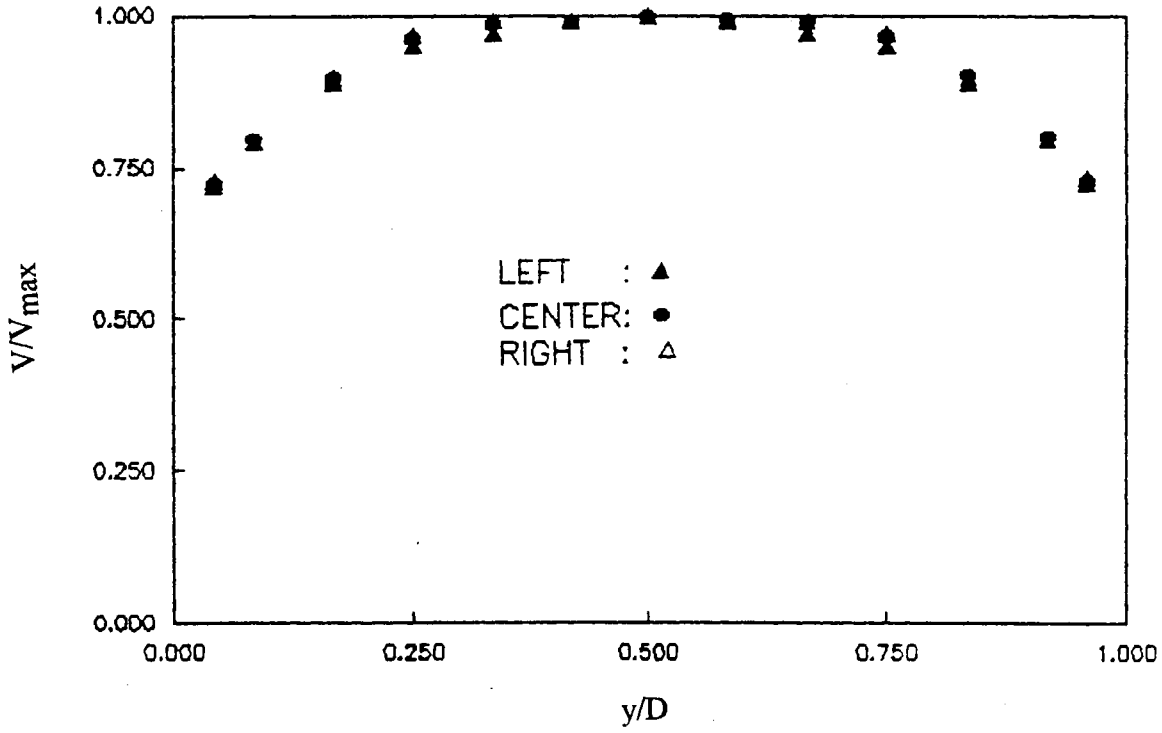

Figure 3.15. Dimensionless Medium Velocity Profiles at the Channel for Three Different Locations

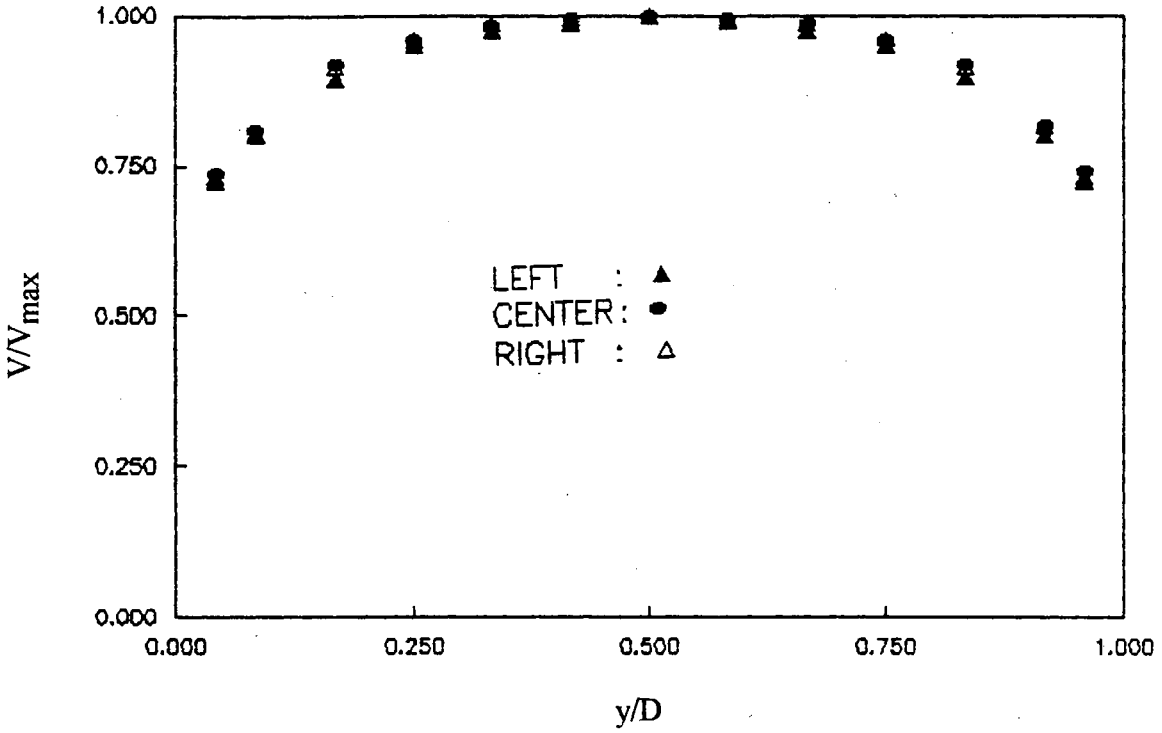

Figure 3.16. Dimensionless High Velocity Profiles at the Channel for Three Different Locations

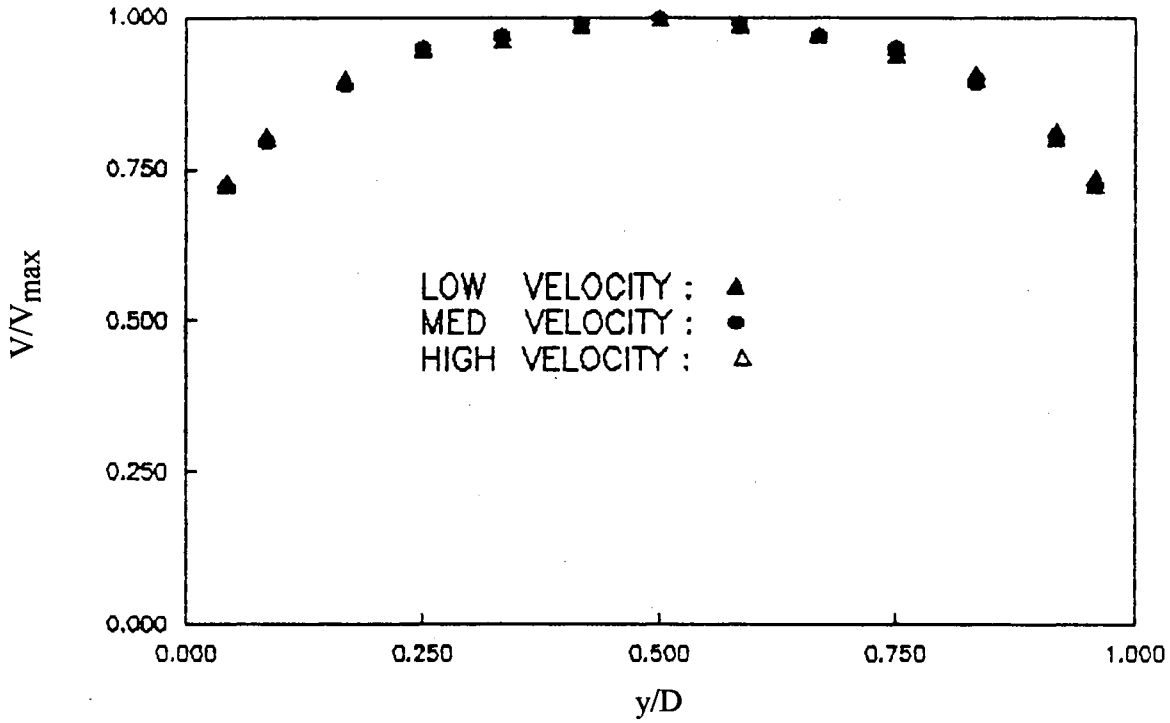

Figure 3.17. Dimensionless Velocity Profiles at the Left of the Channel for Three Different Velocities

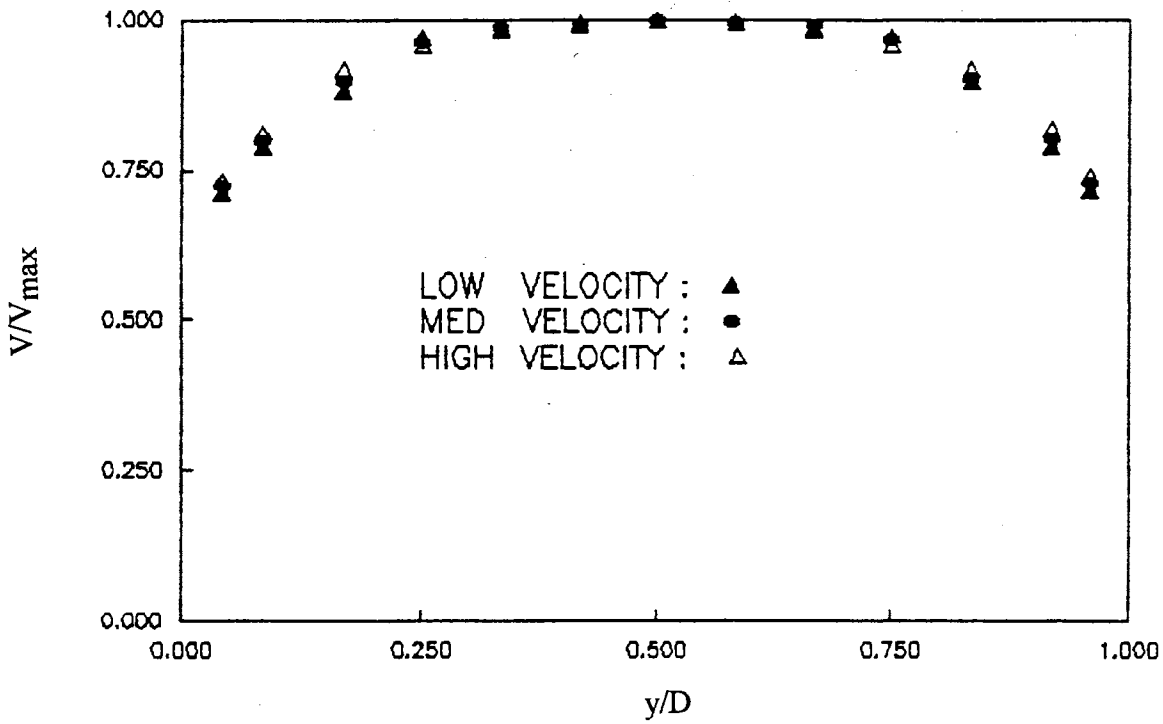

Figure 3.18. Dimensionless Velocity Profiles at the Center of the Channel for Three Different Velocities

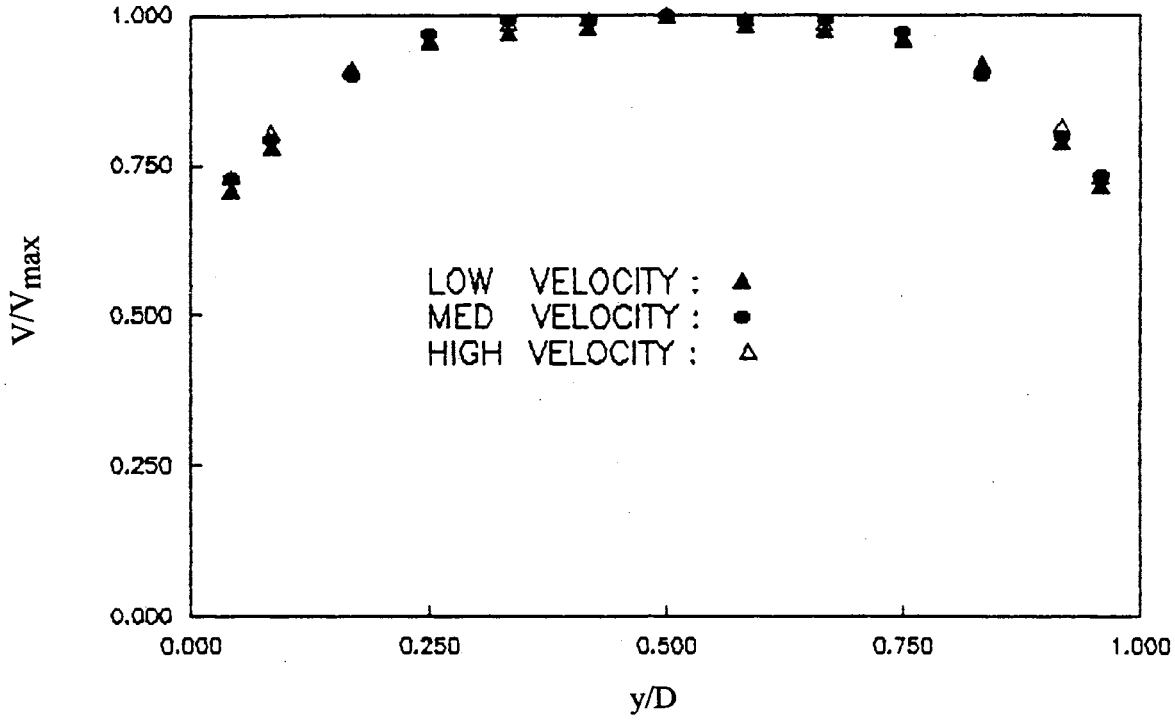

Figure 3.19. Dimensionless Velocity Profiles at the Right of the Channel for Three Different Velocities

Let $$C = \frac{1}{W}\frac{\rho_d}{\rho_{ch}} A_d C_d$$

Hence, $$\overline{V}_{ch} = \frac{1}{D} C V_d$$

where D is the channel height, W = 25.4 cm is the channel width (fixed), ρ_d and ρ_{ch} are the duct and channel air densities, A_{ch} is the channel cross sectional area, A_d is the duct cross-sectional area (duct diameter is 15.24 cm), and C is the "overall correction factor". Combining the above relations with Equations (3.1) and (3.2) gave a value of 6.02 for C. Therefore, the final relation for calculation of channel average velocity from measured duct center-line velocity was:

$$\overline{V}_{ch} = \frac{6.02}{D} V_d \qquad (3.3)$$

where $\overline{V}_{ch}$ and V_d are in m/sec, and D is in cm.

With Equations (3.1) and (3.3), only local velocity at the center of the duct (V_d) should be measured in order to find $\overline{V}_d$ and $\overline{V}_{ch}$. Program VELAIR was modified by incorporating these equations.

To verify the accuracy of these equations, local direct velocity measurements upstream of the component test section at 50.8 cm from the entrance of the rectangular channel for different flow settings (local velocity at the center of the duct was controlled from 1 to 12 m/sec) were performed. The results of these experiments showed that these equations predicted the experimental data with an accuracy of ± 2%. Figure 3.20 shows comparison of measured channel center velocities ($V_{ch,m}$) versus calculated channel center velocities ($V_{ch,c}$), while Figure 3.21 shows measured channel average velocities $\left(\overline{V}_{ch,m}\right)$ versus calculated channel average velocities $\left(\overline{V}_{ch,c}\right)$.

Estimates of uncertainty using method of single-sample experiments (Kline and McClintock, 1953) show the uncertainty in channel average velocity measurements varied from about 0.71% to 8.9% (see Appendix C).

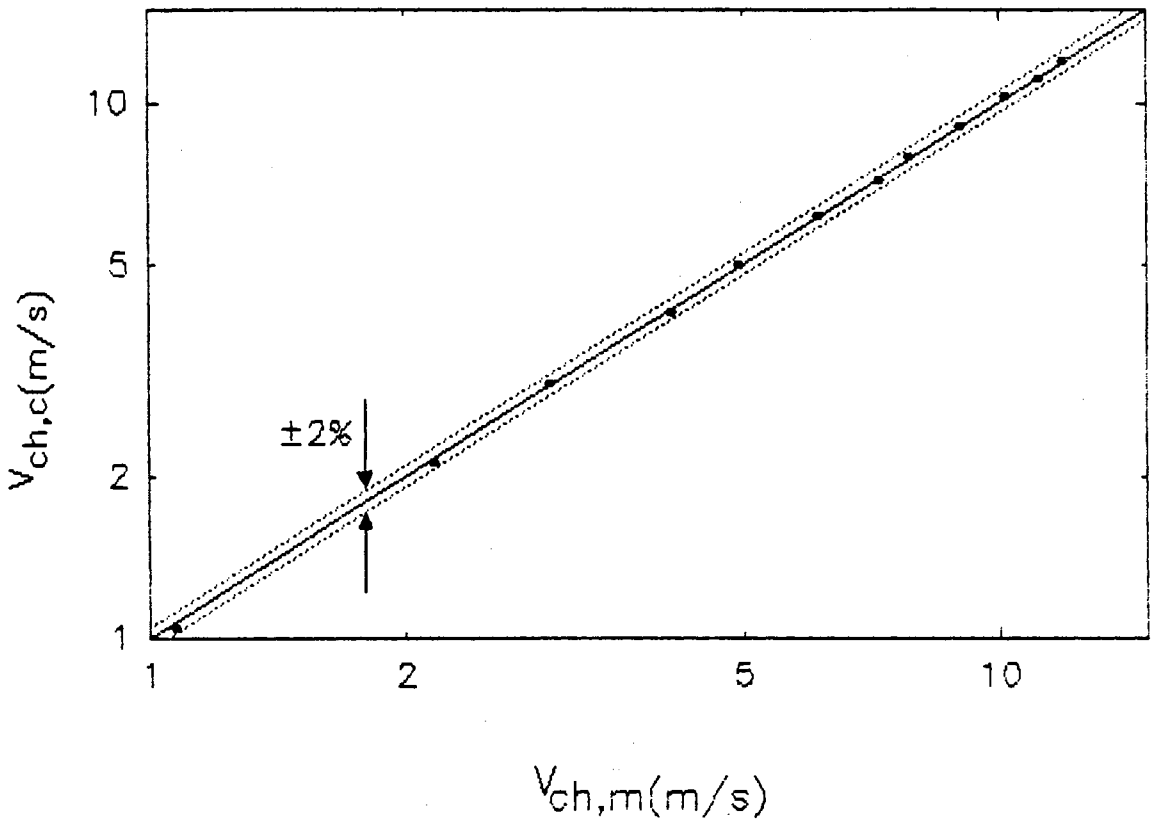

Figure 3.20. Comparison of Measured Local Velocities With Calculated Local Velocities at the Center of Rectangular Channel

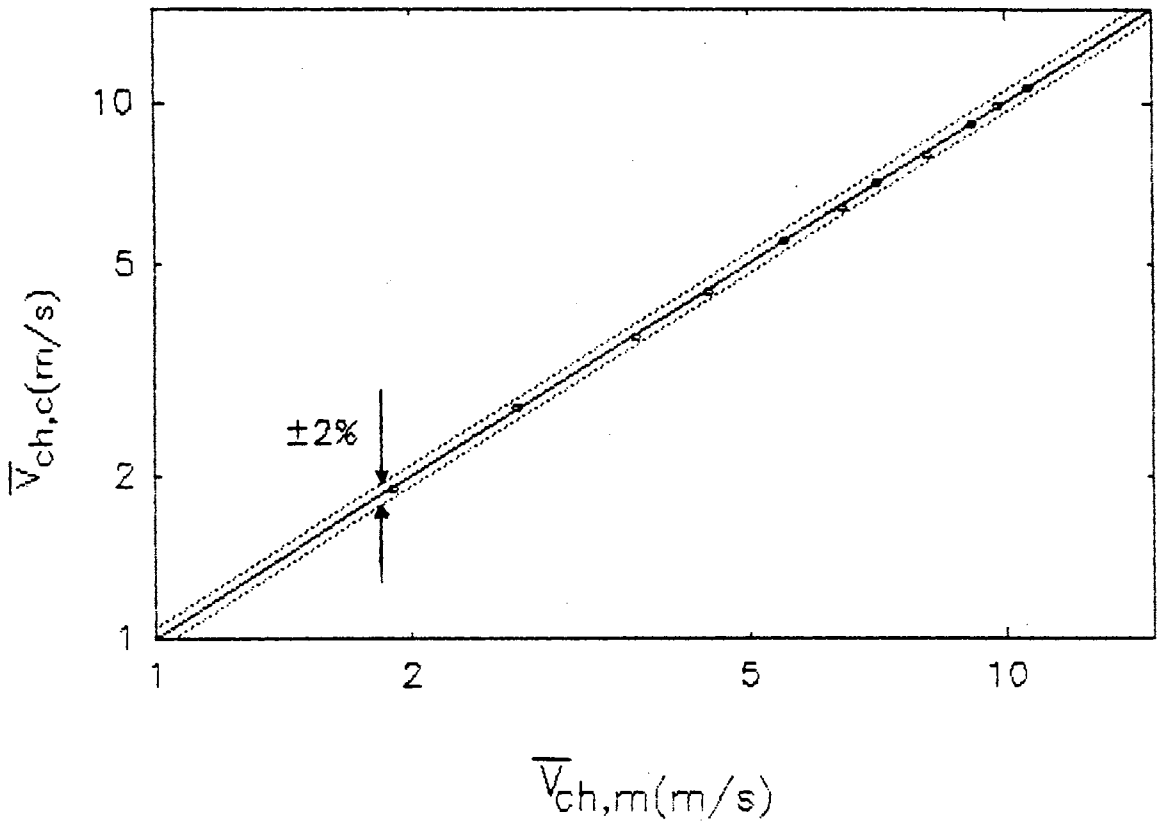

Figure 3.21. Comparison of Measured Average Velocities With Calculated Average Velocities at the Rectangular Channel

3.3 Experimental Procedures and Data Reduction

Before performing any experiment, the following steps should be taken in order to make the setup ready for the purposed experiments:

1. Cover the test section with the fiberglass sheet suitable for the desired arrangement.
2. Install the required components on the test section for the purposed arrangement, and connect the wires to the datalogger and thermal regulator board.
3. Adjust the channel height with the small hydraulic jack under the contraction and three screws under the plexiglass flap attached to the plenum. Then, place the spacers on the two rectangular plexiglass supports and under the channel floor. Do the final adjustment of the channel floor, and then fix it in place with the plastic screws and nuts under the channel floor.
4. Put the upper wall of the test section in place and seal the channel floor, movable part of contraction, and other places. Wait 6 to 8 hours until the sealant dries.
5. Turn on the datalogger, thermal regulator board, and personal computer, and enter the desired power for each component by the keyboard.
6. Turn on the blower, stepper motor and pressure transducer power supply, and enter the required mean velocity (or Reynolds number) at the channel using velocity control option of VELAIR program.
7. Monitor the component temperatures with the datalogger every five minutes until the steady state condition is reached (when temperatures are within $\pm$ 0.5°C).
8. Print out the steady state temperatures of components.

Conduction and radiation are important factors which have to be considered during each experiment. Therefore, the convective heat transfer rate for each component (Q_c) is its input power (Q_t), less losses due to the conduction through the channel floor (Q_k) and thermal radiation to the surroundings (Q_r):

$$Q_c = Q_t - Q_k - Q_r \tag{3.4}$$

conduction losses can be calculated by:

$$Q_k = (T_c - T_\infty)/R_W$$

where T_c is the component temperature, T_∞ is the approach air temperature measured upstream of the test section with a T-type thermocouple connected to the datalogger, and R_W is the thermal resistance of the test section floor obtained by:

$$R_W = \frac{1}{A_k}\left(\frac{t_1}{k_1} + \frac{t_2}{k_2}\right)$$

where:

$A_k = (0.025)^2 m^2$ is the component contact surface area with the channel floor.

$t_1 = 0.0127$m is the plexiglass thickness.

$k_1 = 0.193$ Watt/m°C is the thermal conductivity for commercial plexiglass (Personal communication, Polypenco, Inc., 1991)

$t_2 = 0.0016$ m is the fiberglass thickness

$k_2 = 0.293$ Watt/m°C is the thermal conductivity for NEMA-G11 fiberglass (Personal communication, Polypenco, Inc., 1991)

Therefore,

$$Q_k = \frac{T_c - T_\infty}{110.5°C/Watt} \tag{3.5}$$

Radiation loss can be calculated by

$$Q_r = \sigma \varepsilon A_c (T_c^4 - T_\infty^4)$$

where

$\sigma = 5.729 \times 10^{-8}$ Watt/m^{2}K^4 is the Stefan-Boltzman constant

$\varepsilon = 0.06$ is the emissivity of polished aluminum (Siegel and Howell, 1981)

$A_c = (1 + 4\ t/L)\ (0.0254)^2$ is the component exposed surface area in m^2.

Hence,

$$Q_r = 3.437 \times 10^{-9}\ Ac(T_c^4 - T_\infty^4) \tag{3.6}$$

where T_c is in K and Q_r is in Watts.

Knowing the component temperature (T_c) and the approach air temperature (T_∞), conduction and radiation losses can be calculated from Equations (3.5) and (3.6), respectively. The component convective heat transfer rate (Q_c) can be calculated from Equation (3.4) for a given component input power (Q_t). Thus, the component convective heat transfer coefficient (h) can be found for a single heated component from:

$$h = \frac{Q_c}{A_c (T_c - T_\infty)} \tag{3.7}$$

After finishing one measurement, the same procedure can be repeated for another experiment.

The experimental procedures outlined in this chapter were followed for collection of heat transfer data. The results of these experiments with the related general correlation for different geometric parameters, their detailed discussion and comparison with the work of other investigators, and the influence of conduction losses on component convection heat transfer coefficient are presented in the next chapter.

CHAPTER IV

HEAT TRANSFER RESULTS, DISCUSSION, AND COMPARISONS

In Chapter III, details of our experimental apparatus and procedures for collection of heat transfer data were outlined. The necessity of a systematic and continuous approach in the area of electronic cooling was mentioned, and the experimental setup was designed based on this purpose. It was also explained that the setup has the capability of performing experiments with different arrangements, component heights, channel heights, spanwise and streamwise spacing, component power dissipations, test section orientation (vertical or horizontal), as well as performing experiments for configurations similar to some of the work summarized in Table I, in order to compare and verify the performance of our experimental setup.

In this chapter, heat transfer results are presented. Experiments were performed with different channel average velocities, channel heights, heated component row numbers, component heights, and input power to the heated component. Ranges of conduction and radiation heat transfer for different Reynolds numbers and geometries were first determined. Based on the collected heat transfer data and the influence of all tested effective parameters, a general correlation for prediction of heated component operating temperature was developed. Detailed discussion of the effects of Reynolds number and different tested geometric parameters (H/t, t/L, and r), on convective heat transfer coefficient of the heated component is presented. The results of this study were compared with the results of other investigators, having almost similar geometries and range of Reynolds numbers. These comparisons revealed the accuracy of our general heat transfer correlation, and verified the good performance of our experimental setup. Finally, effects

of conduction heat transfer on heat transfer coefficient, using different board conductivities and Reynolds numbers were investigated.

4.1 Heat Transfer Results

A single component was heated for each set of collected heat transfer data. Ranges of experimental parameters tested are shown in Table II. Figure 4.1 illustrates an in-line arrangement of the components used in the test section, with row-column numbers written above the heated components. Third column was chosen in order to be able to compare the results with other investigators. The works reported in the literature were based on a single heated component placed at the center of the test section, with the same distance from the adjacent side walls of the rectangular channel.

TABLE II

RANGES OF EXPERIMENTAL PARAMETERS TESTED
FOR COLLECTION OF HEAT TRANSFER DATA

t/L	D/t	Heated Component Row Number at Column 3	Approximate channel Average Velocity $\overline{V}_{ch}$ (m/s)
0.5	1.5	1, 2, 3, 4, 5	2, 5, 7.5, 10
	2.25	1, 2, 3, 5, 7, 8	2, 5, 7.5, 10
	3	1, 2, 3, 4, 5, 6	2, 5, 7.5, 10
1	1.5	1,2,3,4,5,8	2, 5, 7.5, 10
	2.25	1, 2, 3, 5, 7, 8	2, 5, 7.5, 10
	3	1, 2, 3, 4, 5, 6, 7	2, 5, 7.5, 10

For each set of these experiments, the procedures outlined in Chapter III were carefully followed. Approach air flow temperature (T_∞), component steady state temperature (T_c), Reynolds number based on component length (Re_L), and the input power

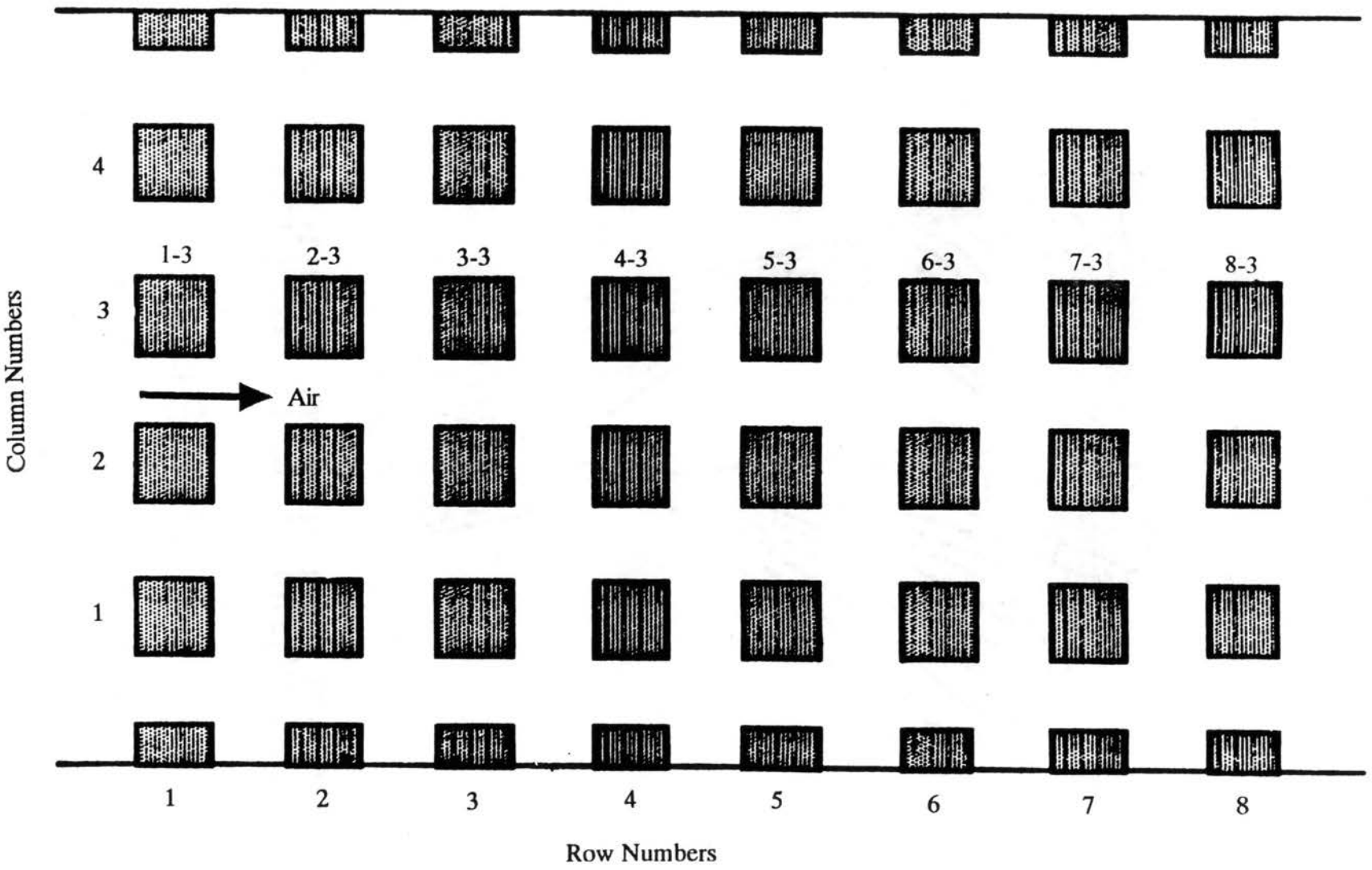

Figure 4.1. In-Line Arrangement of the Components in the Test Section With Row and Column Numbers

to the component (Q_c) were collected. Conduction loss (Q_k), radiation loss (Q_r), convective heat transfer rate (Q_c), and convective heat transfer coefficient (h) were also calculated for each run using Equations (3.5), (3.6), (3.4), and (3.7), respectively. Nusselt number based on component length (L) was found from:

$$Nu_L = hL/k$$

where k is the air thermal conductivity at T_∞.

The Reynolds number, based on component length (L) and channel average velocity ($\overline{V}_{ch}$) is:

$$Re_L = \frac{\overline{V}_{ch} L}{\nu}$$

where ν is the kinematic viscosity of air at T_∞. The choice of component length as the characteristic length for Reynolds and Nusselt numbers was based on the following reasons:

1. All of the geometrical parameters are non-dimensionalized with respect to component length, as mentioned in Section 3.1.4. Components with a fixed length (L = 2.54 cm) but different heights were used for performing systematic experiments with our experimental setup. This length was fixed while varying other parameters, until experiments for all possible variations were performed.
2. Component length is an appropriate conventional basis for meaningful comparisons. The heat transfer results reported by some investigators, even for some set of dissimilar geometries, are possible to be compared with each other and our results by the use of component length as the characteristic length. The Reynolds and Nusselt numbers of some investigators which were not based on their component length were carefully converted to this basis in the next section, in order to make a reasonable comparison.

The collected data and the above calculated parameters are all summarized in Tables III and IV. A complete set of heat transfer data was first collected by keeping the heated

TABLE III

COLLECTED HEAT TRANSFER DATA FOR COMPONENT 2-3 WITH DIFFERENT HEAT DISSIPATION LEVELS AND VELOCITIES (CASE: D/t = 3, S/L = 1, AND t/L = 1)

Q_t (Watt)	Run #	$\overline{V}_{ch}$ (m/s)	Re_L	T_c (°C)	T_∞ (°C)	(T_c-T_∞) (°C)	Q_k (Watt)	Q_k/Q_t x 100	Q_r (Watt)	Q_r/Q_t x 100	Q_L (Watt)	Q_L/Q_t x 100	Q_c (Watt)	h (Watt/m^2°C)	Nu_L
	1	2.11	3552	29.6	22.5	7.1	0.064	6.4	0.008	0.84	0.073	7.3	0.927	40.5	40.1
1	2	4.97	8366	26.5	22.0	4.5	0.041	4.1	0.005	0.53	0.046	4.6	0.954	65.7	65.1
	3	7.57	12742	26.3	22.8	3.5	0.032	3.2	0.004	0.41	0.036	3.6	0.964	85.4	84.6
	4	10.17	17120	25.8	22.8	3.0	0.027	2.7	0.004	0.35	0.031	3.1	0.969	100.2	99.3
	5	2.11	3552	37.5	22.8	14.7	0.133	6.7	0.018	0.91	0.151	7.6	1.849	39.0	38.7
2	6	4.97	8366	30.4	21.3	9.1	0.082	4.1	0.011	0.54	0.093	4.7	1.907	65.0	64.4
	7	7.57	12742	28.2	21.0	7.2	0.065	3.3	0.008	0.42	0.074	3.7	1.926	82.9	82.2
	8	10.17	17120	27.3	21.3	6.0	0.054	2.7	0.007	0.35	0.061	3.1	1.939	100.2	99.3
	9	2.11	3552	42.7	21.9	20.8	0.188	6.3	0.026	0.88	0.215	7.2	2.785	41.5	41.1
3	10	4.97	8366	34.9	21.8	13.1	0.119	4.0	0.016	0.53	0.134	4.5	2.866	67.8	67.2
	11	7.57	12742	32.2	21.5	10.7	0.097	3.2	0.013	0.43	0.110	3.7	2.890	83.7	82.9
	12	10.17	17120	30.9	21.7	9.2	0.083	2.8	0.011	0.37	0.094	3.1	2.906	97.9	97.0
	13	2.11	3552	49.8	22.0	27.8	0.252	6.3	0.037	0.91	0.288	7.2	3.712	41.3	40.9
4	14	4.97	8366	38.7	21.7	17.0	0.154	3.8	0.021	0.53	0.175	4.4	3.825	69.8	69.2
	15	7.57	12742	35.7	22.0	13.7	0.124	3.1	0.017	0.42	0.141	3.5	3.859	87.3	86.5
	16	10.17	17120	34.3	22.5	11.8	0.106	2.7	0.014	0.36	0.121	3.0	3.879	102.4	101.5
	17	2.11	3552	55.7	21.5	34.2	0.310	6.2	0.046	0.92	0.356	7.1	4.644	42.1	41.7
5	18	4.97	8366	43.2	21.9	21.3	0.193	3.9	0.027	0.54	0.220	4.4	4.780	69.6	69.0
	19	7.57	12742	38.9	21.8	17.1	0.155	3.1	0.021	0.42	0.176	3.5	4.824	87.5	86.7
	20	10.17	17120	35.9	21.4	14.5	0.131	2.6	0.018	0.35	0.149	3.0	4.851	103.7	102.8

TABLE IV

COLLECTED HEAT TRANSFER DATA WITH DIFFERENT VELOCITIES AND HEATED COMPONENT ROW NUMBERS (CASE: $D/t = 1.50$, $S/L = 1$, $t/L = 0.50$, AND $Q_t = 4$ WATTS)

r	Run #	$\bar{V}_{ch}$ (m/s)	Re_L	T_c (°C)	T_∞ (°C)	(T_c-T_∞) (°C)	Q_k (Watt)	Q_k/Q_t x 100	Q_r (Watt)	Q_r/Q_t x 100	Q_L (Watt)	Q_L/Q_t x 100	Q_c (Watt)	h (Watt/m^2°C)	Nu_L
	1	2.27	3821	55.8	22.7	33.1	0.300	7.5	0.027	0.67	0.326	8.2	3.674	57.3	56.8
1	2	5.35	9000	41.4	22.5	18.9	0.171	4.3	0.014	0.36	0.185	4.6	3.815	104.5	103.6
	3	7.48	12593	36.8	21.8	15.0	0.136	3.4	0.011	0.28	0.147	3.7	3.853	132.9	131.7
	4	9.90	16669	35.3	22.6	12.8	0.115	2.9	0.009	0.23	0.125	3.1	3.875	156.9	155.5
	5	2.23	3756	57.5	21.9	35.6	0.322	8.1	0.029	0.73	0.351	8.8	3.649	53.0	52.5
2	6	5.24	8819	42.7	21.8	20.9	0.189	4.7	0.016	0.40	0.205	5.1	3.795	93.9	93.1
	7	7.52	12666	39.3	22.3	17.0	0.154	3.9	0.013	0.32	0.167	4.2	3.833	116.3	115.3
	8	9.91	16678	35.2	21.2	14.0	0.126	3.2	0.010	0.25	0.137	3.4	3.863	142.9	141.6
	9	2.21	3728	58.0	21.9	36.1	0.327	8.2	0.030	0.74	0.356	8.9	3.644	52.2	51.7
3	10	5.19	8737	43.6	21.8	21.8	0.197	4.9	0.017	0.42	0.214	5.3	3.786	89.7	88.9
	11	7.47	12584	38.9	21.4	17.6	0.159	4.0	0.013	0.33	0.172	4.3	3.828	112.7	111.7
	12	9.94	16735	37.0	22.6	14.3	0.130	3.2	0.011	0.27	0.140	3.5	3.860	139.1	137.9
	13	2.24	3777	57.2	21.2	36.1	0.326	8.2	0.029	0.73	0.356	8.9	3.644	52.2	51.7
4	14	5.13	8636	43.8	21.7	22.1	0.200	5.0	0.017	0.42	0.217	5.4	3.783	88.4	87.6
	15	7.53	12670	39.6	22.0	17.6	0.159	4.0	0.013	0.33	0.173	4.3	3.827	112.3	111.3
	16	9.88	16635	36.4	21.9	14.5	0.131	3.3	0.011	0.27	0.141	3.5	3.859	137.9	136.7
	17	2.15	3620	59.0	21.8	37.2	0.336	8.4	0.031	0.76	0.367	9.2	3.633	50.5	50.0
5	18	5.21	8766	44.3	22.1	22.3	0.201	5.0	0.017	0.43	0.218	5.5	3.782	87.8	87.0
	19	7.50	12634	39.7	21.9	17.8	0.161	4.0	0.013	0.33	0.174	4.4	3.826	111.0	110.0
	20	9.89	16647	36.8	22.1	14.7	0.133	3.3	0.011	0.27	0.143	3.6	3.857	136.0	134.8

TABLE IV (continued)

COLLECTED HEAT TRANSFER DATA WITH DIFFERENT VELOCITIES AND HEATED COMPONENT ROW NUMBERS (CASE: $D/t = 2.25$, $S/L = 1$, $t/L = 0.5$, AND $Q_t = 4$ WATTS)

r	Run #	$\overline{V}_{ch}$ (m/s)	Re_L	T_c (°C)	T_∞ (°C)	(T_c-T_∞) (°C)	Q_k (Watt)	Q_k/Q_t x 100	Q_r (Watt)	Q_r/Q_t x 100	Q_L (Watt)	Q_L/Q_t x 100	Q_c (Watt)	h (Watt/m^2°C)	Nu_L
	1	1.74	2930	60.0	22.8	37.2	0.336	8.4	0.031	0.77	0.367	9.2	3.633	50.5	50.0
1	2	5.00	8422	42.4	21.9	20.4	0.185	4.6	0.016	0.39	0.200	5.0	3.800	96.1	95.2
	3	7.53	12684	38.3	22.1	16.1	0.146	3.7	0.012	0.30	0.158	4.0	3.842	123.0	121.9
	4	9.99	16827	36.1	22.0	14.1	0.128	3.2	0.010	0.26	0.138	3.5	3.862	141.3	140.0
	5	1.74	2930	60.4	21.4	39.0	0.353	8.5	0.032	0.81	0.385	9.6	3.615	47.9	47.5
2	6	5.6	8422	44.5	22.1	22.4	0.203	5.1	0.017	0.43	0.220	5.5	3.780	87.1	86.3
	7	7.53	12684	39.1	21.6	17.6	0.159	4.0	0.013	0.33	0.172	4.3	3.828	112.6	111.6
	8	9.99	16827	36.4	21.4	15.0	0.136	3.4	0.011	0.28	0.147	3.7	3.853	132.4	131.2
	9	1.74	2930	61.5	22.1	39.4	0.357	8.9	0.033	0.82	0.390	9.7	3.610	47.3	46.8
3	10	5.00	8422	44.8	22.1	22.7	0.205	5.1	0.017	0.43	0.222	5.6	3.778	86.1	85.3
	11	7.53	12684	39.5	21.7	17.9	0.162	4.0	0.013	0.33	0.175	4.4	3.825	110.6	109.6
	12	9.99	16827	36.8	22.0	14.8	0.134	3.3	0.011	0.27	0.144	3.6	3.856	134.9	133.7
	13	1.74	2930	61.8	21.9	39.9	0.361	9.0	0.033	0.83	0.395	9.9	3.605	46.7	46.3
5	14	5.00	8422	44.7	21.8	22.9	0.207	5.2	0.018	0.44	0.225	5.6	3.775	85.2	84.4
	15	7.53	12684	39.0	22.1	16.9	0.153	3.8	0.013	0.31	0.165	4.1	3.835	117.5	116.4
	16	9.99	16827	36.2	21.8	14.4	0.131	3.3	0.011	0.26	0.141	3.5	3.859	138.2	137.0
	17	1.74	2930	61.9	21.8	40.2	0.363	9.1	0.034	0.84	0.397	9.9	3.603	46.4	46.0
7	18	5.00	8422	44.9	21.8	23.1	0.209	5.2	0.018	0.44	0.227	5.7	3.773	84.4	83.6
	19	7.53	12684	39.9	21.7	18.2	0.165	4.1	0.014	0.34	0.178	4.5	3.822	108.5	107.5
	20	9.99	16827	37.5	22.2	15.3	0.138	3.5	0.011	0.28	0.150	3.7	3.850	130.2	129.0
	21	1.74	2930	61.6	21.8	39.8	0.360	9.0	0.033	0.83	0.393	9.8	3.607	46.9	46.5
8	22	5.00	8422	44.7	22.0	22.7	0.206	5.1	0.017	0.44	0.223	5.6	3.777	85.9	85.1
	23	7.53	12684	39.6	21.9	17.7	0.160	4.0	0.013	0.33	0.174	4.3	3.826	111.5	110.5
	24	9.99	16827	36.5	21.6	14.9	0.134	3.4	0.011	0.27	0.145	3.6	3.855	134.1	132.9

TABLE IV (continued)

COLLECTED HEAT TRANSFER DATA WITH DIFFERENT VELOCITIES AND HEATED COMPONENT ROW NUMBERS (CASE: D/t = 3, S/L = 1, t/L = 0.5, AND Q_t = 4 WATTS)

r	Run #	$\bar{V}_{ch}$ (m/s)	Re_L	T_c (°C)	T_∞ (°C)	(T_c-T_∞) (°C)	Q_k (Watt)	Q_k/Q_t x 100	Q_r (Watt)	Q_r/Q_t x 100	Q_L (Watt)	Q_L/Q_t x 100	Q_c (Watt)	h (Watt/m^2°C)	Nu_L
	1	1.78	2998	61.3	23.2	38.1	0.345	8.6	0.032	0.81	0.377	9.4	3.623	49.1	48.7
1	2	4.65	7832	45.0	22.2	22.7	0.206	5.1	0.018	0.44	0.223	5.6	3.777	85.8	85.0
	3	7.69	12953	39.5	22.4	17.1	0.154	3.9	0.013	0.32	0.167	4.2	3.833	116.1	115.1
	4	10.01	16861	36.8	22.4	14.5	0.131	3.3	0.011	0.27	0.142	3.5	3.858	138.0	136.8
	5	1.71	2880	63.0	22.6	40.4	0.366	9.1	0.034	0.85	0.400	10.0	3.600	46.1	45.7
2	6	4.65	7832	47.4	22.7	24.7	0.224	5.6	0.019	0.48	0.243	6.1	3.757	78.6	77.9
	7	7.66	12903	41.3	22.5	18.9	0.171	4.3	0.014	0.36	0.185	4.6	3.815	104.6	103.7
	8	9.98	16810	37.6	22.0	15.7	0.142	3.5	0.012	0.29	0.153	3.8	3.847	126.9	125.8
	9	1.72	2897	64.1	23.2	40.8	0.370	9.2	0.035	0.87	0.404	10.1	3.596	45.5	45.1
3	10	4.63	7799	47.6	22.4	25.2	0.228	5.7	0.020	0.49	0.248	6.2	3.752	76.8	76.1
	11	7.66	12903	41.6	22.2	19.3	0.175	4.4	0.015	0.37	0.189	4.8	3.811	101.9	101.0
	12	9.98	16810	37.7	21.8	15.9	0.144	3.6	0.012	0.29	0.156	3.9	3.844	124.9	123.8
	13	1.77	2981	64.7	22.3	42.4	0.384	9.6	0.036	0.90	0.419	10.5	3.581	43.7	43.3
4	14	4.65	7832	48.2	22.7	25.5	0.231	5.8	0.020	0.50	0.251	6.3	3.749	75.8	75.1
	15	7.63	12852	41.6	22.2	19.4	0.176	4.4	0.015	0.37	0.190	4.8	3.810	101.4	100.5
	16	9.97	16793	37.7	21.5	16.2	0.146	3.7	0.012	0.30	0.158	4.0	3.842	122.7	121.6
	17	1.74	2931	65.3	22.2	43.2	0.391	9.8	0.037	0.92	0.427	10.7	3.573	42.8	42.4
5	18	4.63	7799	50.6	24.8	25.9	0.234	5.9	0.021	0.52	0.255	6.4	3.745	74.8	74.1
	19	7.64	12869	41.8	22.3	19.5	0.176	4.4	0.015	0.37	0.191	4.8	3.809	101.0	100.1
	20	9.97	16793	39.1	22.6	16.5	0.149	3.7	0.012	0.31	0.161	4.0	3.839	120.4	119.3
	21	1.76	2965	65.0	22.3	42.7	0.386	9.7	0.036	0.91	0.423	10.6	3.577	43.3	42.9
6	22	4.65	7832	51.2	25.2	26.0	0.235	5.9	0.021	0.52	0.256	6.4	3.744	74.5	73.8
	23	7.65	12886	41.5	22.1	19.4	0.176	4.4	0.015	0.37	0.190	4.8	3.810	101.4	100.5
	24	9.94	16743	38.5	22.4	16.1	0.146	3.6	0.012	0.30	0.157	3.9	3.843	123.5	122.4

TABLE IV (continued)

COLLECTED HEAT TRANSFER DATA WITH DIFFERENT VELOCITIES AND HEATED COMPONENT ROW NUMBERS (CASE: $D/t = 1.5$, $S/L = 1$, $t/L = 1$, AND $Q_t = 4$ WATTS)

r	Run #	$\bar{V}_{ch}$ (m/s)	Re_L	T_c (°C)	T_∞ (°C)	(T_c-T_∞) (°C)	Q_k (Watt)	Q_k/Q_t x 100	Q_r (Watt)	Q_r/Q_t x 100	Q_L (Watt)	Q_L/Q_t x 100	Q_c (Watt)	h (Watt/m^2°C)	Nu_L
	1	1.86	3133	46.6	22.3	24.3	0.220	5.5	0.031	0.78	0.251	6.3	3.749	47.9	47.5
1	2	5.00	8422	34.8	22.3	12.5	0.113	2.8	0.015	0.38	0.128	3.2	3.872	96.4	95.5
	3	7.58	12768	31.8	22.1	9.7	0.088	2.2	0.012	0.29	0.100	2.5	3.900	124.6	123.5
	4	10.07	16962	30.5	22.2	8.3	0.075	1.9	0.010	0.25	0.085	2.1	3.915	146.2	144.9
	5	1.92	3234	47.2	22.3	24.9	0.226	5.6	0.033	0.81	0.258	6.5	3.742	46.5	46.1
2	6	4.98	8388	36.9	22.2	14.7	0.133	3.3	0.018	0.45	0.151	3.8	3.849	81.2	80.5
	7	7.46	12566	33.9	22.6	11.3	0.102	2.5	0.014	0.34	0.116	2.9	3.884	106.8	105.8
	8	10.07	16962	31.9	22.5	9.4	0.085	2.1	0.011	0.28	0.096	2.4	3.904	128.7	127.5
	9	1.92	3234	46.5	21.5	25.0	0.226	5.7	0.032	0.80	0.258	6.5	3.742	46.4	46.0
3	10	5.00	8422	36.0	22.4	13.6	0.123	3.1	0.017	0.42	0.140	3.5	3.860	88.0	87.2
	11	7.51	12650	32.9	22.3	10.6	0.096	2.4	0.013	0.32	0.109	2.7	3.891	113.5	112.5
	12	10.03	16895	31.4	22.3	9.1	0.082	2.0	0.011	0.27	0.093	2.3	3.907	133.8	132.6
	13	1.92	3234	47.0	21.2	25.9	0.234	5.9	0.033	0.83	0.267	6.7	3.733	44.7	44.3
4	14	5.01	8439	36.7	22.0	14.7	0.133	3.3	0.018	0.45	0.151	3.8	3.849	81.2	80.5
	15	7.63	12852	33.7	22.6	11.1	0.100	2.5	0.014	0.34	0.114	2.8	3.886	108.5	107.5
	16	10.03	16895	31.3	21.8	9.5	0.086	2.2	0.011	0.28	0.098	2.4	3.902	126.8	125.7
	17	1.92	3234	47.2	21.2	26.0	0.236	5.9	0.034	0.84	0.269	6.7	3.731	44.4	44.0
5	18	5.01	8439	36.5	22.6	13.9	0.126	3.2	0.017	0.43	0.143	3.6	3.857	86.0	85.2
	19	7.55	12717	33.6	22.2	11.4	0.103	2.6	0.014	0.35	0.117	2.9	3.883	105.6	104.7
	20	10.09	16996	31.1	21.4	9.7	0.087	2.2	0.012	0.29	0.099	2.5	3.901	125.3	124.2
	21	1.92	3234	46.8	22.0	24.8	0.224	5.6	0.032	0.80	0.256	6.4	3.744	46.8	46.4
8	22	10.09	16996	31.7	22.4	9.3	0.084	2.1	0.011	0.28	0.095	2.4	3.905	130.6	129.4

TABLE IV (continued)

COLLECTED HEAT TRANSFER DATA WITH DIFFERENT VELOCITIES AND HEATED COMPONENT ROW NUMBERS (CASE: $D/t = 2.25$, $S/L = 1$, $t/L = 1$, AND $Q_t = 4$ WATTS)

r	Run #	$\bar{V}_{ch}$ (m/s)	Re_L	T_c (°C)	T_∞ (°C)	(T_c-T_∞) (°C)	Q_k (Watt)	Q_k/Q_t x 100	Q_r (Watt)	Q_r/Q_t x 100	Q_L (Watt)	Q_L/Q_t x 100	Q_c (Watt)	h (Watt/m^2°C)	Nu_L
	1	1.80	3032	48.1	21.8	26.3	0.238	6.0	0.034	0.85	0.272	6.8	3.728	43.9	43.5
1	2	5.03	8473	36.6	22.7	14.0	0.126	3.2	0.017	0.43	0.144	3.6	3.856	85.6	84.8
	3	7.56	12734	33.1	22.1	11.0	0.099	2.5	0.013	0.33	0.133	2.8	3.887	109.9	108.9
	4	10.04	16911	31.5	22.3	9.1	.083	2.1	0.011	0.27	0.094	2.3	3.906	132.5	131.3
	5	1.80	3032	50.2	22.0	28.2	0.225	6.4	0.037	0.93	0.292	7.3	3.708	40.8	40.4
2	6	5.03	8473	38.5	22.5	16.0	0.145	3.6	0.020	0.50	0.165	4.1	3.835	74.1	73.4
	7	7.56	12734	34.9	22.2	12.7	0.115	2.9	0.016	0.39	0.131	3.3	3.869	94.2	93.4
	8	10.00	16844	33.2	22.7	10.5	0.095	2.4	0.013	0.32	0.107	2.7	3.893	115.3	114.3
	9	1.80	3032	51.2	22.5	28.7	0.259	6.5	0.038	0.95	0.297	7.4	3.703	40.0	39.6
3	10	5.03	8473	38.7	22.4	16.3	0.148	3.7	0.020	0.51	0.168	4.2	3.832	72.9	72.2
	11	7.56	12734	34.4	21.8	12.6	0.114	2.9	0.015	0.38	0.129	3.2	3.871	95.2	94.3
	12	10.04	16911	33.0	22.4	10.6	0.096	2.4	0.013	0.32	0.109	2.7	3.891	113.8	112.8
	13	1.80	3032	52.7	21.8	30.9	0.280	7.0	0.041	1.03	0.321	8.0	3.679	36.9	36.6
5	14	5.03	8473	39.0	22.4	16.6	0.151	3.8	0.021	0.52	0.171	4.3	3.829	71.3	70.7
	15	7.56	12734	35.0	21.8	13.2	0.119	3.0	0.016	0.40	0.135	3.4	3.865	90.8	90.0
	16	10.04	16911	32.7	21.2	11.5	0.104	2.6	0.014	0.34	0.118	2.9	3.882	104.7	103.8
	17	1.80	3032	52.9	22.1	30.8	0.279	7.0	0.041	1.03	0.320	8.0	3.680	37.0	36.7
7	18	5.03	8473	39.2	22.0	17.2	0.155	3.9	0.021	0.53	0.177	4.4	3.823	69.0	68.4
	19	7.56	12734	35.7	22.3	13.4	0.122	3.0	0.016	0.41	0.138	3.4	3.862	89.1	88.3
	20	10.04	16911	33.4	21.7	11.8	0.106	2.7	0.014	0.35	0.121	3.0	3.879	102.3	101.4
	21	1.80	3032	52.4	22.7	29.7	0.269	6.7	0.040	0.99	0.308	7.7	3.692	38.6	38.3
8	22	5.03	8473	39.7	22.7	17.1	0.154	3.9	0.021	0.53	0.176	4.4	3.824	69.5	68.9
	23	7.56	12734	35.1	22.0	13.1	0.119	3.0	0.016	0.40	0.135	3.4	3.865	91.5	90.7
	24	10.04	16911	33.6	22.3	11.4	0.102	2.6	0.014	0.34	0.116	2.9	3.884	106.1	105.1

TABLE IV (continued)

COLLECTED HEAT TRANSFER DATA WITH DIFFERENT VELOCITIES AND HEATED COMPONENT ROW NUMBERS (CASE: D/t = 3, S/L = 1, t/L = 1, AND Q_t = 4 WATTS)

r	Run #	$\bar{V}_{ch}$ (m/s)	Re_L	T_c (°C)	T_∞ (°C)	(T_c-T_∞) (°C)	Q_k (Watt)	Q_k/Q_t x 100	Q_r (Watt)	Q_r/Q_t x 100	Q_L (Watt)	Q_L/Q_t x 100	Q_c (Watt)	h (Watt/m^2°C)	Nu_L
	1	2.11	3554	46.8	21.9	24.9	0.225	5.6	0.032	0.80	0.258	6.4	3.742	46.6	45.7
1	2	5.03	8473	37.3	21.9	15.4	0.139	3.5	0.019	0.47	0.158	4.0	3.842	77.3	76.6
	3	7.57	12751	34.1	22.2	11.9	0.108	2.7	0.014	0.36	0.122	3.1	3.878	101.0	100.1
	4	10.17	17130	32.7	21.9	10.8	0.098	2.4	0.013	0.32	0.111	2.8	3.889	111.6	110.6
	5	2.11	3554	49.8	22.0	27.8	0.252	6.3	0.037	0.91	0.288	7.2	3.712	41.3	40.9
2	6	4.97	8371	38.7	21.7	17.0	0.154	3.8	0.021	0.53	0.175	4.4	3.825	69.8	69.2
	7	7.57	12751	35.7	22.0	13.7	0.124	3.1	0.017	0.42	0.141	3.5	3.859	87.3	86.5
	8	10.17	17130	34.3	22.5	11.8	0.106	2.7	0.014	0.36	0.121	3.0	3.879	102.4	101.5
	9	2.11	3554	50.3	22.3	28.0	0.254	6.3	0.037	0.92	0.290	7.3	3.710	41.0	40.6
3	10	4.97	8371	39.4	22.0	17.3	0.157	3.9	0.022	0.54	0.179	4.5	3.821	68.3	67.7
	11	7.57	12751	35.7	21.9	13.7	0.124	3.1	0.017	0.42	0.141	3.5	3.859	87.1	86.3
	12	10.17	17130	33.5	21.9	11.6	0.105	2.6	0.014	0.35	0.118	3.0	3.882	104.6	103.7
	13	2.06	3470	51.9	22.3	29.6	0.270	6.7	0.039	0.98	0.309	7.7	3.691	38.6	38.3
4	14	4.97	8371	40.8	22.3	18.5	0.168	4.2	0.023	0.58	0.191	4.8	3.809	63.7	63.1
	15	7.57	12751	36.7	22.0	14.7	0.133	3.3	0.018	0.45	0.151	3.8	3.849	81.2	80.5
	16	10.17	17130	34.6	22.3	12.3	0.111	2.8	0.015	0.37	0.126	3.1	3.874	98.0	97.1
	17	2.06	3470	52.4	22.0	30.4	0.275	6.9	0.040	1.01	0.316	7.9	3.684	37.6	37.3
5	18	4.97	8371	41.0	22.3	18.7	0.169	4.2	0.024	0.59	0.193	4.8	3.807	63.1	62.5
	19	7.57	12751	36.8	22.1	14.7	0.133	3.3	0.018	0.45	0.151	3.8	3.849	81.2	80.5
	20	10.17	17130	34.4	21.7	12.7	0.115	2.9	0.015	0.39	0.130	3.3	3.870	94.5	93.7
	21	2.06	3470	52.5	22.2	30.3	0.274	6.9	0.041	1.01	0.315	7.9	3.685	37.7	37.4
6	22	4.97	8371	40.9	22.0	19.0	0.172	4.3	0.024	0.59	0.195	4.9	3.805	62.2	61.6
	23	7.57	12751	36.8	22.1	14.7	0.133	3.3	0.018	0.45	0.151	3.8	3.849	81.2	80.5
	24	10.17	17130	34.1	21.8	12.2	0.111	2.8	0.015	0.37	0.126	3.1	3.874	98.1	97.2
7	25	4.97	8371	40.9	22.3	18.7	0.169	4.2	0.024	0.59	0.193	4.8	3.807	63.2	62.6

component at a fixed place (row 2, column 3), and varying the input power and Reynolds number. This was necessary, as shown in Table III, in order to show that the percentage of conduction and radiation losses were independent of input power to the heated component. Table IV shows collected heat transfer data for different ranges of experimental parameters in the order shown in Table II. Estimates of uncertainty using single-sample experiments method (Kline and McClintock, 1953) show the uncertainty in the calculated heat transfer coefficients in Table IV varied from a minimum of 2.1% to a maximum of 8.6% (see Appendix C). However, for intermediate values of velocities (3 to 5 m/sec) and higher input power to the component, which is more closer to the electronic cooling application, this value is always less than 6%. Repeatability was checked on the heat transfer measurements. Repeated measurements using the same heated components, the same input power, the same instruments, the same geometric parameters and approach Reynolds numbers, on successive days showed ±1% scatter. More details about these two tables are presented in the next section.

4.1.1 Ranges of Conduction and Radiation Losses

With a quick look at Tables III and IV, the following conclusions for conduction and radiation can be obtained:

1. Percentage of conduction loss (Qk/Qt x 100) decreases with increasing Reynolds number. From Table III, percentage of conduction loss seems to be independent of input power to the component. However, Table IV indicates that the loss due to conduction is a weak function of heated component row number (r), channel height (D/t), and component height (t/L). In general, it is true that for a fixed t/L (fixed component surface area exposed to convection and radiation, i.e Ac), percentage of conduction loss is inversely proportional to the convective heat transfer coefficient or Nusselt number. This fact can be

analytically proven using Equations (3.4) through (3.7), ignoring negligible loss due to radiation. On the other hand, with increasing t/L and holding other effective parameters constant, Ac increases and causes more heat dissipation due to convection and radiation, and less losses due to conduction heat transfer. The range of conduction loss in Table IV is from a minimum of 1.9% to a maximum of 9.8%, depending strongly on the flow approach velocity and the component height, and weakly on the heated component row number and the channel height. More detailed discussion and analysis for influence of effective parameters on conduction loss are presented in Section 4.2.

2. Percentage of radiation loss (Qr/Qt x 100) is independent of input power to the heated component, and decreases with increasing the approach Reynolds number. As shown in Table IV, radiation loss is a weak function of the heated component row number, component height, and channel height. In this table radiation losses range from a minimum of 0.23% to a maximum of 1.01%, depending strongly on the approach Reynolds number, and weakly on the heated component row number and other geometric parameters.
3. Percentage of total heat loss due to conduction and radiation (QL/Qt x 100) decreases with an increase in the approach mean air velocity, and is independent of the input power to the heated component. As shown in Table IV, range of total loss due to the conduction and radiation is from a minimum of 2.1% to a maximum of 10.7%, depending strongly on the flow approach velocity and the component height, and weakly on the heated component row number and the channel height.

The above conclusions for the ranges of conduction and radiation losses match the results of other investigators (see for example Arvizu, 1981; Buller and Kilburn, 1981; Wirtz and Dykshoorn, 1984).

4.1.2 Heat Transfer Correlations

An interactive curve fitting computer program called RQ was used for developing the heat transfer correlations. This program was originally developed by Professor J. P. Chandler, Computer Science Department, Oklahoma State University. The program was modified by D. R. Maiello and L. M. Tam under supervision of Professor A. J. Ghajar, School of Mechanical and Aerospace Engineering, OSU, for interactive use on personal computers and heat transfer applications. The general form of equation used in this program for correlating the collected heat transfer data was:

$$Nu_L = A_1(Re_L)^{A2}(R)^{A3}(H/t)^{A4}(t/L)^{A5}$$

where Nu_L is the Nusselt number of the heated component collected during each experiment, Re_L, R, H/t and t/L are the corresponding tested experimental parameters. R is a new parameter for the effect of row number, and defined as the ratio of the distance between the leading edge of the component at the first row (beginning of the test section) and the center of the heated component, to the total length of the test section:

$$R = \frac{(r-1)(1+S/L)+\frac{1}{2}}{(N-1)(1+S/L)+1} \qquad (4.1)$$

where N is the total number of rows in the test section, and the equation holds for $r < N$. Once the collected data for Nu_L and the corresponding tested experimental parameters are entered in the RQ program, the coefficients A_1, A_2, A_3, A_4, and A_5 are determined by the computer program.

Based on the first set of collected heat transfer data, a primary heat transfer correlation was developed using RQ curve fitting computer program and the simplest form of the equation as: $Nu_L = A_1(Re_L)^{A2}$. This primary correlation was then modified gradually by entering new tested experimental parameters tabulated in Table II during the course of the experiments. This modification procedure helped in observing the influence of the involved effective parameters which will be discussed in detail in the next section.

After the final modification, the following single general correlation was developed for the range of tested experimental parameters presented in Table II:

$$Nu_L = 0.280\,(Re_L)^{0.61}\,(R)^{-0.05}\,(H/t)^{-0.11}\,(t/L)^{-0.22} \qquad (4.2)$$

where

$$2880 \le Re_L \le 17130, \quad 0.5 \le H/t \le 2.0, \quad 0.5 \le t/L \le 1.0, \quad S/L = 1.0$$

and R is given by Eq. (4.1).

This correlation is applicable to any single heated component in an in-line array of similar rectangular components having different geometries, heated component row numbers, and approach velocities within the above range. Equation (4.2) does not accurately predict the heat transfer coefficient of the heated component at the last row (row 8), because of the exposure of the component's back surface at this row. For this reason the collected data for heated component at row 8 were not used for developing the general correlation. Figure 4.2 conveys the deviations between the experimental heat transfer data (Nu_{exp}) collected in Table IV and the predicted results (Nu_{cal}) presented by Eq. (4.2). The correlation gives a representation of the experimental data to within +10.5% and -12.6%. In the development of the correlation, a total of one hundred and twenty nine experimental data points were used. The absolute average deviation between the results predicted by Eq. (4.2) and the experimental data is 3.7%. About thirty one percent of the data (40 data points) were predicted with more than ±5% deviation and sixty nine percent of the data (89 data points) with less than ±5% deviation (see Fig. 4.2). As shown in the figure, only three data points (2.3% of the data) were predicted with more than ±10% deviation and one hundred and twenty six data points (97.7% of the data) with less than ±10% deviation.

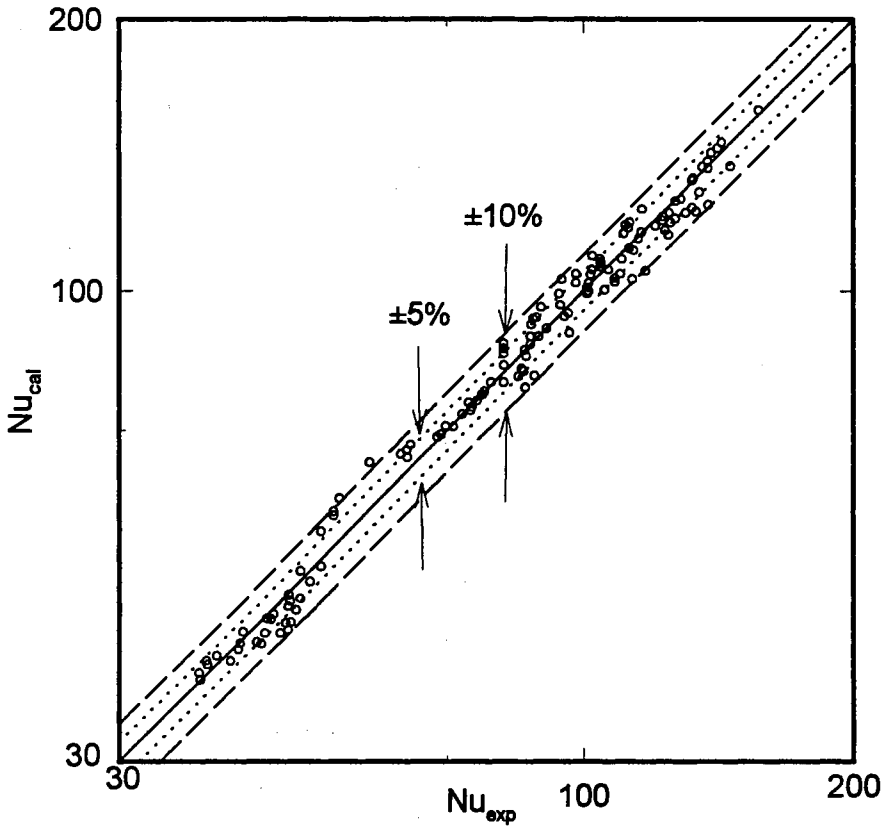

Figure 4.2. Comparison of Predicted Heat Transfer Results with the Experimental Data Tabulated in Table IV

More detailed discussion about the effects of Reynolds number and the other tested geometric parameters on the heat transfer of the heated component, along with the appropriate figures and comparisons with the results of previous investigators are presented in the next section.

4.1.3 Discussion and Comparisons of the Results

The experimental results of this study have shown that the heat transfer behavior of a single heated component in a regular in-line array of rectangular components can be described by a correlation of the form $Nu_L = C_g Re_L^n$. For different geometric tested parameters shown in Table II, the exponent value, n, was found to be constant and equal to 0.61. The geometric coefficient, C_g, varies with different array densities and is only a function of geometric parameters (r, D/t, and t/L). Figures 4.3 through 4.9 show the effects of Reynolds number and other tested geometric parameters on the heat transfer of the heated component. A detailed discussion of these figures and comparison of the experimental results of this study with the results of other investigators are presented next.

Evidence of $h \sim Re^n$ dependence has been observed for many years in forced convective electronic cooling. It is evident that larger Reynolds numbers mean more air movement around the heated component which causes more heat dissipation. Figures 4.3 through 4.7 show the effects of Reynolds number on the heated component Nusselt number for different array geometries. These figures convey the fact that there is a regular increase in the value of heat transfer coefficient, corresponding to a regular increase in the value of Reynolds number.

In addition to the Reynolds number, there are three other important geometric tested parameters which affect the value of heat transfer coefficient of a single heated rectangular component, placed in an in-line array of rectangular components. These parameters are:

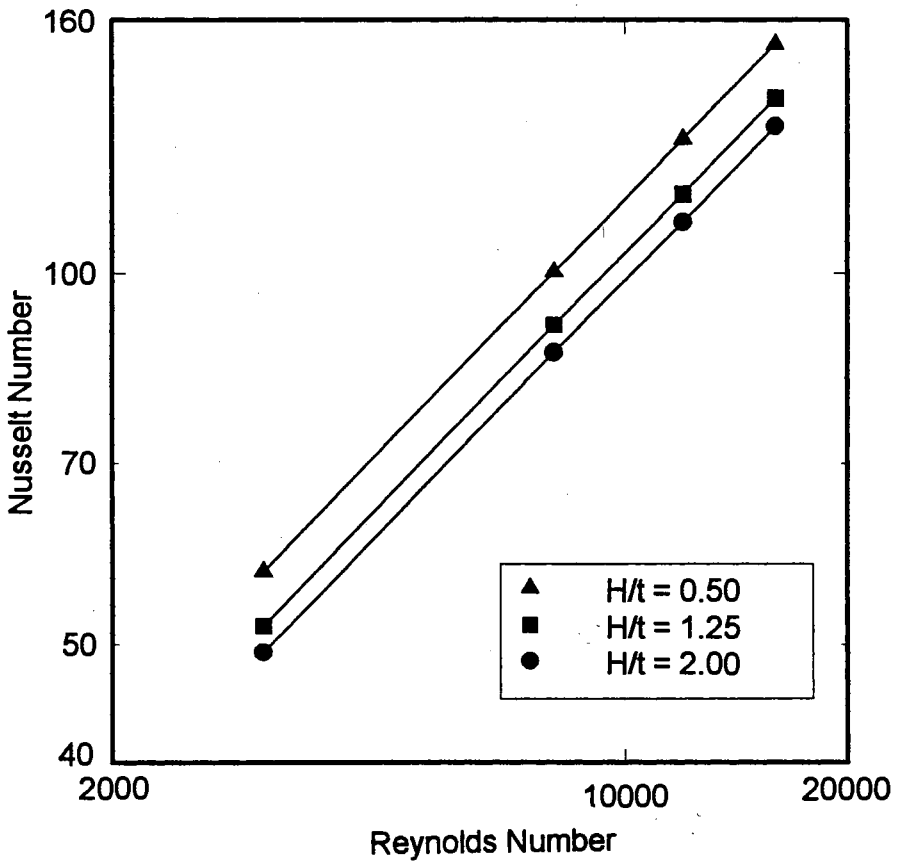

Figure 4.3. Heated Component Nusselt Number as a Function of Reynolds Number for the First Row and t/L = 0.5, Parametric in H/t

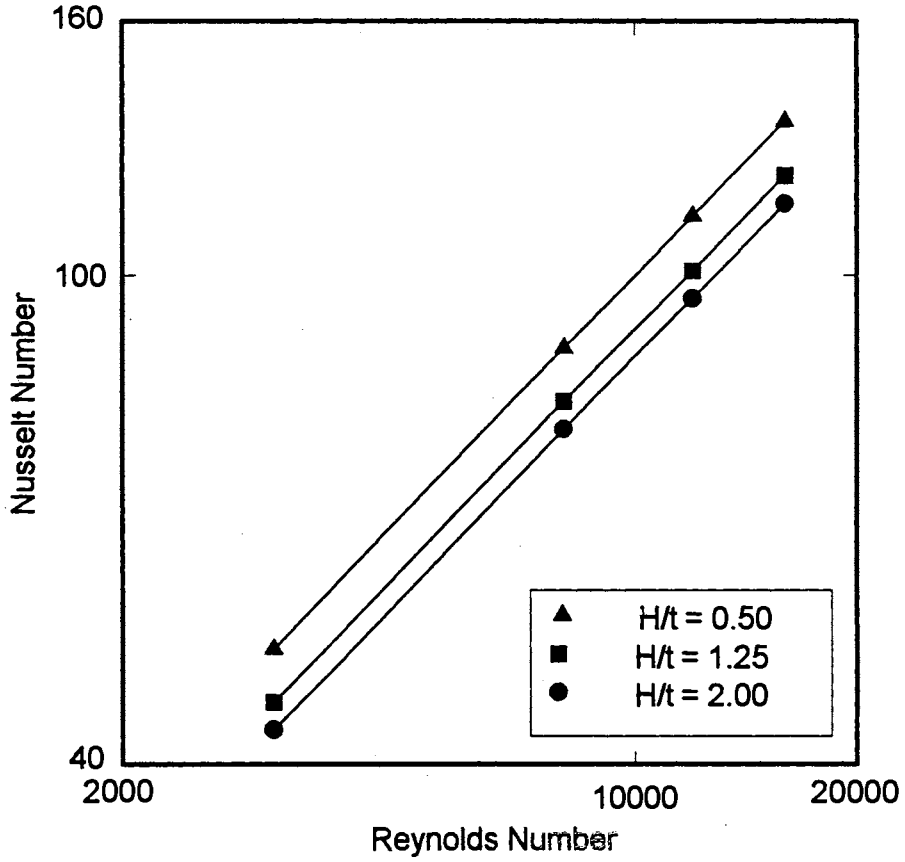

Figure 4.4. Fully Developed Heated Component Nusselt Number (Fifth Row) as a Function of Reynolds Number for t/L = 0.5, Parametric in H/t

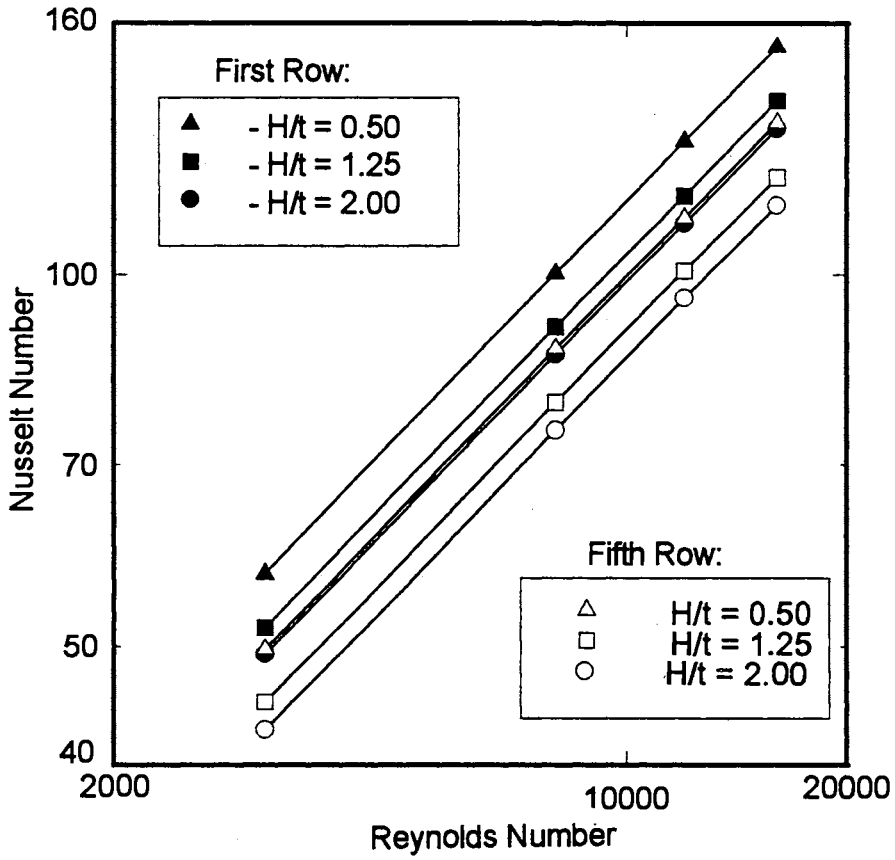

Figure 4.5. Comparison of Heated Component Nusselt Number at the First Row with Fully Developed Nusselt Number (Fifth Row), as a Function of Reynolds Number for t/L = 0.5, Parametric in H/t

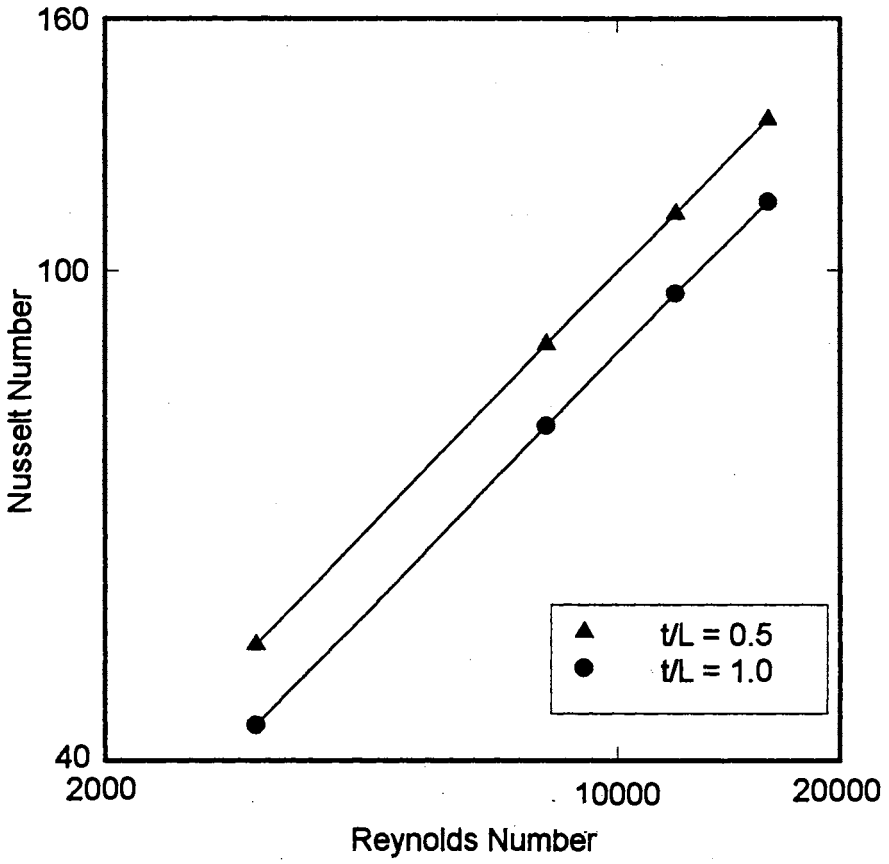

Figure 4.6. Fully Developed Heated Component Nusselt Number (Fifth Row) as a Function of Reynolds Number for H/t = 0.50, Parametric in t/L

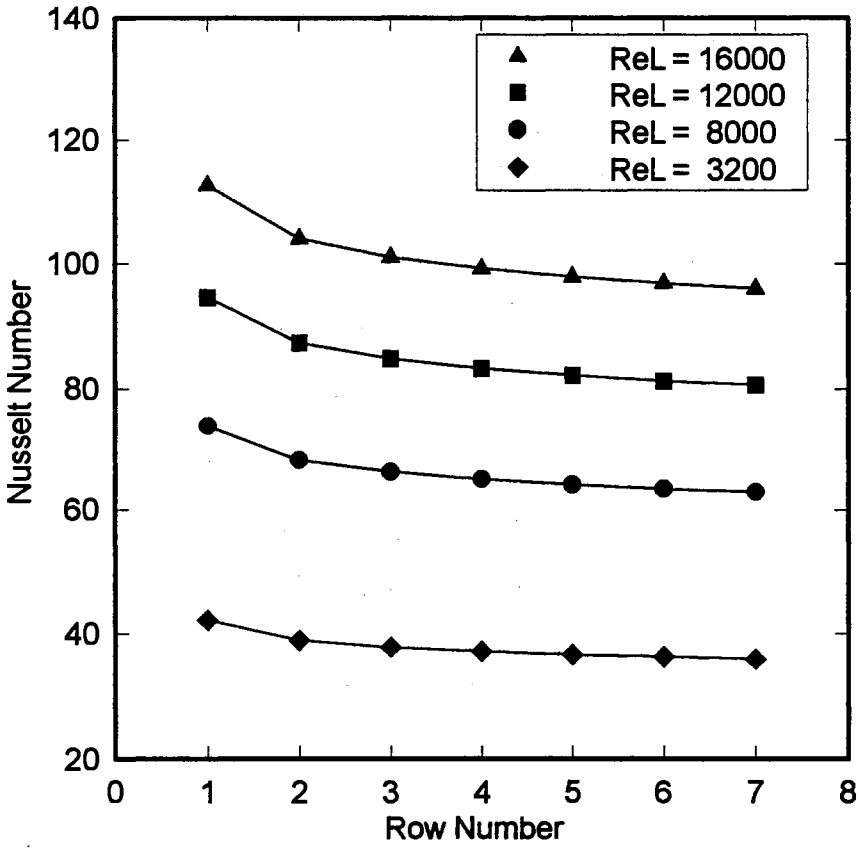

Figure 4.7. Heated Component Nusselt Number as a Function of Row Number for Different Reynolds Numbers for the Case of H/t = 2, and t/L = 1

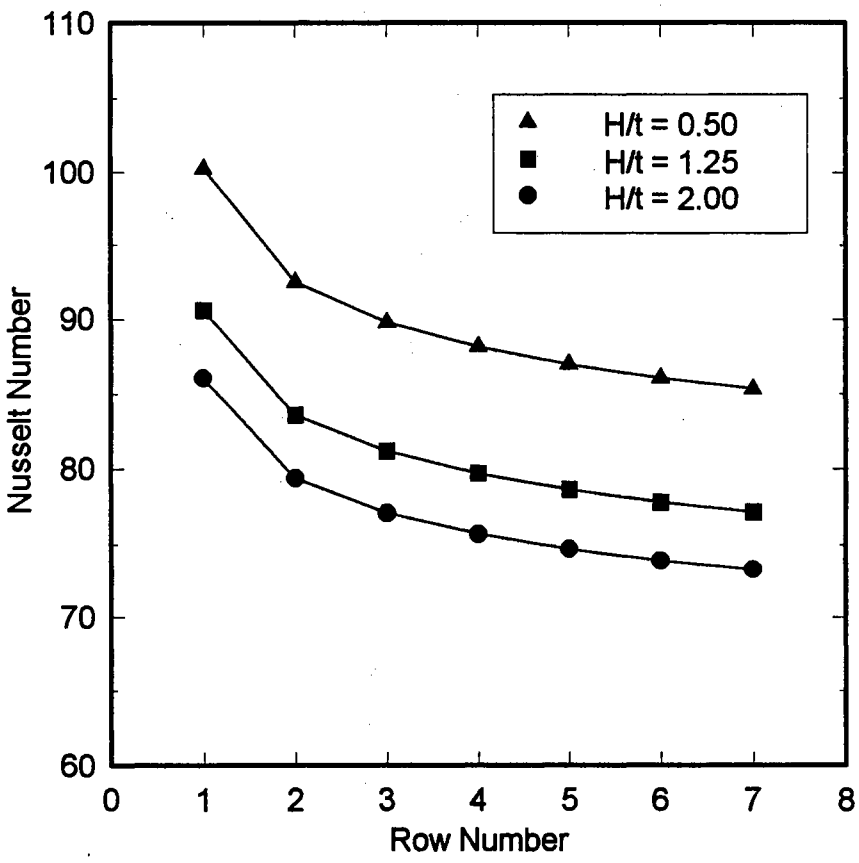

Figure 4.8. Heated Component Nusselt Number as a Function of Row Number for t/L = 0.5 and Re_L = 8000, Parametric in H/t

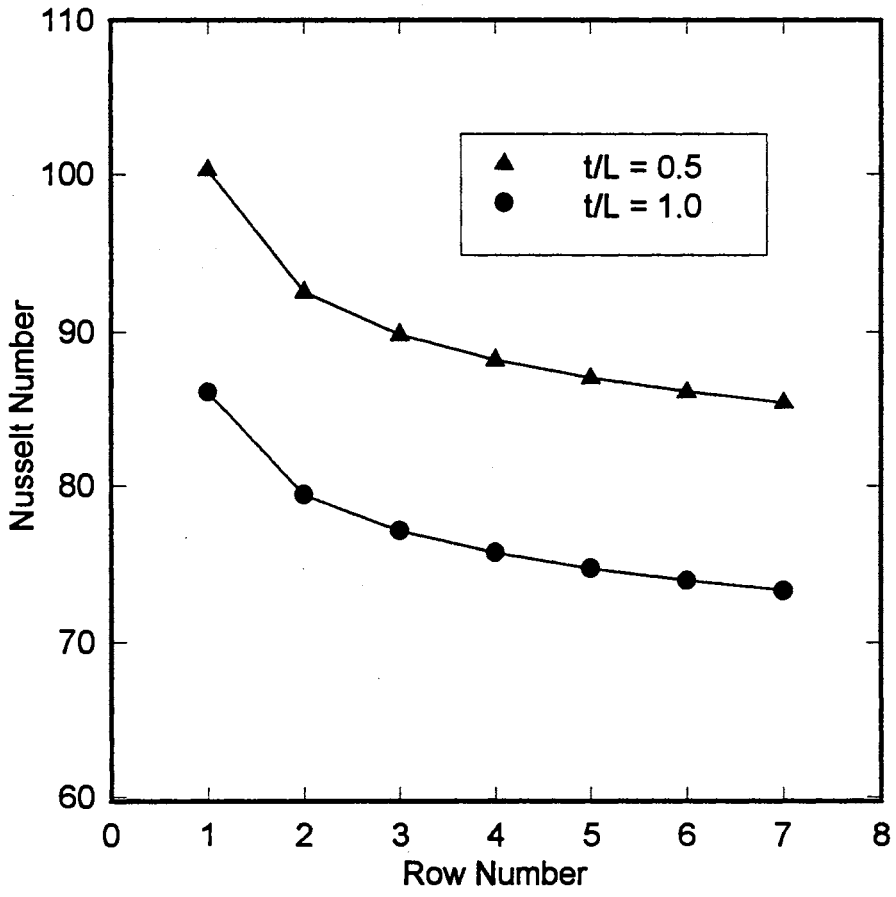

Figure 4.9. Heated Component Nusselt Number as a Function of Row Number for H/t = 0.50 and Re_L = 8000, Parametric in t/L

1. r(heated component row number) - When examining the results, it must be kept in mind that there will be irregularities due to the exposure of the first and last rows. The first row will lose a disproportionate amount of heat through its front surface (the surface facing the air flow) due to the increased air velocity over the surface. Similarly, the eighth (last) row will lose more heat through its back surface than other components due to its exposure. These losses will affect the remaining sides.

   The results of this study show that components along the first row experience heat transfer which is 8 to 17% greater than those of succeeding rows. Figure 4.7 shows the variation of Nusselt numbers as a function of row number for different Reynolds numbers. These data correspond to the dimensionless component height of t/L = 1.0 and the dimensionless channel height of H/t = 2.00. It should be noted that five additional figures for different combinations of H/t and t/L showing the same trend as Figure 4.7 could have also been presented. As shown in Figure 4.7, for a fixed Reynolds number, the heat transfer of the heated component at the first row is 8.4%, 11.6%, 13.7%, 15.2%, 16.4%, and 17.5% greater than the heat transfer of the second to seventh row, respectively. It is clear from this figure that as the row number increases, the difference between h for the two neighboring rows becomes smaller. This difference reduces to 1.0% for the fifth and sixth rows. Therefore, the Nusselt number of the heated component at the fifth and subsequent rows is defined as the "periodically fully-developed" Nusselt number. Sparrow et al. (1982) found that it took five rows of components for the heat transfer to be truly "periodically fully-developed", while Wirtz and Dykshoorn (1984) reported three rows. However, they did not clearly define the meaning of "periodically fully-developed" heat transfer i.e., what is the

percentage difference between the Nusselt number at the row they attained fully-developed, and its first downstream row.

The variation of the heated component Nusselt number as a function of Reynolds number for the first row and fifth row (fully-developed) for different channel heights are shown in Figs. 4.3 and 4.4. The data plotted in these two figures correspond to a fixed component height (t/L = 0.5). It can be seen from these two figures that the heat transfer for the first row (see Fig. 4.3) is 15.2% greater than the corresponding fully-developed Nusselt number shown in Fig. 4.4. This finding is in agreement with the experimental heat transfer results reported in the literature (Arvizu, 1981; Sparrow et al, 1982; Wirtz and Dykshoorn, 1984; etc.) which indicates that the components along the first row of an in-line arrangement experience heat transfer which is 10 to 20% greater than that of succeeding rows. In order to clearly compare the heated component Nusselt numbers shown in Figs. 4.3 and 4.4, these two figures were combined into a single figure as Fig. 4.5.

2. H/t (dimensionless channel height) - Figures 4.3 and 4.4 depict the heated component Nusselt number versus Reynolds number for the entrance and fully-developed regions, respectively, for t/L = 0.5 and a range of channel heights, while Fig. 4.8 shows the Nusselt number of the heated component as a function of row number for t/L = 0.5 and Re_L = 8,000, for different channel heights. From these figures it can be seen that for a fixed Reynold number, as the channel height is increased, the heat transfer decreases both for the entrance and fully developed regions. Since a fixed Re_L represents a fixed mean velocity, as H/t increases (see Fig. 3.4), the portion of air flow over the component is decreased, thus reducing the heat transfer. This expression justifies the assumption of other investigators, that the heat transfer of a single

component depends on the velocity around it. For example, see Moffat, et al. (1985).

During the process of development of the general heat transfer correlation presented by Eq. (4.2), it was found that the exponent, -0.11, was the best fit for the heat transfer data tabulated in Table IV. This negative exponent shows that the heat transfer is more sensitive to the values of H/t less than unity. This fact can be seen more clearly in Fig. 4.8, that for a fixed row number, the heated component Nusselt number for H/t = 0.5 is 10.5% more than what is depicted for H/t = 1.25, and this percentage reduces to 5.3% for comparable Nusselt number of a fixed row for H/t = 1.25 and 2. This reveals that as H/t increases, while holding the other parameters constant, the Nusselt number becomes less sensitive, and at some critical value of H/t, the change in heat transfer is negligible. In other words, if the heated component Nusselt is plotted versus H/t while holding the other parameters constant, the slope would be steeper for H/t < 1 than the slope for H/t >1.

3. t/L (dimensionless component height) - Figure 4.6 shows the fully-developed Nusselt number as a function of Reynolds number for H/t = 0.5, and two different tested dimensionless component heights (t/L), while Fig. 4.9 plots the heated component Nusselt number versus row number for H/t = 0.5, Re_L = 8,000, and two different tested t/L. It can be seen from these two figures that as t/L is increased, the heat transfer decreases. This fact can be justified by defining a new-parameter called Surface Blocking Ratio (SBR). SBR is the ratio of the surface of the component blocked by its neighboring components in the direction of air flow, to the total surface of the heated component exposed to convection. This ratio is t/L/(1 + 4t/L) for the first and last rows, and 2t/L/(1 + 4t/L) for the components in the other rows. Comparing this new defined parameter (SBR) for the two cases of t/L = 0.5 and 1.0, it reveals that

for the case of t/L = 0.5, less fractional surface of the heated component is blocked by its neighboring components in the direction of the air flow, which in turn causes more fractional surface exposed to convection, thus more convective heat transfer. It was found that the exponent, -0.22, was the best fit for the heat transfer data tabulated in Table IV. This negative exponent shows that the heated component Nusselt number is more sensitive to the values of t/L < 1. It is believed that if more experiments are performed for a range of t/L > 1, some critical value for t/L can be found that for t/L greater than this critical value, the variation of Nusselt number of the heated component will be negligible. However, in electronic cooling t/L is less than unity for most practical cases.

In the above analysis, the effects of Reynolds number and each single geometric parameter (r, H/t, and t/L) on the heated component Nusselt number were discussed separately in detail. However, during the analysis, it was found that effects of these geometric parameters on the convective heat transfer of the heated component are not independent of each other. In the following, two important conclusions which were made for the effect of geometric parameters on each other and their combined effects on the Nusselt number of a heated component are presented.

1. In the general correlation presented by Eq. (4.2), the exponents for H/t and t/L were -0.11 and -0.22, respectively. As mentioned earlier, these two exponents were the best fit for the experimental heat transfer data tabulated in Table IV. These two exponents are interrelated and for some set of values for H/t and t/L, they cancel each other and Eq. (4.2) could be simplified. For example, for the case of H/t = 2 and t/L = 0.5, Eq. (4.2) predicts the same result as the case of H/t = 0.5 and t/L = 1. This fact can be seen from the raw data for these two cases in Table IV, which for most of the data points, the difference is less than 3% which is within our experimental error. In general Eq. (4.2) predicts the

same heat transfer result for the case of H/t = x, t/L = 1/X, and the case of H/t = 1/x, t/L = 1, while holding the other parameters constant, since $(H/t)^{-.11}$ $(t/L)^{-.22}$ in both cases simplifies to $(1/X)^{-.11}$. It is believed that if more experiments were performed for larger ranges of H/t and t/L, these two geometric parameters could be combined in order to introduce a new single geometric parameter which represents effects of both H/t and t/L on the Nusselt number of the heated component.

2. During the process of development of the general correlation, two separate subcorrelations were found for the cases of t/L = 0.5 and 1, having the same exponent for Re_L and H/t, but different exponents for the effect of row number (R). These two exponents were -0.04 and -0.06 for t/L = 0.5 and 1, respectively. This difference in exponent of R means that for the case of t/L = 0.5, the heat transfer coefficient is less dependent on the row number and takes less number of rows of components for the heat transfer to reach fully-developed region than the case of t/L = 1. This fact can be seen from the data tabulated in Table IV, which shows that for the case of t/L = 0.5, the average difference of the heated component Nusselt number between the first and second rows is 6.5% while this value is 10% for the case of t/L = 1. It is believed that this difference is partially due to the effect of Surface Blocking Ratio (SBR) which was discussed earlier. If more experiments for the larger range of t/L were performed, it might be possible to find a relation between the exponent of R and SBR. However, for this study the above two mentioned subcorrelations were combined to represent a single general correlation presented by Eq. (4.2). The error due to this combination is within our experimental error, and does not affect the final result.

Thus far the heat transfer results, the general heat transfer correlation based on the results along with a detailed discussion of the effects of Reynolds number and other tested

geometric parameters on the heat transfer coefficient have been presented. In the following, the collected heat transfer results and the general heat transfer correlation presented by Eq. (4.2) will be compared with the results of other investigators reported in the open literature. These comparisons will show that the results of this study are in good agreement with the results of other investigators. This in turn verifies the good performance of our experimental setup and the accuracy of the general heat transfer correlation given by Eq. (4.2).

In electronic cooling, the component heat fluxes are roughly limited to what is suggested by Kraus and Bar-Cohen (1983), as shown in Fig. 4.10. This figure agrees well with the heat transfer data summarized in Tables III and IV, as well as the general heat transfer correlation presented by Eq. (4.2).

The experimental heat transfer results of other investigators are compared with our results in Table V. This table only shows ranges of their tested parameters which were comparable with the results of this study, and their corresponding correlations for both heat transfer coefficient (h) and Nusselt number (Nu_L). In these correlations, h is in Watt/m^2°C. More details about the experimenters experimental setups and their involved parameters can be found in Table I. Reynolds and Nusselt numbers of these studies were based on different characteristic lengths, such as the channel height (D), component height (t), component length (L), etc. To be able to compare the results of these investigators with our heat transfer results, their reported correlations were carefully converted on the basis of our characteristic length (L=2.54 cm). Furthermore, Eq. (4.2) was simplified according to their "Ranges of Comparable tested experimental parameters" and entered in the "Simplified Form of Eq. (4.2)" Column in Table V. It appears from this table that the range of the exponent on Reynolds number varies from 0.54 to 0.72. The heat transfer results reported in the open literature indicate the bounds on the exponent, n, to be 0.5 to 0.8. This range on the exponent applies to geometries of both small scale and large scale sizes and from

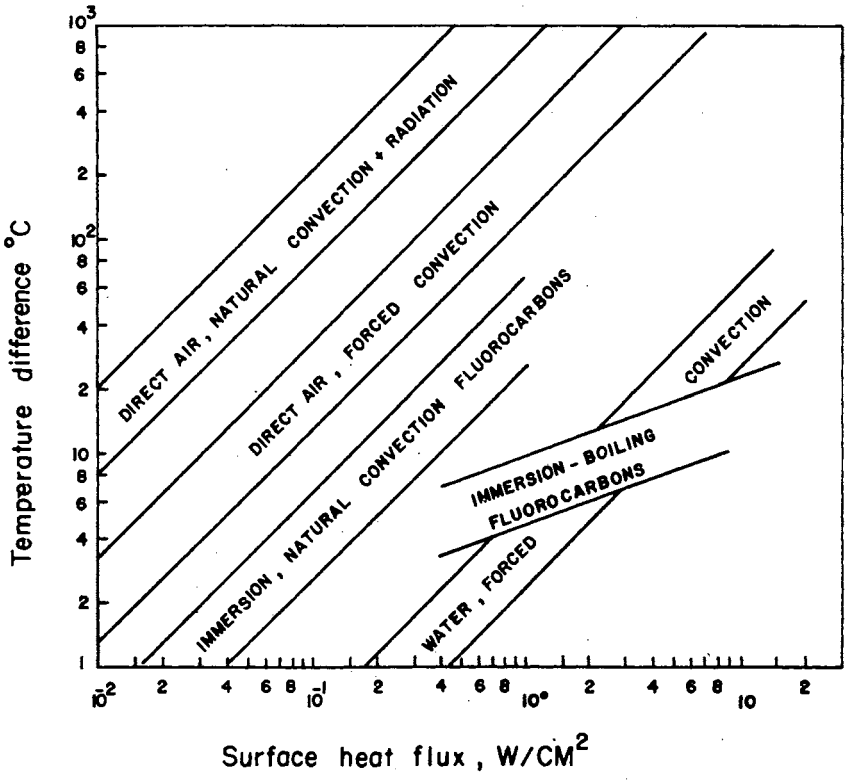

Figure 4.10. Temperature Differences Attainable as a Function of Heat Flux for Various Heat Transfer Modes and Various Coolant Fluids (Kraus and Bar-Cohen, 1983)

TABLE V

COMPARISON OF HEAT TRANSFER RESULTS WITH THE RESULTS OF OTHER INVESTIGATORS

Study	Case	Ranges of comparable tested experimental parameters					Suggested Correlation	Simplified Form of Eq. (4.2)	%Difference	
		Re_L	t/L	H/t	r	S/L			Lowest Re_L	Highest Re_L
Sparrow et. al 1982	Dense flatpacks	1905 to 6667	0.375	1.67	5	0.25	$h = 0.095 (Re_L)^{0.72}$ $Nu_L = 0.094 (Re_L)^{0.72}$	$h = 0.340 (Re_L)^{0.61}$ $Nu_L = 0.337 (Re_L)^{0.61}$	+35.9%	+26.4
Arvizu, 1981	Sparse cubes	2419 to 14514	1	3.62	5	1	$h = 0.441 (Re_L)^{0.55}$ $Nu_L = 0.437 (Re_L)^{0.55}$	$h = 0.252 (Re_L)^{0.61}$ $Nu_L = 0.250 (Re_L)^{0.61}$	-9.6%	+1.5%
Buller and Kilburn, 1981	Single flatpack	806 to 4032	0.196	5.31	1	N/A	$h = 0.667 (Re_L)^{0.54}$ $Nu_L = 0.661 (Re_L)^{0.54}$	$h = 0.398 (Re_L)^{0.61}$ $Nu_L = 0.394 (Re_L)^{0.61}$	-4.9%	+6.3%
Wirtz and Dykshoorn 1985	Sparse flatpack	1613 to 16127	0.25	3.6	3	1	$h = 0.358 (Re_L)^{0.6}$ $Nu_L = 0.355 (Re_L)^{0.6}$	$h = 0.353 (Re_L)^{0.61}$ $Nu_L = 0.350 (Re_L)^{0.61}$	+5.8%	+7.9%
Lehmann and Wirtz, 1985	Sparse flatpack	2680 to 12000	0.25	1.25	11	1	$h = 0.268 (Re_L)^{0.65}$ $Nu_L = 0.266 (Re_L)^{0.65}$	$h = 0.377 (Re_L)^{0.61}$ $Nu_L = 0.374 (Re_L)^{0.61}$	+2.5%	-3.5%

single roughness element to arrays of roughness elements. The upper limit on the exponent, i.e., n = 0.8 is precisely the value reported for turbulent flow through smooth parallel planes (see Kays and Crawford, 1980). It is not too surprising that, as the regular in-line array of rectangular components become very dense, i.e., S/L << 1, the Reynolds number exponent increases to approach the behavior of turbulent flow between smooth parallel planes, i.e., $h \sim Re^{0.8}$.

The heat transfer results of this study were compared with the results of Sparrow, et al. (1982) in Fig. 4.11 for their reported ranges of tested experimental parameters. We measured higher heat transfer rates and a slightly weaker dependence on the flow rate. This is not surprising since Sparrow, et al's. arrays were densely packed (S/L = 0.25) whereas ours should be considered sparse with S/L = 1. It is well known that the large cavities between arrays, such as in the present experiments, will interact more strongly with the channel flow above the array, producing a higher turbulence level in the flow. This higher freestream turbulence will produce higher heat transfer coefficients and a weaker dependence on the Reynolds number. Furthermore, they used naphthalene sublimation technique, and found the value of Nusselt number by invoking the mass-transfer analogy. This may be the second reason for their heat transfer results being lower than ours.

Figure 4.12 shows comparison of the heat transfer results of the present study with the work of Arvizu (1981) for his reported ranges of tested experimental parameters tabulated in Table V. This figure shows that his results are in good agreement and within a few percent of our results for t/L = 1, H/t = 3.62, S/L = 1, and r = 5. This slight difference may be due to the fact that the general heat transfer correlation presented by Eq. (4.2) is limited to the ranges of $0.5 \leq H/t \leq 2.0$ and $2880 \leq Re_L \leq 17130$, while Arvizu's H/t and Re_L were 3.6 and 2419, respectively.

Buller and Killurn (1981) used a single heated flatpack with attached pins. Our heat transfer results were compared with their results as shown in Fig. 4.13, for their reported ranges of tested experimental parameters. This figure shows that the Buller and Killurn's

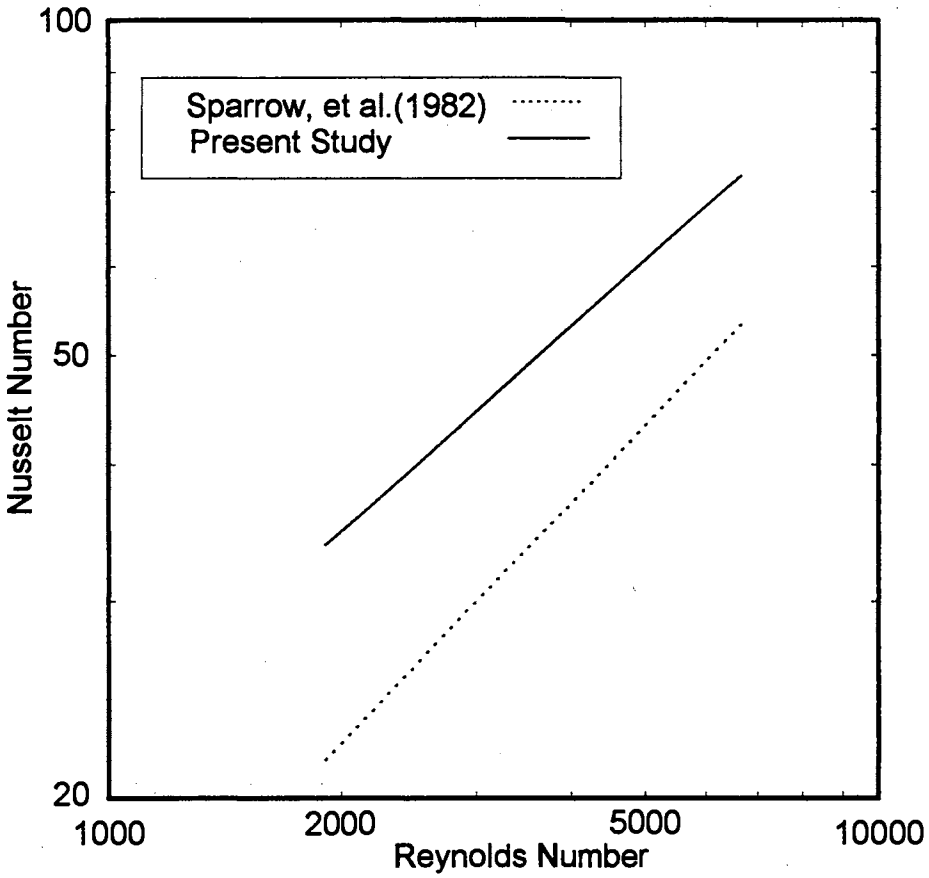

Figure 4.11. Variation of the Nusselt Number with Respect to the Reynolds Number-Comparison with Sparrow et al. (1982)

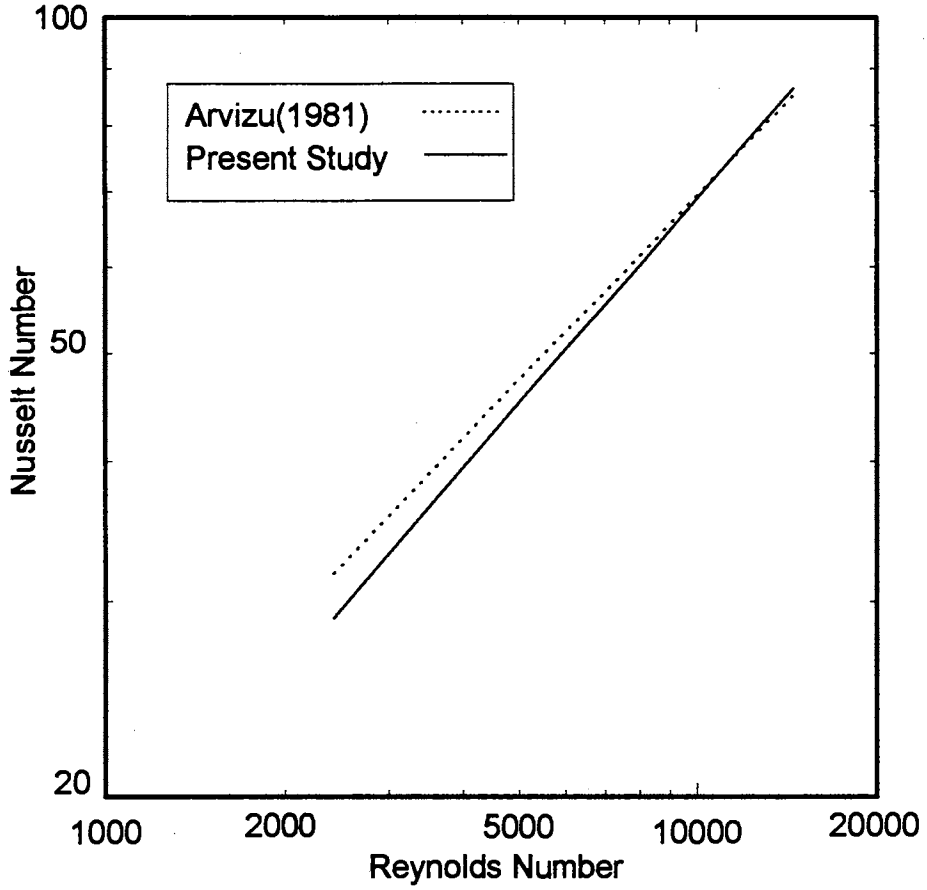

Figure 4.12. Variation of the Nusselt Number with Respect to the Reynolds Number-Comparison with Arvizu (1981)

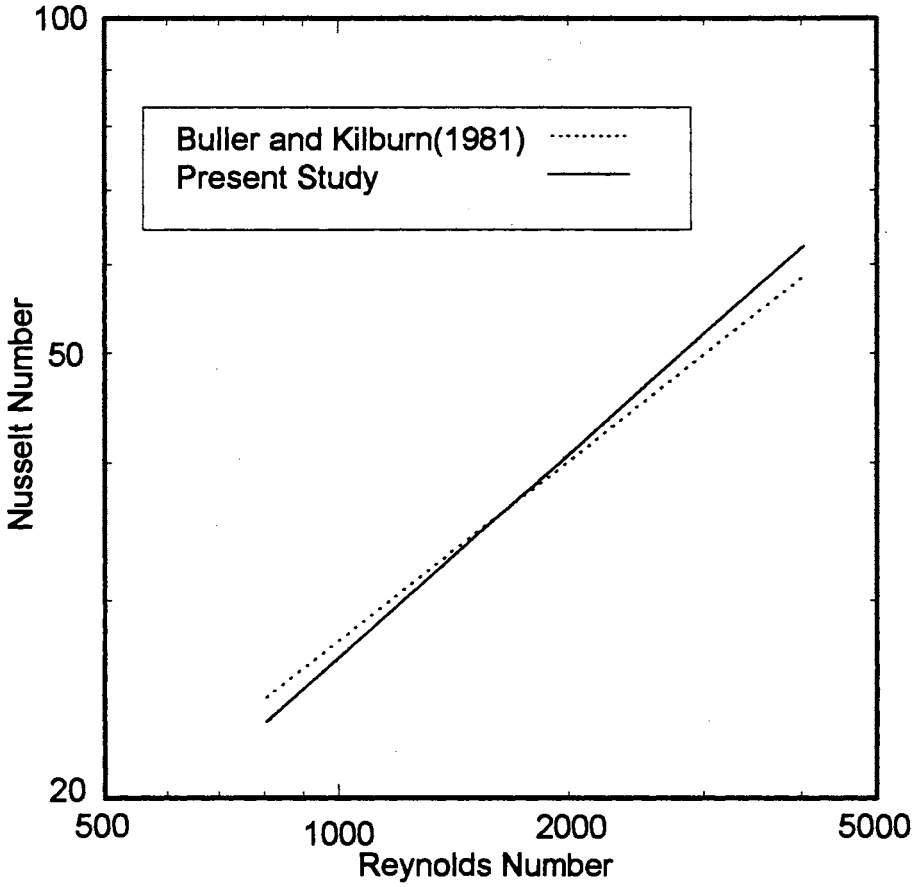

Figure 4.13. Variation of the Nusselt Number with Respect to the Reynolds Number-Comparison with Buller and Kilburn (1981)

heat transfer results are within a few percent of our results with a slightly weaker dependence on the Reynolds number. However, since they used single heated flatpack with attached pins, their heat transfer results should be higher than the results of this study. On the other hand, their ranges of tested experimental parameters were different from ranges for which Eq. (4.2) is suggested. These two factors may offset each other. Since detailed dimensions of the attached pins and other parameters were not reported, further discussion about this comparison is impossible. Their characteristic length (l) was defined as:

$$l = \left[\left(\frac{A_f}{C_f} \right) \left(\frac{A_t}{L} \right) \right]^{1/2}$$

where A_f was component frontal surface area, C_f was circumference of component frontal surface, A_t was component total wetted area, and L was component length. Their Reynolds number was based on l and the velocity component was evaluated through the constricted test area. Correlating the heat transfer coefficient to this Reynolds number would automatically include partial effects of t/L, S/L, and H/t.

Figure 4.14 shows comparison of our heat transfer results with the work of Wirtz and Dykshoorn (1985) for their reported ranges of tested experimental parameters tabulated in Table V. This figure shows that their results are a few percent higher than ours, while the exponent of their Reynolds number is almost the same as ours. Although this percent difference is not considerable (5.8% to 7.9% as tabulated in Table V), it may be partially due to the use of Eq. (4.2) outside of its recommended range for t/L and H/t.

The present experimental heat transfer results were compared with the work of Lehmann and Wirtz (1985) as shown in Fig. 4.15, for their ranges of tested experimental parameters. This figure shows the good agreement of our results with theirs, while our results are slightly less sensitive to the Reynolds number. As seen in Table V, their results are within +2.5% to -3.5% of our results for the range of Reynolds numbers from 2680 to

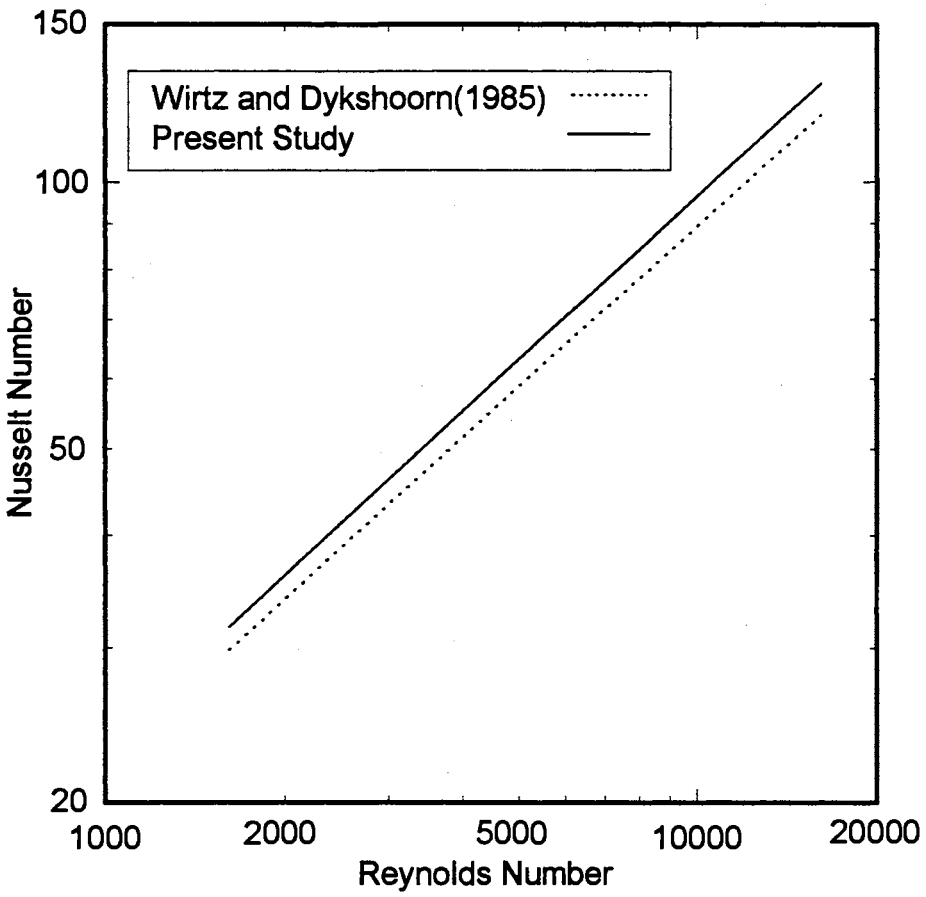

Figure 4.14. Variation of the Nusselt Number with Respect to the Reynolds Number-Comparison with Wirtz and Dykshoorn (1985)

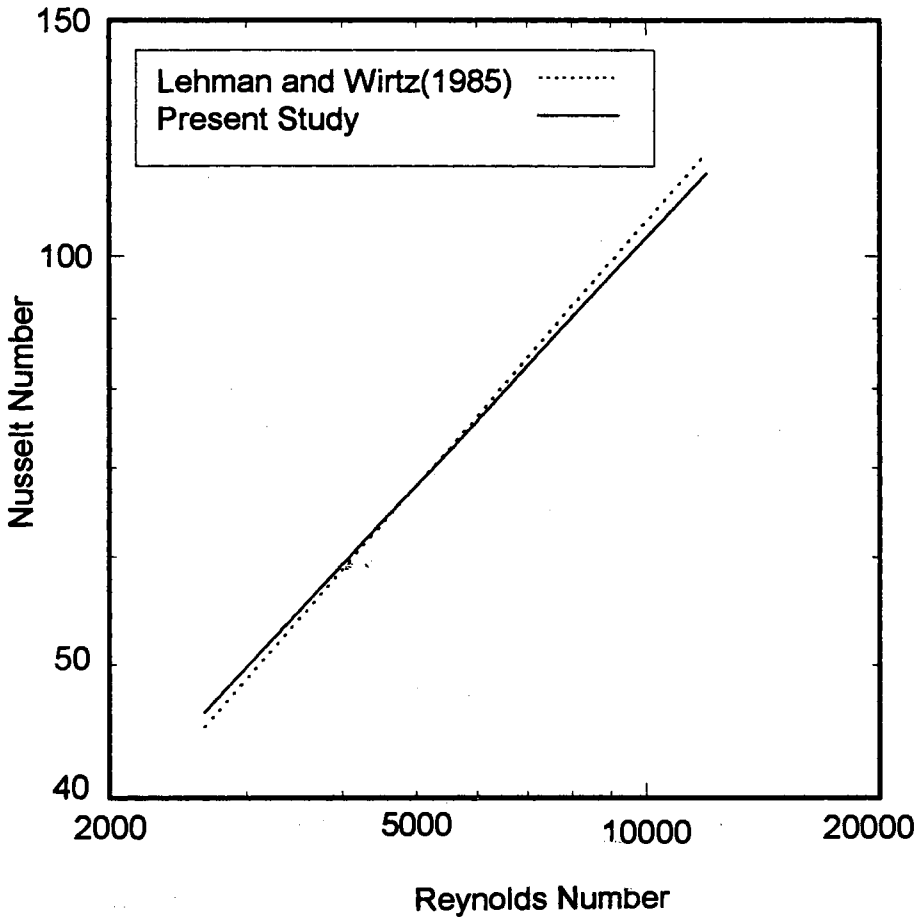

Figure 4.15. Variation of the Nusselt Number with Respect to the Reynolds Number-Comparison with Lehmann and Wirtz (1985)

12000. Their ranges of tested experimental parameters were closer to ours (see Table II) than the work of other investigators tabulated in Table V.

Table V along with Figs. 4.12, 4.14, and 4.15 show that our experimental heat transfer results are in good agreement with the results of other investigators having the same dimensionless component spacing, i.e., S/L = 1. As seen in Table V, the percent difference between our results and their work is within +7.9% to -9.6%. This agreement reveals the accuracy of our general heat transfer correlation presented by Eq. (4.2), and verifies the good performance of our experimental setup.

4.2 Effects of Conduction and Board Conductivity on Heat Transfer Coefficient

Accurate prediction of component operating temperature depends on the heat transfer coefficient, which, in turn, is influenced by board conductivity and conduction heat transfer to the board. An experimental investigation was conducted to examine the effects of board conductivity and conduction losses of the heated component, on the convective heat transfer coefficient and consequently on the operating temperature of the heated component. Experiments were performed with different board materials, each one arranged with an in-line array of four rows by three columns of highly polished aluminum cubes, in a horizontal rectangular wind tunnel. Each component was individually powered with a resistor element. Data were collected for different ranges of channel average air velocities, component placement, as well as input power to the heated component. The heat flux and temperature were measured on all sides of the middle heated components in each row of the array by a direct measurement heat flow sensor equipped with a thermocouple. The heat transfer by conduction through the back of the board was measured directly beneath and surrounding the heated components. The experimental results indicate that the conduction heat transfer through the board and consequently the thermal behavior of the system were strongly affected by the Reynolds number of the flow,

placement of the component, and the board conductivity. For the experiments conducted in this study, heat transfer by conduction accounted for 1 to 91% of the total power applied to the component and the component temperature varied from 25 to 132°C.

A brief review of this investigation will be presented in this section. More information about this study can be found in Arabzadeh et al. (1993).

4.2.1 Previous Studies

An extensive review of the literature pertinent to convective cooling of electronic boards has been compiled by Incropera (1988). Most previous investigators did not adequately address the problem of conduction, since they tried to minimize the conduction effects by using insulating materials. This kept the problem simple and tractable, and made it possible to do well controlled experiments and simple analyses. There has been no systematic attempt to study and incorporate the effect of conduction in a circuit board. Because the majority of the heat is ultimately removed through convection, the effects of conduction are often overlooked. If conductive board is used, the problem will be more complex, since the conduction coupling between the components and the board can represent a significant thermal path for dissipation of heat. This was one of the main purposes of this study.

Wagner (1984) used an epoxy-glass board with different thick layers of copper in order to investigate effects of board conductivity on temperature distribution on the back of the board. A heat source of low power (1.0 W) was placed at the center of the board to represent a silicon integrated chip. Conduction losses were calculated rather than being directly measured. The experiments were performed with only one low velocity (1.0 m/s), therefore effects of different Reynolds numbers were not investigated.

Ortega and Moffat (1986) used a board consisting of balsa wood epoxied onto plexiglass in an effort to minimize conduction heat transfer through the board. Ortega and

Kabir (1991) also used balsa wood mounted on plexiglass for the board. Kang et al. (1990) tried to limit conduction by using three masonite boards separated by 6 mm air gaps. Roeller et al. (1990) used a thermally symmetric channel design on a cardboard board to minimize conduction heat transfer through the board.

Studies using convection in fluids other than air generally had insignificant amounts of conduction. For example, Garimella and Eibeck (1990) estimated that the conduction for their setup cooled by forced convection in water accounted for less than 1% of the total heat dissipated.

Some investigators have attempted to account for conduction by numerical or analytical methods. Laderman et al. (1987) conducted a numerical study of several conduction heat transfer schemes and examined the sensitivity of the component junction and board temperatures to certain parameters which affect conduction.

Some studies effectively correlated models with experimental results. Fitch (1990) proposed a model using a thermal resistance network which included the effects of conduction. Experiments were also conducted and the temperatures were found to correlate well with the proposed model.

Ortega and Kabir (1991) developed an analytical model for the conduction from a component to the board. This model suggested that conduction varies linearly with a modified driving temperature. This model correlated well with experimental conduction flux data calculated from thermocouple temperatures within the component.

Manno and Azar (1991) examined the effect of intercomponent coupling which included conduction and radiation. All the correlations which were examined underpredicted component temperatures. They note that this is potentially due to underestimating conduction losses. They conclude that the non-convective mechanisms, which consist mainly of conduction, account for approximately 34% of the total heat dissipated from a powered component.

Some experimenters have examined the influence of conduction on certain quantities. Azar and Moffat (1991) studied the effect of conduction on the heat transfer coefficient. Only the convective flux from the top of the component was experimentally measured using a heat flux sensor. They assumed that the convective heat flux from the other surfaces of the component (front, back, and sides) is equal to the heat flux from the top (as will be shown, not a particularly good assumption). Employing this assumption, from an energy balance, they determined the total conductive heat flux of the component. Conduction percentages between 24.3% and 60.0% were reported.

While there has been considerable interest in the effect of conduction, there has not been a systematic attempt to experimentally determine the influence of varying Reynolds number, component placement, and board conductivity on the conduction heat transfer to the board, component temperature, and heat transfer coefficient. One of the objectives of this study was to conduct such experiments in a horizontal rectangular wind tunnel using polished aluminum cubes to simulate electronic components.

4.2.2 Experimental Setup and Procedures

The same experimental apparatus which was explained in detail in Chapter III, was used to perform conduction experiments. Only the test board on which the array of components were mounted changed, and positioned in the test section in place of the plexiglass ceiling (see Fig. 4.16). The test board occupied the entire width and length of the test section and rested flush with the ceiling of the rest of the channel. Three boards of different materials were used. The materials were chosen in order to have a significant variation in thermal conductivity. The materials chosen were fiberglass (0.160 cm thick) with a thermal conductivity of 0.293 W/m-K, aluminum 2219 alloy (0.155 cm thick) with a thermal conductivity of 130 W/m-K, and balsa wood (0.645 cm thick) with a thermal conductivity of 0.07 W/m-K.

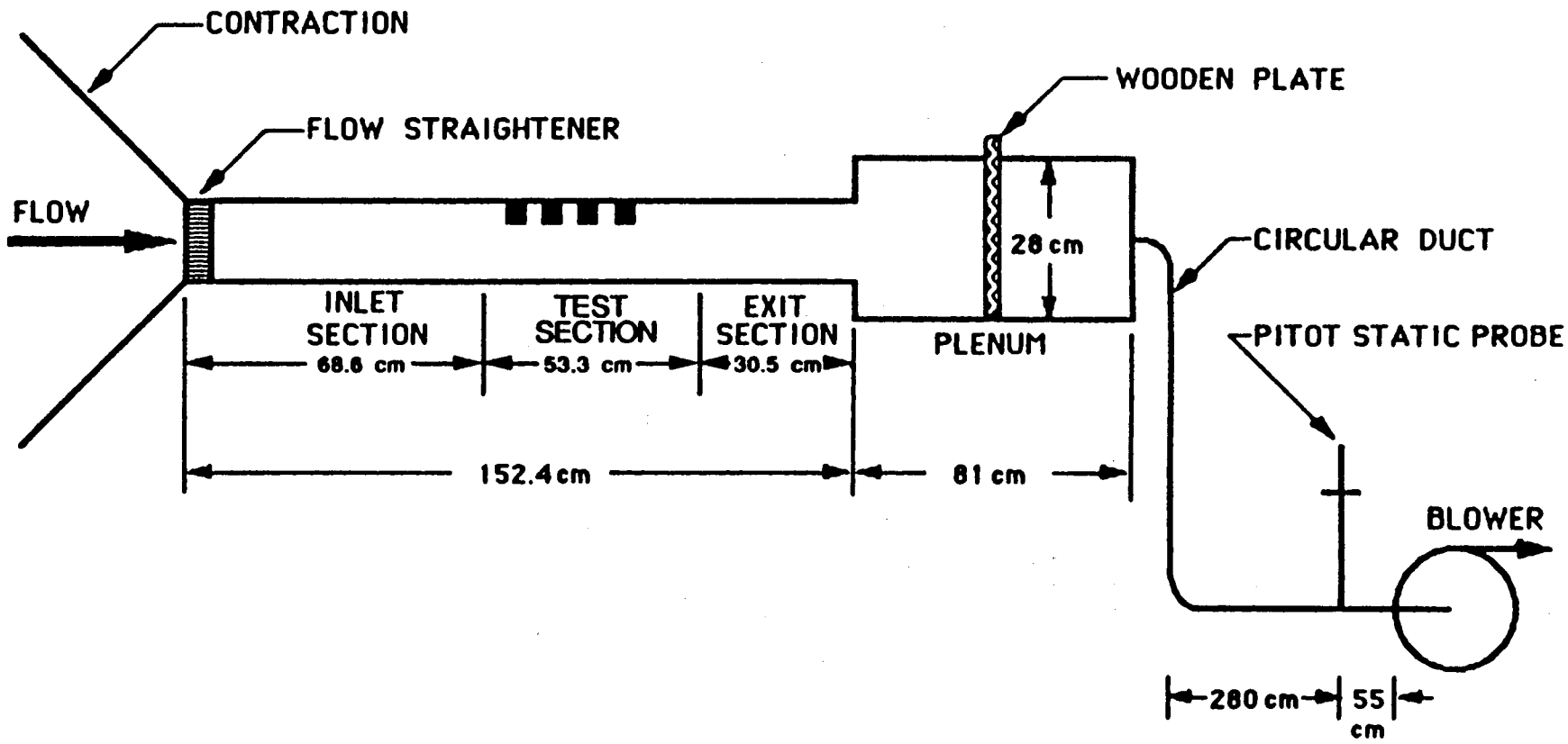

Figure 4.16. Schematic of Experimental Apparatus for Performing Conduction Experiments

The components were arranged in an array with four rows in the streamwise direction and three columns in the cross-stream direction (see Fig. 4.17). The dimensionless length ratios which define the geometrical characteristics of the array are:

$t/L = 1$; $S/L = 0.3$; $(H+t)/L = 3$

The difference between component height and channel height ($H = D - t = 2L$), is the characteristic length used for calculation of the Reynolds number. Components were oriented such that the lead wires through which current is supplied to the resistor emerge from the downstream side of the cube. These wires were secured against the board and followed the board to the end of the test section where they emerged from the air channel via holes sealed with putty.

Electronic chips were modeled by highly polished aluminum cubes (2.54 cm per side) with a thermal conductivity of 216.3 W/m-K. The components were heated using resistance heating. Each component was equipped with a 475 ohm ceramic resistor placed at the center of the component (see Fig. 4.18). The rest of the cavity in the back of the block was filled with Omegabond 101 thermally conductive epoxy.

The heat flux and temperature on all five exposed surfaces (inside the wind tunnel) and the back of the board (outside of the wind tunnel) for the middle heated components in each row of the array were measured by a direct measurement heat flow sensor equipped with a built-in T-type thermocouple. These sensors were 1.27 cm square, and placed exactly at the center of heated component surface using Omegatherm 201 a very high thermally conductive silicon paste. It is important to note that these sensors measure radiation as well as convection losses. For monitoring the heat flux on all sides of the components, the voltage signals from the heat flux sensors were passed through a high gain DC amplifier. The output of the amplifier was then connected to a personal computer equipped with an A/D board. Estimates of uncertainty of the measured heat fluxes with negligible thermal contact resistance between the module and the board was determined to be ±5% (Kline and McClintock, 1953). This estimate of uncertainty increased to about

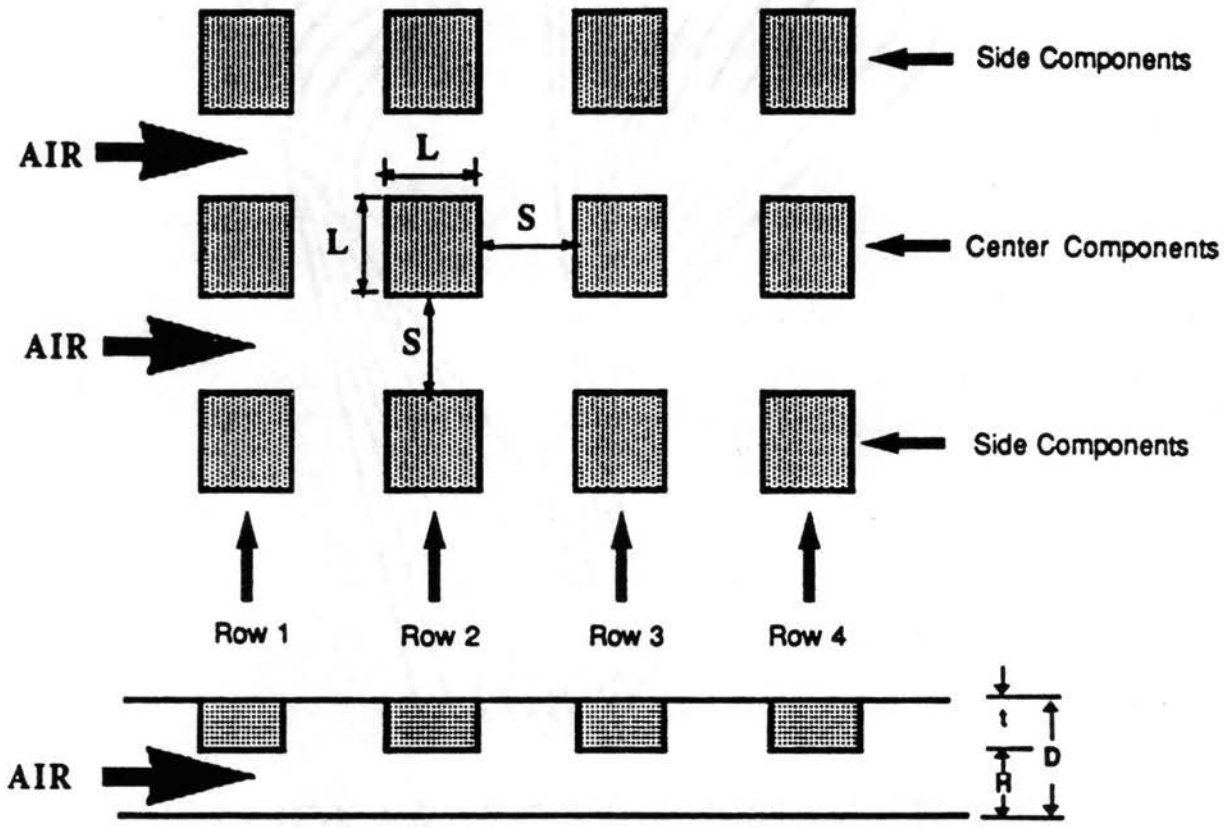

Figure 4.17. Top and Side Views of the In-line Arrangement of the Components in the Test Section (used for conduction experiments)

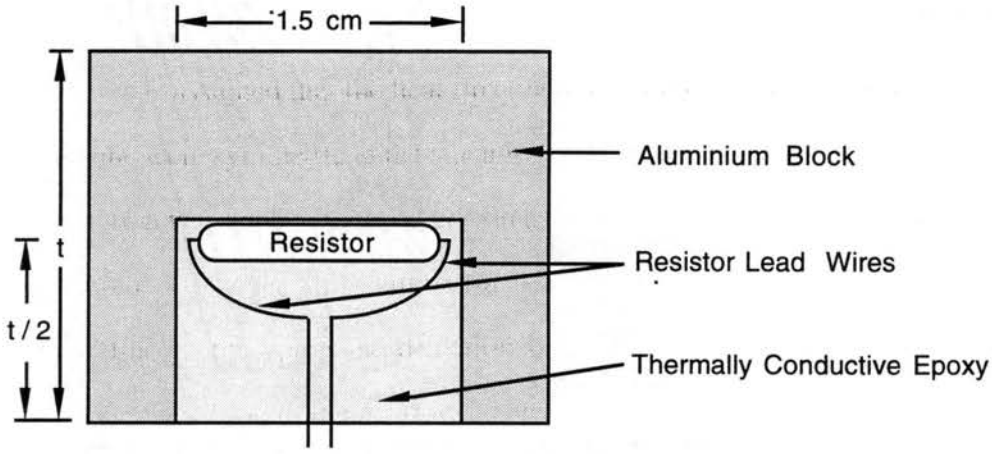

Figure 4.18. Detail of a Heated Component Used for Conduction Experiments

16% when an estimate of the maximum possible value of thermal contact resistance for the experiments was included in the uncertainty analysis.

4.2.3 Results and Discussion

Table VI summarizes the experiments that were conducted to show the influence of varying Reynolds number, component placement, and board conductivity on conduction heat transfer to the board, component temperature, and heat transfer coefficient. The data were collected for the middle heated components of an array of twelve components placed in four rows (stream-wise) and three columns. During the data collection, all of the center components were heated simultaneously. Table VI summarizes the three different power distributions (referred to as cases) that were used for the experiments. This table gives a summary of the specific data taken for each case using each of the three boards. As indicated in Table VI, the Reynolds number based on the difference between component height and channel height (H), was either 3800 or varied from 1450 to 30400.

When examining the results, it must be kept in mind that there will be irregularities due to the exposure of the first and last rows. The first row will lose a disproportionate amount of heat through its front surface (the surface facing the air flow) due to the increased air velocity over that surface. Similarly, the fourth (last) row will lose more heat through its back surface than other components due to its exposure. These losses will affect the remaining sides.

Conduction heat flux for each of the heated components is directly measured beneath the component on the back of the board (outside of the wind tunnel), using a heat flux sensor. This value will be referred to as the "direct conduction". Direct conduction is not the total conduction heat transfer from the heated component. A large portion of the heat (depending on the board conductivity) will be dissipated by conduction from the surface of the board both inside and outside of the channel in all directions around the

TABLE VI

HEAT TRANSFER DATA COLLECTED FOR DIFFERENT BOARD MATERIALS AND LEVELS OF POWER SUPPLIED TO THE MIDDLE COMPONENTS

Case	Power Supplied (Watts)	Fiberglass Board	Aluminum Board	Balsa Wood Board
1	1	I,T,S,F,B,C,EB,L	I,T,S,F,B,C,EB,L	I,C
2	3	I,T,S,F,B,C,EB,Re	I,T,C	I,C
3	4.5	I,T,S,F,B,C,EB,L,Re	I,T,S,F,B,C,EB,L,Re	I,T,C,Re

I = inlet air temperature
T = flux and temperature for the top of the component
S = flux and temperature for the side of the component
F = flux and temperature for the front of the component
B = flux and temperature for the back of the component
C = flux and temperature for the bottom of the board
EB = an energy balance was performed
L = lateral conduction from the back of the board was measured
Re = flux and temperature for the bottom of the board was taken for eight Reynolds numbers ranging from 1450 to 30400

* Unless otherwise specified, all data was taken at a Reynolds number of 3800

bottom of the heated component. This will be referred to as the "lateral conduction". As mentioned before, the readings from heat flow sensors for the five exposed surfaces were the sum of convective and radiative heat fluxes. Subtracting this total convective and radiative heat transfer from the input power to the component, gives the "total conduction" heat transfer. Dividing the "direct conduction", and the "total conduction" by the input power to the heated component, gives the "direct conduction percentage", and the "total conduction percentage", respectively. The difference between the total and direct conduction is the lateral conduction. Efforts were made to account for the lateral conduction by direct measurements. In order to accomplish this, experiments were performed with a single heated component placed 91.5 cm from the entrance of the rectangular channel on two different boards, a 0.155 cm thick aluminum board, and a layer of 0.16 cm thick fiberglass board placed on a 1.27 cm thick commercial plexiglass. The back of the board (outside of the wind tunnel) was divided into uniform grids of the size 1.27 cm x 1.27 cm, same size as the heat flux sensors, up to a distance of 5L around the

component. Conduction heat flux and temperature of each individual grid was carefully measured by the heat flux sensors. Two different input power levels (1 and 4.5 W) and several different air velocities ranging from 2 to 12 m/s were used. These detailed measurements revealed that it was not possible to account for all of the lateral conduction, since part of the heat was dissipated by conduction from the inside part of the board around the component.

Figure 4.19(a) shows one of these grid systems used to measure the local conduction heat fluxes from the back of the aluminum board around the component in terms of mW, and temperature above T_∞ in °C, for a fixed 4.5 W input power to the component and 7.5 m/s channel average air velocity. The bottom of the heated component is highlighted in Fig. 4.19(a) by the thick lines. The top number shown inside of each grid is the local temperature above T_∞ in °C, while the bottom number is the local conduction heat flux in mW. It was assumed that the heat flux and temperature distributions about the component center-line were symmetric in the streamwise direction.

This assumption was applied to those grids that their heat flux and temperature were not directly measured. However, this symmetric assumption can not be made about the component center-line in the spanwise direction because of the thermal wake effect upstream of the component due to the air flow. The variations of temperature rise above T_∞ and the lateral conduction in the streamwise and spanwise directions given in Fig. 4.19(a) are depicted in two distinct 3-D plots in Figs. 4.19(b) and 4.19(c). Adding all of these local conduction heat fluxes gives 1.079 W. Measured convective and radiative heat fluxes from the exposed surfaces through the sensors were 0.161, 0.182, 0.173, 0.173, and 0.128 W from the top, front, left side, right side, and back of the component, respectively. Adding these values and subtracting from 4.5 W input power, gives 3.683 W which should be the total conduction loss. However, total measurement of the conduction loss from the back of the board up to 5L around the component (from Fig. 4.19(a)) was

0.78 5.26						1.00 5.42	1.00 5.42						0.89 6.59
						1.06 5.93	1.06 5.93						
						1.44 6.09	1.44 6.09						
						1.5 6.5	1.5 6.5						
						1.61 7.2	1.61 7.2						
						1.94 7.4	1.94 7.4					1.56 7.1	
		1.67 8.3	2.00 8.7	1.28 7.1	2.28 8.9	2.17 8.2	2.17 8.2	2.28 8.9	1.28 7.1	2.00 8.7	1.67 8.3		
		1.67 8.3	2.17 9.0	2.17 7.6	2.78 9.6	2.67 9.6	2.67 9.6	2.78 9.6	2.17 7.6	2.17 9.0	1.67 8.3		
		2.11 9.1	2.44 9.4	2.61 10.1	3.11 11.2	3.33 10.2	3.33 11.0	3.11 11.2	2.61 10.1	2.44 9.41	2.11 9.1		
		2.39 9.1	2.72 9.9	3.06 11.2	3.61 10.3	4.44 13.1	4.56 15.7	3.94 14.2	3.06 11.2	2.72 9.9	2.39 9.1		
1.67 6.1	1.94 6.1	2.22 7.0	2.67 6.9	3.06 7.6	3.78 8.7	**5.11** **13.2**	**6.00** **19.2**	4.72 14.3	3.61 10.7	2.94 9.4	2.50 8.4	2.00 7.4	1.83 7.3
1.67 6.1	1.94 6.1	2.22 7.0	2.67 6.9	3.06 7.6	3.78 8.7	**5.28** **16.5**	**6.06** **16.7**	4.67 12.6	3.61 10.4	2.89 9.1	2.39 8.2	1.94 7.6	1.83 7.8
		2.2 7.5	2.07 8.0	1.94 8.4	3.00 8.6	4.56 8.1	4.56 8.1	3.00 8.6	1.94 8.4	2.07 8.0	2.2 7.5		
		2.08 7.2	1.98 7.4	1.67 7.4	2.72 7.3	3.39 6.8	3.39 6.8	2.72 7.3	1.67 7.4	1.98 7.4	2.08 7.2		
		2.17 7.9	2.11 7.5			2.83 6.6	2.83 6.6			2.11 7.5	2.17 7.9		
		1.94 7.4	1.83 7.4			2.17 6.0	2.17 6.0			1.94 7.4	1.83 7.4		
						1.89 5.8	1.89 5.8						
0.167 5.2						1.61 6.3	1.61 6.3						0.22 5.3

↑
Air Flow

Figure 4.19(a). Local Temperatures Above T_∞ in °C (top numbers in the grids), and Local Conduction Losses in mW (bottom numbers) Around the Heated Component on the Back of the Aluminum Board.

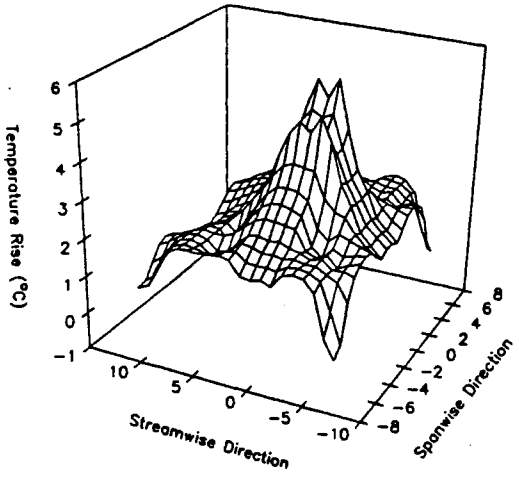

Figure 4.19(b). Variation of Local Temperature Above T_∞ Around the Heated Component on the Back of the Aluminum Board.

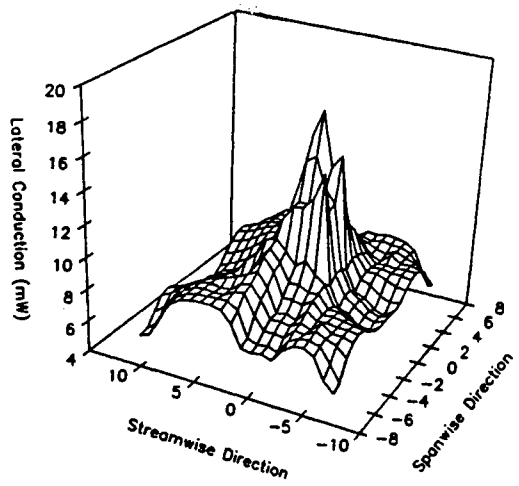

Figure 4.19(c). Variation of Local Conduction Loss Around the Heated Component on the Back of the Aluminum Board.

only 1.079 W. This value was 0.241 W for the fiberglass board for the same input power and channel average air velocity, while the total conduction obtained from the energy balance was 0.469 W. From this comparison, it seems that the correct way to account for the total conduction heat transfer is to use an energy balance by subtracting the total measured convective and radiative heat fluxes of the exposed surfaces from the input power to the component.

4.2.3.1 Effect of Board Conductivity The amount of conduction losses can greatly affect the component operating temperature and therefore the reliability of the system as a whole. In this study, conduction was controlled by changing board material. Boards with different thermal conductivities allowed different amounts of conduction. Balsa wood with a low thermal conductivity (0.07 W/m-K) was used to minimize conduction, while aluminum with a high thermal conductivity (130 W/m-K) was used to maximize conduction.

Figure 4.20 shows the temperature rise of the middle components for case 3 using three different boards. The different board conductivities had a large effect upon the component temperature rise. In other words, with a fixed input power to the component, the higher conductive board has more conduction heat transfer through the back of the board and less convection and radiation through the exposed surfaces, hence less component temperature rise. For example, the temperature rise of the heated component at row 1 was 13°C, 40.5°C, and 50°C for the aluminum, fiberglass, and balsa wood, respectively. Similarly, these temperature rises for row 4 were 16°C, 60.2°C, and 80°C for the three respective boards. The difference in temperature rise is very significant when a 10°C increase is considered to double the component failure rate (Weiss et al. 1989). This figure also reveals the hydrodynamic and thermal effects of upstream components on the temperature rise of downstream components, since all of the middle components were

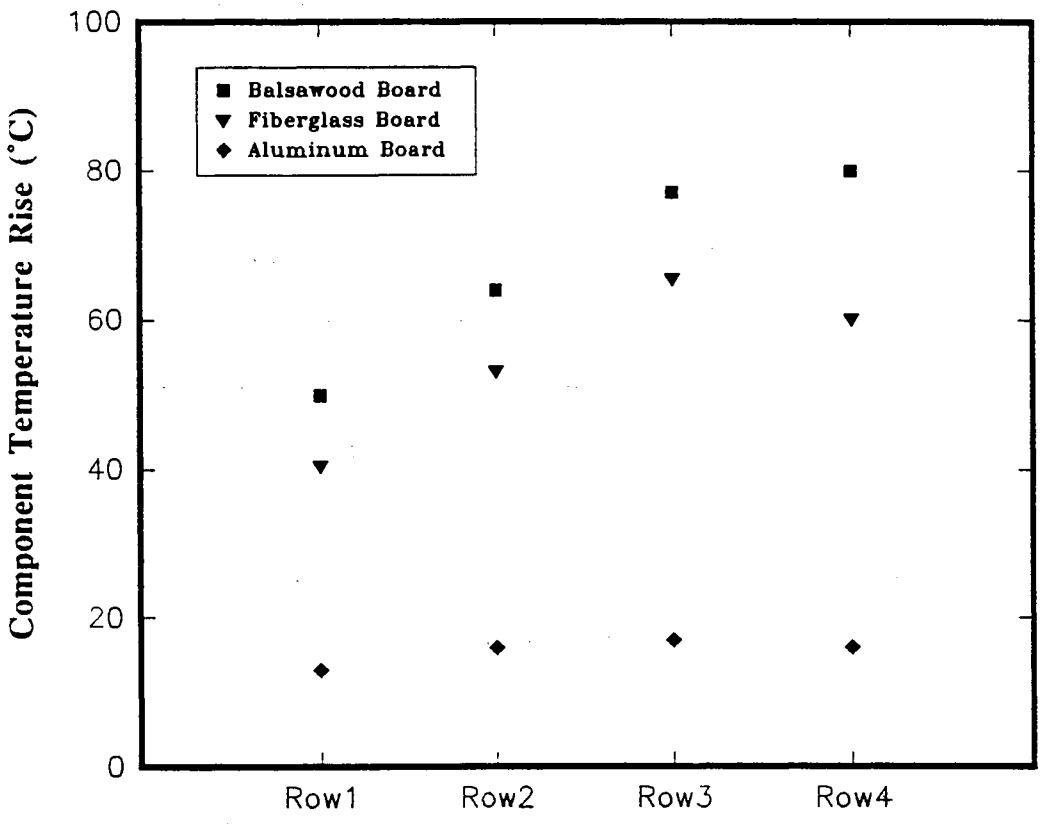

Figure 4.20. Effect of Board Conductivity on Component Temperature Rise for Different Component Placement of Case 3

heated simultaneously. As mentioned earlier, there are some irregularities due to the exposure of the last row. It is recommended that the component with higher power be placed in row 1 in electronic packaging, since its operating temperature will be lower, thereby providing higher reliability.

Figures 4.21 and 4.22 complement the results shown in Fig. 4.20. Figure 4.21 shows the effect of board conductivity on the total conduction percentage of the heated component at row 3 for case 3 with different Reynolds numbers, while Fig. 4.22 depicts effect of board conductivity on component temperature rise at row 3 for case 3 with different Reynolds numbers. Comparing Figs. 4.20 and 4.21 for a fixed Reynolds number of 3800 and input power of 4.5 W, the component temperature rise at row 3 is 17°C, 65.6°C, and 77°C (see Fig. 4.20), while the total conduction percentage is 89%, 21%, and 6% (see Fig. 4.21) for the aluminum, fiberglass, and balsa wood boards, respectively. It is important to note that with a fixed Reynolds number, the board with the higher thermal conductivity, dissipates more heat through the back of the board by conduction (see Fig. 4.21), rather than by convection and radiation through the exposed surfaces, which in turn, causes less temperature rise of the heated component (see Figs. 4.20 and 4.22). Figure 4.21 also shows that the total conduction percentage decreases with increasing Reynolds number. For example, for a Reynolds number of 1470, the total conduction percentage is 91%, 26.7%, and 7.2%, while for a Reynolds number of 30450, the total conduction percentage is 78.3%, 5%, and 1.2% for the aluminum, fiberglass, and balsa wood boards, respectively. Higher Reynolds number means faster air movement around the exposed surfaces of the component causing more heat dissipation by convection and less by conduction. This increase in convection heat transfer reduces the operating temperature of the heated component as can be seen in Fig. 4.22. The temperature rise for the balsa wood board was 110°C at the lowest Reynolds number. This was 28°C higher than that for the fiberglass board. The temperature rise for the fiberglass board was in turn, 57°C higher than that for the aluminum board. At high Reynolds number, the temperature rise for the

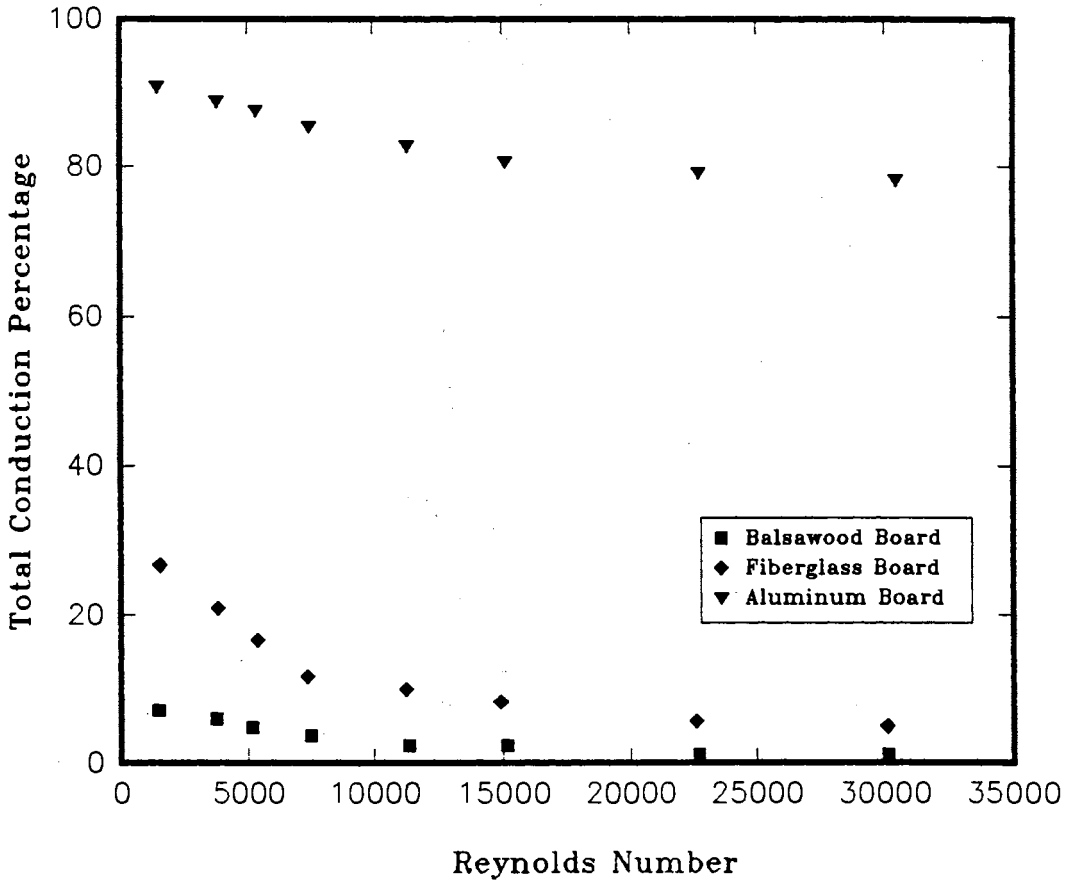

Figure 4.21. Effect of Board Conductivity on Total Conduction Percentage for Different Reynolds Numbers (Row 3 of Case 3)

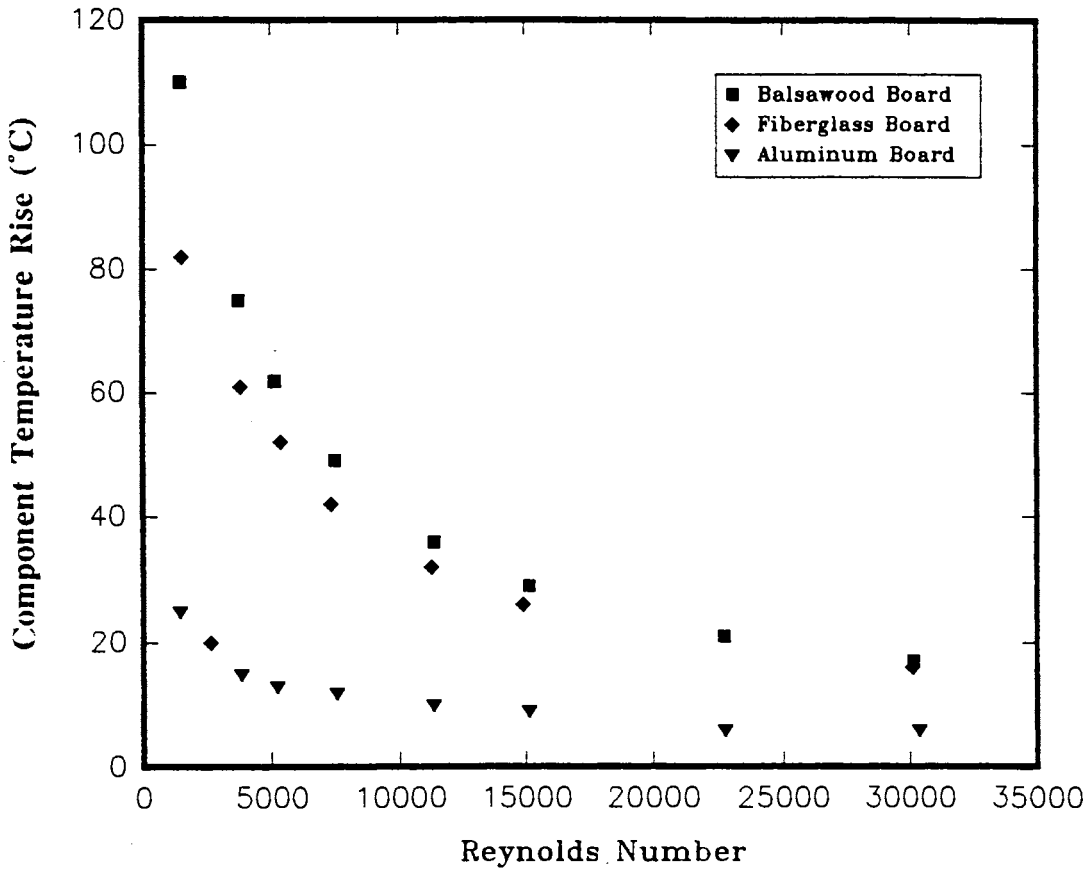

Figure 4.22. Effect of Board Conductivity on Component Temperature Rise for Different Reynolds Numbers (Row 3 of Case 3)

balsa wood board was only 1°C higher than that for the fiberglass board. However, the temperature rise for the fiberglass board was 10°C higher than that for the aluminum board.

The role of board conductivity on direct and lateral conduction losses can be further analyzed by revisiting the data of Fig. 4.21. If for this data "lateral conduction" contributions are ignored and only "direct conduction" effects are considered, the results will appear as Fig. 4.23. Comparison of Figs. 4.23 and 4.21 show that conduction percentage for aluminum is less than fiberglass and balsa wood for the same operating conditions. This is obviously not true. As discussed earlier, a great portion of conduction heat transfer for a conductive board (aluminum) is by lateral conduction, while for a relatively non-conductive board (balsa wood) this portion is very small. For example, for a fixed Reynolds number of 1470, the direct conduction percentage is 4%, 16.5%, and 6.5%, while the total conduction percentage is 91%, 26.7%, and 7.2% for the aluminum, fiberglass, and balsa wood boards, respectively. This means that heat transferred by lateral conduction is 87% for aluminum, 10.2% for fiberglass, and only 0.7% for balsa wood board.

The effects of board conductivity and Reynolds number on conduction losses are not addressed as a major contribution to the heat transfer in most of the work done in electronic cooling. This is perhaps because most of those measurements were conducted at higher Reynolds numbers regimes using nonconductive board. In fact, this is also shown in this study on Fig. 4.21 for Reynolds numbers above 10,000 (total conduction percentage is less than 9 for balsa wood and fiberglass board). Results of this work could become more useful if more measurements are performed for a set of lower Reynolds numbers. A correlation may be obtained between the percentage of conduction losses and Reynolds numbers for a range of Reynolds numbers below 2000.

4.2.3.2 Influence of Conduction and Board Conductivity on the Heat Transfer Coefficient

The total rate of heat transfer from the exposed surfaces measured with the

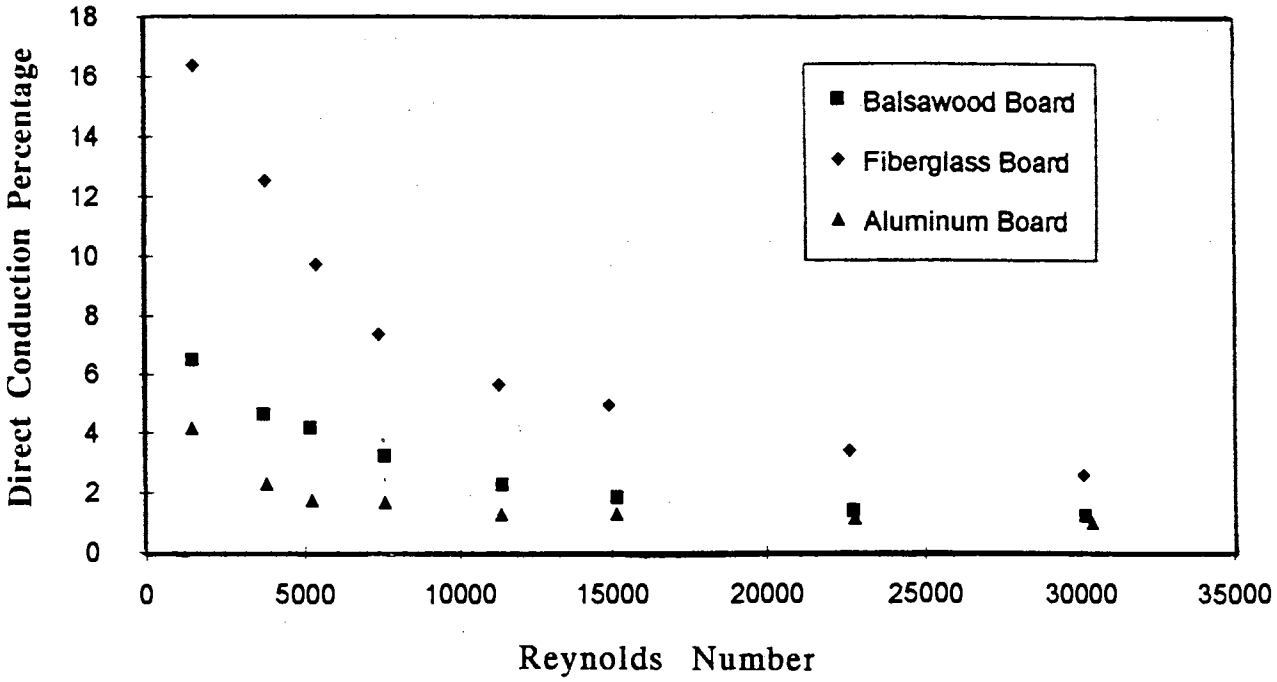

Figure 4.23. Effect of Board Conductivity on Direct Conduction Percentage for Diffent Reynolds Numbers (Row 3 of Case 3)

heat flow sensors by the experimenter, is the sum of convective and radiative heat transfers. The net rate of thermal radiation heat exchange between the surfaces and the surroundings (Q_r) can be calculated from Stefan-Boltzmann law, which in general is less than 1% of the total power supplied, as shown in Tables III and IV. Therefore, the experimenter can directly find the value of the convective heat transfer of the heated component (Q_c), then the value of the heat transfer coefficient (h) can be determined from Eq. (3.7):

$$h = Q_c/A_c\,(T_c - T_\infty) \tag{3.7}$$

where A_c is the total exposed surfaces of the heated component, T_c is the average temperature of the exposed surfaces, and T_∞ is the approaching air temperature. Working with heat flux sensors is tedious, time consuming, and causes flow disturbance due to presence of exposed wires. Therefore, most of the experimenters preferred temperature measurements rather than using heat flow sensors. They found the convective heat transfer by employing Eq. (3.4):

$$Q_c = Q_t - Q_k - Q_r \tag{3.4}$$

where Q_t is the total input power to the component, and Q_k is the calculated conduction heat transfer using the board thermal conductivity. However, typically the industrial users directly apply the heat transfer coefficient offered by the experimenter in order to predict the operating temperature of the heated component:

$$T_c = T_\infty + (Q_c/hA_c) \tag{4.3}$$

The actual heat transfer coefficient (h_a) can be found by using the correct measured value of total conduction loss in Eq. (3.4). However, almost all of the experimenters used one-dimensional calculated conduction loss in Eq. (3.4) in order to find the calculated heat transfer coefficient (h_c) from Eq. (3.7). Figure 4.24 shows comparison of these two values for the heated component at row 3 of case 3 for fiberglass board at different Reynolds numbers. This figure reveals that the calculated heat transfer coefficient is overestimated for all of the Reynolds numbers. The average difference between h_c and h_a

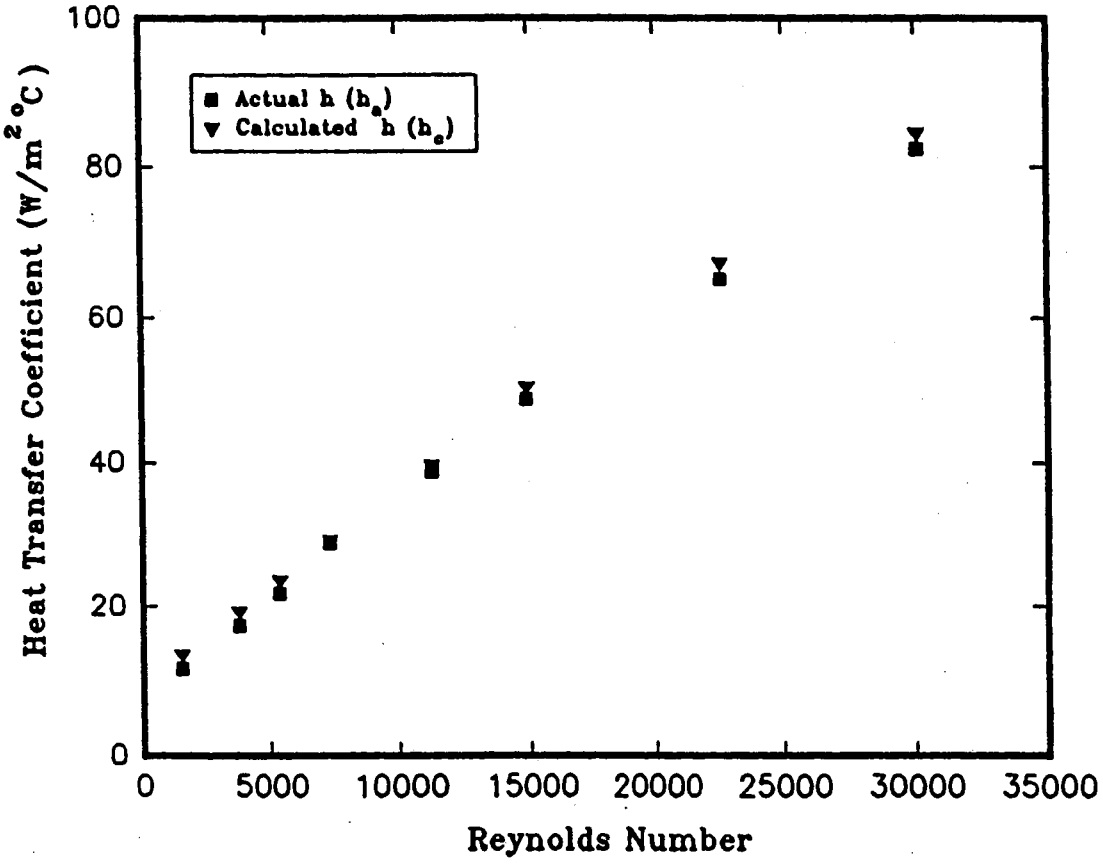

Figure 4.24. Comparison of Actual and Calculated Heat Transfer Coefficients for Different Reynolds Numbers (Row 3 of Case 3 for Fiberglass Board)

is 5.8% with a maximum of 16% at the lowest Reynolds number. This difference would be higher if the board with higher conductivity is used, since the percentage of lateral conduction is higher which is not taken into account in the one-dimensional conduction loss calculation. An attempt was made to directly compare the actual heat transfer coefficients obtained in this study with the data in the literature. The arrays tested by previous investigators were different in size and geometry, as well as the material used for the board and simulated component(s). Hence, the results of these studies can not be directly compared with one another, as though to test for agreement or disagreement. However, Fig. 4.24 depicts a general comparison of the heat transfer results of this study with those experimenters who ignored lateral conduction loss and only considered one-dimensional calculated conduction loss using the board thermal conductivity. It should be mentioned that the board used for collection of the main experimental heat transfer results tabulated in Tables III and IV, was a non-conductive board (a layer of 0.16 cm thick fiberglass placed on 1.27 cm thick commercial plexiglass). Since the conductivity of this composite board is much less than the conductivity of the fiberglass alone, therefore, average difference between h_c and h_a is less than what is shown in Fig. 4.24. In order to investigate this difference, experiments were performed with a single heated component placed 91.5 cm from the entrance of the rectangular channel, on this composite board (a layer of 0.16 cm thick fiberglass placed on a 1.27 cm thick commercial plexiglass). Different approach velocities and input power were used. It was found that the average difference between h_a and h_c for this board was less than 2.6% which was within the range of our experimental error. For this reason the conduction losses (Q_k) reported in Tables III and IV were based on a one-dimensional assumption.

In most practical applications of convective cooling in air, there will be some heat lost due to conduction. If the experimenter either ignores or underestimates these losses, then by employing Eqs. (3.4) and (3.7), Q_c and h will be overestimated. Use of this overestimated heat transfer coefficient by the industrial user, causes underprediction of the

component operating temperature in Eq. (4.3). On the other hand, if the user uses the accurate value of h offered by the experimenter, but either ignores or underestimates the conduction losses, then Q_C in Eq. (3.4) will be overestimated, which in turn, causes overprediction of the component operating temperature in Eq. (4.3). While having the operating temperature lower than what predicted, is generally not a problem from the reliability aspect, it is preferable to predict the component operating temperature as accurately as possible. This important task can be accomplished by the correct estimation of the conduction losses.

The value of the conduction losses and the consistency between the experimenter and the industrial user in the way they estimated this value, plays a major role in accurate prediction of the operating temperature, and it can cause serious problems if there is a failure of communication. Taking into account the accurate value of conduction losses, could allow greater packaging densities and therefore better overall circuit performance.

CHAPTER V

SUMMARY, CONCLUSIONS AND RECOMMENDATIONS

Summary and Conclusions

While forced air cooling continues to be adequate for many relatively low power dissipation applications, techniques for prediction of the component operating temperature are actively being investigated for future generations of electronic equipment such as high performance computers. Sufficient knowledge of the convective heat flux distribution over the exposed surfaces of an electronic printing wiring board is required as a guide to accurately predict the operating temperature of the heated component. The convective heat flux is mainly affected by the array geometry and the air flow rate.

In Chapter I, the effects of four key parameters (D/t, S/L, t/L, and the heated component row number) on the heat transfer coefficient of *any single heated rectangular component placed in an in-line array of unheated similar rectangular components* became evident. The investigators who obtained their correlations with taking any of these parameters into account were summarized in Table I. This table showed that none of the reported correlations included the effects of all of these four parameters. Since the arrays tested were different in geometry as well as size, the urge to combine the reported correlations and deduce a single correlation which covers the effects of all these four parameters is also impossible. Therefore, the reported correlations work only for the experimenter's experimental setup, or with limitations for setups that are somewhat similar. These correlations are not "transportable" to setups having different geometries. In spite of having expanded heat transfer database in the area of forced convective electronic cooling,

there is still no single correlation available that can predict the heat transfer behavior of *any single heated rectangular component placed in any in-line array of unheated similar rectangular components* having arbitrary geometries.

Research on air cooling should be more responsive to the inherent complexities of "real world" applications while at the same time retaining sufficient generality to be "transportable" from one application to another. Lack of this generality in the reported correlations established the need for the present research.

This study was undertaken to investigate the combined effects of most influential geometric parameters (D/t, t/L,and r), air flow rate, and conduction loss on the heat transfer coefficient of *any single heated rectangular component placed in an in-line array of unheated similar rectangular components.* A versatile experimental setup was designed and constructed for this purpose. The setup allows to perform experiments with different channel heights, component heights, spanwise and streamwise spacings, component arrangements (in-line and staggered), as well as test section orientations (vertical or horizontal). The setup will also allow accurate control and measurement of the channel average velocity, heated component temperature, and input power to the selected component(s).

Systematic experiments were performed for a range of different geometric parameters (D/t, t/L, and r), air flow rates and input powers to the heated component (see Tables II, III, and IV) placed in regular in-line array of similar rectangular components. A set of separate experiments with a different test section arrangement was also performed, in order to examine the effects of conduction losses and board conductivity on the heat transfer coefficient and consequently on the operating temperature of the heated component. Effects of air flow rate, each of the geometric parameters, input power, board material, conduction and radiation losses, on the heat transfer coefficient of the heated component were individually analyzed and discussed in detail.

The findings and accomplishments of this experimental investigation may be summarized as follows:

1. It was found that the percentages of conduction and radiation losses, and the heat transfer coefficient of the heated component were independent of the input power to the heated component (see Table III).
2. Percentage of conduction losses for the experimental data tabulated in Table IV, was found to vary from a minimum of about 2% to a maximum of about 10%, depending strongly on the flow approach velocity and the components' height, and weakly on the heated component row number and the channel height.
3. Percentage of radiation losses for the experimental data tabulated in Table IV, was found to vary from a minimum of about 0.2% to a maximum of about 1%, depending strongly on the approach Reynolds number, and weakly on the heated component row number, components' height, and channel height.
4. The results of this study showed that components along the first row experienced heat transfer which was 8 to 17% greater than those of succeeding rows (see Figs. 4.7 through 4.9). As the row number increased, the difference between h for the two neighboring rows became smaller. It generally took five rows of components for the heat transfer coefficient to be truly "periodically fully-developed."
5. For a fixed Reynolds number, as the channel height was increased, the heat transfer coefficient of the heated component decreased both for the entrance and fully developed regions (see Figs. 4.3, 4.4, and 4.8).
6. It was found that for a fixed Reynolds number, as the components' height was increased, the heat transfer coefficient of the heated component decreased (see Figs. 4.6 and 4.9). This fact was justified by defining a new parameter called Surface Blocking Ratio (SBR). SBR was defined as the ratio of the surface of

the heated component blocked by its neighboring components, to the total surface of the heated component exposed to convection.

7. This study showed that for a conductive board, such as an aluminum board, lateral conduction was generally higher than 50% of the total conduction. Total conduction heat transfer of the heated component was defined as the sum of two terms: "Direct Conduction" and "Lateral Conduction". The "Direct Conduction" is a one-dimensional conduction and was accounted for the amount of heat dissipated directly beneath the heated component on the back of the board. The "Lateral Conduction" is the heat dissipated by conduction from all around the component either to the inside or outside surface of the board. Almost all of the previous investigators ignored lateral conduction, and only accounted for one-dimensional conduction, i.e., direct conduction. Ignoring this significant value, overestimates the heat transfer coefficient. This causes underprediction of the operating temperature of the chip by the industrial user; hence reduction in the overall reliability of the system.
8. The experimental heat transfer data of this study were used to develop a general empirical correlation presented by Eq. (4.2). This correlation expresses the local convective heat transfer coefficient of *any single heated component placed in an arbitrary regular in-line array of unheated rectangular components with S/L = 1.* Equation (4.2) has sufficient generality in order to be "transportable" to any in-line array of rectangular components having arbitrary geometries i.e., different D/t, t/L, and r.
9. The heat transfer results of this study were compared with the results of other investigators reported in the open literature. These comparisons revealed that the results of this study were in good agreement with the results of other investigators. This in turn verified the good performance of our experimental

setup, and the accuracy of the general heat transfer correlation presented by Eq. (4.2).

The generality of the proposed correlation can be further increased by including the effect of S/L into Eq. (4.2). Experiments with different S/L ratios are underway (Kim, 1993). The results of these experiments will complement the database developed in this study, and could be easily incorporated into the proposed heat transfer correlation.

The general correlation presented in this study can be used to predict the *self heating temperature rise* of the heated component due to its own internal heating. The *temperature rise due to the thermal wakes of upstream components* can be calculated using the available correlations in the literature (Arvizu, 1981; Arvizu and Moffat, 1982; Anderson and Moffat, 1990; etc.). However, during the data collection, the temperature rise of downstream unheated components were also collected in order to cross check the works of these investigators. With combining the results of this study and the available correlations for thermal wakes due to upstream components, it is possible to predict the temperature rise of *any rectangular component placed in any in-line array of arbitrarily heated similar rectangular components.*

The heat transfer results of this study can be used as the preliminary database, for prediction of heat transfer behavior of any rectangular array with a desired complexity, such as arrays with different component sizes, missing components, etc. This fact is evident, since the in-line array can gradually be changed toward the desired complexity, and heat transfer behavior of the array should be experimentally determined during this process of change until the final change is achieved. Therefore, the heat transfer behavior of in-line array should be initially known, in order to move systematically toward the desired complex situation.

Recommendations

Based on the results obtained in this study the following recommendations may be stated:

1. In the general correlation presented by Eq. (4.2), the exponents for H/t and t/L were found to be interrelated, and for some set of values for H/t and t/L they cancel each other and Eq. (4.2) could be simplified. More experimental data for larger ranges of H/t and t/L are needed in order to introduce a new single geometric parameter which represents effects of both H/t and t/L on the heat transfer coefficient of the heated component.
2. During the process of experimentation and development of the general correlation, it was found that the exponent of R in Eq. (4.2) was a function of t/L. More experiments for the larger range of t/L are needed in order to find a relation between the exponent of R and the Surface Blocking Ratio (SBR).
3. Board conductivity can have significant direct effect on the operating temperature of the heated component. This study showed that the temperature rise of the heated component mounted on a conductive board such as aluminum was generally much less than what was for a relatively non-conductive board such as fiberglass or balsa wood board. However, in the electronic equipment, packages are mounted on the printing wiring board (PWB) where layers of electrical conductor networks are fabricated to connect the different packages. Hence, the material used for PWB should be electrically non-conductive. This causes a problem, since generally any heat conductive material is also electrically conductive and vice versa. More research should be conducted in this area to further quantify the influence of board material in order to find a suitable material to be able to transfer more heat by conduction and reduce the operating temperature of the heated component.

4. Systematic experiments should be performed by gradually changing the rectangular in-line array toward more complex arrays, such as arrays with staggered arrangements, arrays with different component sizes, arrays with missing components, arrays having different angles with the direction of approach velocity, etc. During the process of this change, the heat transfer behavior of the array should be experimentally determined and Eq. (4.2) should be gradually modified.

Finding the general correlations in order to predict the operating temperature of any rectangular component placed in *an arbitrary array of rectangular components*, is the "overall objective" of electronic cooling. However, at the present time, the world of electronic cooling is far away from this main purpose.

BIBLIOGRAPHY

Anderson, A. M. and Moffat, R. J. (1988), Direct Air Cooling of Electronic Components: Reducing Element Temperature by Controlled Thermal Mixing, Fundamentals of Forced Convection Heat Transfer, ASME HTD-vol. 101, pp. 9-16.

Anderson, A. M. and Moffat, R. J. (1990), A New Type of Heat Transfer Correlation for Air Cooling of Regular Arrays of Electronic Components, Proc. of the Thermal Modeling and Design of Electronic System and Devices, ASME HTD-vol. 153, pp.27-40.

Arabzadeh, M., Ogden, E. L., and Ghajar, A. J. (1993), Conduction Heat Transfer Measurements for an Array of Surface Mounted Heated Components, Proceedings of the 1993 ASME Winter Annual Meeting.

Arvizu, D. E. (1981), Experimental Heat Transfer from an Array of Heated Cubical Elements on an Adiabatic Channel Wall, Ph.D. Thesis, Stanford University.

Arvizu, D. E. and Moffat, R. J. (1982), The Use of Superposition in Calculating Cooling Requirements for Circuit Cards Containing Arrays of Electronic Components, Proc. of the 32nd Electronics Components Conference, IEEE, EIA, and CHMT.

Ashiwake, N., Nakayama, W., Daikoku, T. and Kobayashi, F. (1983), Forced Convective Heat Transfer from LSI Packages in an Air-Cooled Wiring Card Array, Heat Transfer in Electronic Equipment, ASME HTD-vol. 28, pp. 32-35.

Azar, K., and Moffat, R. J. (1991), Heat Transfer Coefficient and Its Estimation in Electronic Enclosures, Proceedings of the 1991 National Electronics Packaging and Production Conference (East), Boston, June 1991.

Biber, C. R. and Sammakia, B. G. (1986), Transport From Discrete Heat Components in a Turbulent Channel Flow, ASME paper No. 86-WA/HT-68.

Buller, M. L., and Kilburn, R. F. (1981), Evaluation of Surface Heat Transfer Coefficients for Electronic Module Packages,Heat Transfer in Electronic Equipment, ASME HTD-vol. 20, pp. 25-28.

Chang, M. J., Shyu, R. J. and Fang, L. J. (1987), An Experimental Study of Heat Transfer from Surface Mounted Components to a Channel Airflow, ASME Paper No. 87-HT-75.

Chou, J. and Lee, J. (1987), Reducing Flow Non-Uniformities in LSI Packages by Vortex Generators, Proc. of The International Symposium on Cooling Technologies for Electronic Equipment, Honolulu, Hawaii, pp. 583-594.

Choudhury, D. (1993), A Study of Two Benchmark Heat Transfer Problems Using Fluent, Solution to CFD Benchmark Problems in Electronic Packaging, ASME HTD-vol. 225, pp. 21-30.

Copeland, D.W. (1992), Effects of Channel Height and Planar Spacing on Air Cooling of Electronic Components, ASME Journal of Electronic Packaging, vol. 114, pp. 420-424.

Fitch, J. S. (1990), A One-Dimensional Thermal Model for the VAX 9000 Multi-Chip Units, Thermal Modeling and Design of Electronic Systems and Devices, Presented at the Winter Annual Meeting of ASME, Dallas, November 1990.

Garemilla, S. V. and Eibeck, P. A. (1990), Heat Transfer Characteristics of an Array of Protruding Elements in Single Phase Forced Convection, Int. J. Heat Transfer, vol. 33, No. 12, pp. 2659-2669.

Hollworth, B. R. and Fuller, H. A. (1987), Heat-Transfer and Pressure Drop in a Staggered Array of Air-Cooled Components, Proc. of The International Symposium on Cooling Technologies for Electronic Equipment, Honolulu, Hawaii, pp. 732-748.

Incropera, F. P., ed. (1986), Research Needs in Electronic Cooling, Proceedings of National Science Foundation Workshop, Andover, MA, June 4-6.

Incropera, F. P. (1987), Research Needs in Electronic Cooling, Proceedings of the International Symposium on Cooling Technology for Electronic Equipment, Honolulu, HI, Mar. 17-21, pp. 749-761.

Incropera, F. P. (1988), Convection Heat Transfer in Electronic Equipment Cooling, ASME Journal of Heat Transfer, vol. 110, pp. 1097-1111.

Kang, B. H., Jaluria, Y., and Tewari, S. S. (1990), Mixed Convection Transport from an Isolated Heat Source Module on a Horizontal Plate, Journal of Heat Transfer, vol. 112, pp. 653-661.

Kays, W. M. and Crawford, M. E. (1980), Convective Heat and Mass Transfer, McGraw-Hill, New York.

Kim, D. (1993), Experimental Study of the Effect of Component Spacing on Forced Air Cooling of Regular In-Line Array of Electronic Components, M.S. Report, Oklahoma State University, Stillwater, Oklahoma, December, 1993.

Kline, S. J. and McClintock, F. A. (1953), Describing Uncertainties in Single-Sample Experiments, Mech. Eng., pp. 3-8.

Kraus, A. D. and Bar-Cohen, A. (1983), Thermal Analysis and Control of Electronic Equpment, McGraw-Hill, New York.

Laderman, A. J., Osborn, D. B., Grabow, R. M., and Bury, M. C. (1987), Parametric Study of Conduction Cooling for High Power Density Electronics, Proceedings of the International Symposium of Electronic Technology for Electronic Equipment, Honolulu, March 1987.

Lehmann, G. L. (1985), Experimental Investigation of Convective Heat-Transfer From Surface Mounted Repeating Ribs in a Transitional Channel Flow, Ph.D. Thesis, Clarkson University, Potsdam, NY.

Lehmann, G. L. and Wirtz, R. A. (1985), The Effect of Variations in Stream-Wise Spacing and Length on Convection from Surface Mounted Rectangular Components, Heat Transfer in Electronic Equipment, ASME HTD-vol. 48, pp. 39-47.

Linton, R. L. and Agonafer, D. (1993), Benchmark Problems for System-Level Elctronics Cooling, Solution to CFD Benchmark Problems in Electronic Packaging, ASME HTD-vol. 225, pp. 37-43.

Manno, V. P., and Azar, K. (1991), Impact of Heat Transfer Coefficient Models on the Simulation of Electronic Enclosure Thermal Response, Proceedings of the 1991 National Electronic Packaging and Production Conference (East), Boston, June 1991.

Moffat, R. J., and Anderson, A. M. (1990), Applying Heat Transfer Coefficient Data to Electronic Cooling, Int. Journal of Heat and Mass Transfer, ASME HTD-vol. 112, pp. 882-890.

Moffat, R. J., Arvizu, D. E. and Ortega, A. (1985), Cooling Electronic Components: Forced Convection Experiments with an Air-Cooled Array, Heat Transfer in Electronic Equipment, ASME HTD-vol. 48, pp. 17-27.

Nakayama, W. (1986), Thermal Management of Electronic Equipment: A Review of Technology and Research Topics, Applied Mechanics Reviews, vol. 39, pp. 1847-1868 .

Ogden, E. L. (1992), The Effect of Certain Parameters on Conduction and the Component Temperature for an Array of Heated Components, M.S. Report, Oklahoma State University, Stillwater, Oklahoma, December, 1992.

Ortega, A., and Kabir, H. (1991), Substrate Conduction Mechanisms in Convectively Cooled Simulated Electronic Packages, Seventh IEEE Semi-Therm Symposium.

Ortega, A. and Moffat, R. J. (1986), Experiments on Buoyancy-Induced Convection Heat Transfer From an Array of Cubical Elements on a Vertical Channel Wall, Ph.D. Thesis, Stanford University, Stanford, CA.

Patankar, S. V. (1993), CFD Benchmark Problems for Electronic Packaging: Some Desirable Characteristics, Solution to CFD Benchmark Problems in Electronic Packaging, ASME HTD-vol. 225, pp. 31-35.

Rajagopalan, M. (1991), A Microcomputer-Based Data Acquisition System and Software for Research in Electronic Cooling, M.S. Report, Oklahoma State University, Stillwater, Oklahoma, May, 1991.

Ratts, E., Amon, C. H., Mikic, B. B., and Patera, A. T. (1987), Cooling Enhancement of Forced Convection Air Cooled Chip Array Through Flow Modulation Induced by Vortex-Shedding Cylinders in Cross-Flow, Proc. of The International Symposium on Cooling Technologies for Electronic Equipment, Honolulu, Hawaii, pp. 651-662.

Roeller, P. T., Stevens, J., and Webb, B. W. (1990), Heat Transfer and Turbulent Flow Characteristics of Isolated Three Dimensional Protrusions in Channels, Thermal Modeling and Design of Electronic Systems and Devices, ASME HTD-vol. 153, pp. 7-13.

Santos, W. F. N. and Souza Mendes, P. R. (1986), Heat Transfer and Pressure Drop Experiments in Air-Cooled Electronic Component Arrays, AIAA Paper No. 86-1301 presented at the AIAA/ASME 4th Joint Thermophysics and Heat Transfer Conference, Boston, MA.

Siegel, R. and Howell, J.R. (1981), Thermal Radiation Heat Transfer, 2Ed., Hemisphere, New York.

Sparrow, W. M., Niethammer, J. E. and Chaboki, A. (1982), Heat Transfer and Pressure Drop Characteristics of Rectangular Modules Encountered in Electronic Equipment, Int. Journal of Heat and Mass Transfer, vol. 25, no. 7, pp. 961-973.

Sparrow, E. M., Vemuri, S. B. and Kadle, D. S. (1983), Enhanced and Local Heat Transfer, Pressure Drop and Flow Visualization for Arrays of Block-Like Electronic Components, Int. Journal of Heat and Mass Transfer, vol. 26, no. 5, pp. 689-699, .

Sparrow, E. M., Yanezmoreno, A. A. and Otis, D. R. (1984), Convective Heat Transfer Response to Height Differences in an Array of Block-Like Electronic Components, Int. Journal of Heat and Mass Transfer, vol. 27, no. 3, pp. 469-473.

Torikoshi, K., Kawazoe, M. and Kurihara, T. (1988), Convective Heat Transfer Characteristics of Arrays of Rectangular Blocks Affixed to One Wall of A Channel, ASME HTD-vol.100, pp. 59-65.

Wagner, G. R. (1984), "Circuit Board Material/Construction and its Effect on Thermal Management", Section 3, Chapter 2 in Thermal Management Concepts in Microelectronic Packaging: From Component to System, ISHM Technical Monograph Series 6984-003, S.S. Furkay, R.F. Kilburn and G. Monti, Editors, Published by the International Society for Hybrid Microelectronics, Silver Spring, MD.

Wang, Y. and Ghajar, A. J. (1991), Effect of Component Geometry and Layout on Flow Visualization for Surface Mounted Electronic Components: A Smoke Flow Visualization Study, Proc. of the 1991 ASME Winter annual Meeting, HTD-vol.183, pp. 25-31.

Weiss, J., Fortner, P. Pearson, B., Watson, K. and Monroe, T. (1989), Modeling Air Flow in Electronic Packages, Mechanical Engineering, vol. 111, No. 9, pp. 56-58.

Wirtz, R. A. and Dykshoorn, P. (1984), Heat Transfer from Arrays of Flat Packs in a Channel Flow, Proc. Fourth Annual Int. Electronic Packaging Society Conf., pp. 318-326.

Wirtz, R. A., Hollworth, B. R. and Fuller, H. A. (1985), An Infrared Thermographic Study of Convection in an Array of Surface Mounted Components, Proc. Fifth Annual Int. Electronic Packaging Society Conf., pp. 496-507.

APPENDIX A

INPUT/OUTPUT OF RED40 AND PROGRAM VELAIR

A SAMPLE OF INPUT DATA FILE FOR RED40 PROGRAM

```
* 10/23/90 01:33
  *01+0100.0 F
  *02+0099.0 F
  *03+0082.1 F
  *04+0078.8 F
  *05+0088.8 F
  *06+0088.8 F
  *07+0088.8 F
  *08+0088.8 F
  *09+0088.8 F
  *10+0088.8 F
  *11+0088.8 F
  *12+0088.8 F
  *13+0088.8 F
  *14+0088.8 F
  *15+0088.8 F
  *16+0088.8 F
  *17+0088.8 F
  *18+0088.8 F
  *19+0088.8 F
  *20+0088.8 F
  *21+0088.8 F
  *22+0088.8 F
  *23+0088.8 F
  *24+0088.8 F
  *25+0088.8 F
  *26+0088.8 F
  *27+0088.8 F
  *28+0088.8 F
  *29+0088.8 F
  *30+0088.8 F
  *31+0088.8 F
  *32+0088.8 F
  *33+0088.8 F
  *34+0088.8 F
  *35+0088.8 F
  *36+0088.8 F
  *37+0088.8 F
  *38+0088.8 F
  *39+0088.8 F
  *40+0088.8 F
```

```
* 10/23/90 01:34
  *01+0100.1 F
  *02+0099.1 F
  *03+0082.4 F
  *04+0078.8 F
  *05+0088.8 F
  *06+0088.8 F
  *07+0088.8 F
  *08+0088.8 F
  *09+0088.8 F
  *10+0088.8 F
  *11+0088.8 F
  *12+0088.8 F
  *13+0088.8 F
  *14+0088.8 F
  *15+0088.8 F
  *16+0088.8 F
  *17+0088.8 F
  *18+0088.8 F
  *19+0088.8 F
  *20+0088.8 F
  *21+0088.8 F
  *22+0088.8 F
  *23+0088.8 F
  *24+0088.8 F
  *25+0088.8 F
  *26+0088.8 F
  *27+0088.8 F
  *28+0088.8 F
  *29+0088.8 F
  *30+0088.8 F
  *31+0088.8 F
  *32+0088.8 F
  *33+0088.8 F
  *34+0088.8 F
  *35+0088.8 F
  *36+0088.8 F
  *37+0088.8 F
  *38+0088.8 F
  *39+0088.8 F
  *40+0088.8 F
```

```
* 10/23/90 01:35
  *01+0100.2 F
  *02+0099.2 F
  *03+0082.5 F
  *04+0078.8 F
  *05+0088.8 F
  *06+0088.8 F
  *07+0088.8 F
  *08+0088.8 F
  *09+0088.8 F
  *10+0088.8 F
  *11+0088.8 F
  *12+0088.8 F
  *13+0088.8 F
  *14+0088.8 F
  *15+0088.8 F
  *16+0088.8 F
  *17+0088.8 F
  *18+0088.8 F
  *19+0088.8 F
  *20+0088.8 F
  *21+0088.8 F
  *22+0088.8 F
  *23+0088.8 F
  *24+0088.8 F
  *25+0088.8 F
  *26+0088.8 F
  *27+0088.8 F
  *28+0088.8 F
  *29+0088.8 F
  *30+0088.8 F
  *31+0088.8 F
  *32+0088.8 F
  *33+0088.8 F
  *34+0088.8 F
  *35+0088.8 F
  *36+0088.8 F
  *37+0088.8 F
  *38+0088.8 F
  *39+0088.8 F
  *40+0088.8 F
```

A SAMPLE OF OUTPUT FILE FOR RED40 PROGRAM

INPUT DATA FILE = INPUT OUTPUT DATA FILE = OUTPUT

THE TEMPERATURES ARE IN DEG C

CHANNEL NO.	MEAN TEMP	LOWEST TEMP	HIGHEST TEMP
1	37.83	37.78	37.89
2	37.28	37.22	37.33
3	27.96	27.83	28.06
4	26.00	26.00	26.00
5	31.56	31.56	31.56
6	31.56	31.56	31.56
7	31.56	31.56	31.56
8	31.56	31.56	31.56
9	31.56	31.56	31.56
10	31.56	31.56	31.56
11	31.56	31.56	31.56
12	31.56	31.56	31.56
13	31.56	31.56	31.56
14	31.56	31.56	31.56
15	31.56	31.56	31.56
16	31.56	31.56	31.56
17	31.56	31.56	31.56
18	31.56	31.56	31.56
19	31.56	31.56	31.56
20	31.56	31.56	31.56
21	31.56	31.56	31.56
22	31.56	31.56	31.56
23	31.56	31.56	31.56
24	31.56	31.56	31.56
25	31.56	31.56	31.56
26	31.56	31.56	31.56
27	31.56	31.56	31.56
28	31.56	31.56	31.56
29	31.56	31.56	31.56
30	31.56	31.56	31.56
31	31.56	31.56	31.56
32	31.56	31.56	31.56
33	31.56	31.56	31.56
34	31.56	31.56	31.56
35	31.56	31.56	31.56
36	31.56	31.56	31.56
37	31.56	31.56	31.56
38	31.56	31.56	31.56
39	31.56	31.56	31.56
40	31.56	31.56	31.56

THE START TIME (HRS AND MINS) = 1.33
THE FINAL TIME (HRS AND MINS) = 1.35
DURATION OF EXPERIMENT (HRS AND MINS) = .02
EXPERIMENT WAS CONDUCTED ON 10/23/90 BY: MASOUD

```
/*
                                VELAIR PROGRAM

  This program can be used for three purposes :

1. To reach a desired velocity of wind tunnel by changing the damper position
   of the blower using a 60 oz in , 200/revolution stepper motor. Range of
   desired velocity is from 0.0 to 12. meter per second with the accuracy of
   0.05 m/s.

2. To measure the velocity and Reynolds # either at the duct or test section
   at a fixed damper position.

3. To back calculate velocity of either test section or duct by using a given
   Reynolds # as an input.

   An MKS 223B pressure transducer with the range of 0.5 inches of water and
   5 volts (+ or -) output signal is used for A/D conversion. */



#include <stdio.h>
#include <conio.h>
#include <math.h>
#include "dos.h"
#include <stdlib.h>

                                /* Definition of addresses from DAS -8 manual */

#define   BASADR      0x300
#define   ADHI        BASADR+1
#define   STATUS      BASADR+2
#define   CONTROL     BASADR+2


float rd_ad();

main()

{

                                /* Declaration of variables */

int io=0,chno,i,choice,in=1,vch,velch,hit,key;
int loop,dur,dir,lowbyte,hibyte,ask,cho;
char sign;
float reyn,tk,dvis,dvise,v,vel,temp,sum=0.0,data,sq,da,dat,press;
float chtd,rho,pstat,dyn,ave,duct,corr,hgatm,atmp,vcorr;
float vtest,vel1,vel2,cht1,cht2,reyn1,reyn2,sqr,x,xx,a,vref,checkv;
double kvis;
float b = 0.000001458,s = 110.4;        /* Sutherland  & Gas Constants */

FILE *ofp;
```

```
ofp = fopen("velair.dat","w");        /* Output file - Velair.dat */
textbackground(LIGHTGREEN);
textcolor(BLACK);
 clrscr();

 printf("\n\n\n\n\n\n\n\n");


printf("\t  FORCED CONVECTIVE COOLING IN COMPUTERS & ELECTRONIC EQUIPMENT\n");
printf("\t  ***************************************************************\n");
printf("\n\n\n\t            Velocity Control of Wind tunnel\n");
printf("\n\n\n\t               Type <RETURN>\n");
getchar();

clrscr();

                                  /*  Program begins */
while(in == 1){
sum = ave = 0.0;
clrscr();

                                  /* Two input options */

printf("\n\n\n\n\n\n\n\n\t          Inputs \n");
printf("\t          ******\n");
printf("\n\t Do you want to calculate experimental parameters for\n");
printf("\t                    - a given Re.no.      ->1 ");
printf("\n\t                     - a measured Velocity   ->2 ");
printf("\n\t Input no. and <RETURN>                          ->");
scanf("%d",&cho);

while(cho < 1 || cho > 2){
printf("\n\t Error in input ! Try again                    ->");
scanf("%d",&cho);
 }
                                  /* Reynolds number */
if(cho == 1){
printf("\n\t Input the desired Re.no (AT DUCT)              ->");
scanf("%f",&reyn);
}


printf("\n\t Duct diameter(inches)                          ->");
scanf("%f",&duct);

                                  /* Channel number for A/D conversion */

if(cho == 2){
chno =  5;

                                  /* Option for velocity measurement or control */

printf("\n\t Velocity measurement                          ->1");
```

```
printf("\n\t Velocity Control                    ->2");
printf("\n\t                  Choice          ->");
scanf("%d",&vch);

                              /* Characteristic length */

printf("\n\t Char.length (inches) -TEST SECTION          ->");
scanf("%f",&dyn);

                              /* Control the velocity */
if(vch == 2){
printf("\n\t Control Average Velocity at the -Duct       ->1");
printf("\n\t                  -Test section    ->2");
printf("\n\t                Your input and <RETURN>   ->");
scanf("%d",&velch);


printf("\n\t Desired Average Velocity(m/sec)             ->");
scanf("%f",&vref);

if(velch == 2){
vtest = vref;       /* Calculating the corresponding velocity at the duct */
vref  = 1.0882 * 0.945 * vref * 10.0 * dyn / (duct * duct * 3.1415927 / 4.0);

  }

 if(velch == 1){     /* Calculating the corresponding  velocity at the test section */
 vtest = 1./(1.0882 * 0.945) * vref * 3.1415927 * duct * duct / 4.0 / (dyn * 10.0);
  }
 }
}

printf("\n\t Barometric pressure (mm of Hg)              ->");
scanf("%f",&hgatm);
atmp = 101325.0 * hgatm/760.0; /* Converting barometric pressure to atmospheres */

                              /* Air temperature */

printf("\n\t Air Temperature (deg C)?                    ->");
scanf("%f",&temp);
clrscr();

                              /* Display input channel number on screen */

if(cho == 2){
printf("\n\t Input Channel No. -> %d",chno);
sum = rd_ad(chno);

 ave = sum/1000.0;
 press = 0.0999 * ave - 0.0014;   /* Pressure transducer calibration equation*/


 pstat = -press * 249.1 + atmp;
```

```
if(press >= 0.0){
press = press;
sign = '+';
 }

if (press <= 0.0){
press = -press;
sign = '-';
 }


        /* The following are the air constants calculations Conversion
          factor to convert pressure in inches to atm in Pa's */

tk = temp + 273.15;
rho = pstat / (287.0*tk);
dvis =  b * sqrt(tk)/(1.0 + (s/tk));
kvis = dvis/rho;

v = 22.297799 * sqrt (press / rho) * 0.945; /* Average Velocity at the DUCT */


                                    /* Beginning of velocity control */

if(vch == 2){

if(sign == '-'){
v = -v;
 }

checkv = vref - v;     /* Checking whether desired a verage velocity has
                                been reached */


                                    /* Loop begins for velocity control */

while((checkv > 0.05) || (checkv < -0.05)){
gotoxy(50,10);
printf("\n\t  Velocity Control in process ! \n");


while(checkv > 0.05){

gotoxy(50,13);
printf("\n\t Desired Average Velocity (DUCT) = %6.3f m/sec",vref);
printf("\n\t Actual  Average Velocity (DUCT) = %6.3f m/sec\n",v);


if(checkv >= 3.0){
loop = 100;}

else
  if(checkv >= 2.0){
  loop = 50;}
```

```
else
 if(checkv >=1.0){
 loop = 30;}

else
 if(checkv >=0.3){
 loop = 10;}

else{
loop = 1;}

v = 0.0;
checkv = 0.0;            /* D/A conversion for clockwise direction */
outportb(CONTROL,0x0);
for(io=0; io <= loop;++io){
outportb(CONTROL,0x20);
delay(20);
outportb(CONTROL,0x0);
 }

sum = rd_ad(chno);       /* Checking actual velocity again */
ave = sum/1000.0;
press = 0.0999 * ave - 0.0014;
pstat = -press * 249.1 + atmp;
rho = pstat / (287.0 * tk);
gotoxy(50,10);

if(press > 0.0){
sign = '+';
 }

if(press < 0.0){
press = -press;
sign = '-';
 }

v = 22.297799 * sqrt (press / rho) * 0.945;

if(sign == '-'){
v = -v;
 }

checkv = vref - v;            /* Error check */

if(v >= 13.5){
clrscr();
printf("\n\n\t  Actual Velocity = %6.3f m/sec",v);
printf("\n\t Desired Velocity = %6.3f m/sec",vref);
printf("\n\n\n\n\t Approaching the MAX.PRESSURE OF 0.5 inch!");
printf("\n\t You could damage the PRESSURE TRANSDUCER !\n\n\n");
printf("\n\n\n\n\n\n\n Stop - program VELAIR terminated\n");
exit(1);
 }
```

```
 }


 while(checkv < -0.05){

gotoxy(50,13);
printf("\n\t Desired Average Velocity (DUCT) = %6.3f m/sec",vref);
printf("\n\t Actual  Average Velocity (DUCT) = %6.3f m/sec\n",v);


 if(checkv < -3.0){
 loop = 100;}

 else
  if(checkv <= -2.0){
  loop = 50;}

 else
       if(checkv <= -1.0){
       loop = 30;}
 else
       if(checkv <= -0.3){
       loop = 10;}

 else{
 loop = 1;}


 v = 0.0;
 checkv = 0.0;
 outportb(CONTROL,0x10);          /* D/A conversion for C-Clockwise */

 for(io=0; io <= loop ;++io){
 outportb(CONTROL,0x30);
 delay(20);
 outportb(CONTROL,0x10);
  }

 sum = rd_ad(chno);               /* Checking actual velocity */
 ave = sum/1000.0;
 press = 0.0999 * ave - 0.0014;
 pstat = -press * 249.1 + atmp;

if(press > 0.0){
sign = '+';
  }

if(press < 0.0){
press = -press;
sign = '-';
  }

rho = pstat / (287.0 * tk);
```

```
  v = 22.297799 * sqrt (press / rho) * 0.945;

  if(sign == '-'){
  v = -v;
   }

  checkv = vref - v;              /* Checking error */

          }
         }
   }
   /* End of velocity control */


                                              /* Calculations for duct */
vel1 = vel = v;
cht1 = duct * 0.0254;
reyn1 = reyn = vel * cht1 /kvis;

                                              /* Calculations for test section */
cht2 = dyn * 0.0254;
vel2 = 1./(1.0882 * 0.945) * (v * duct * duct * 3.1415927 / 4.0) / (10.0 * dyn);
reyn2 = vel2 * cht2 / kvis;
   }

/* End for choice 2 */


if(cho == 1){                    /* Back calculations option begins to */
chtd = duct * 0.0254;              /* calculate voltage for a given Re */
tk   = 273.15 + temp;
dvis = b*sqrt(tk)/(1.0 + (s/tk));
x = chtd * chtd /(dvis * dvis);
a = x * tk * 572.83845;            /* Eqn of the form ax**2 + bx + c = 0 */
sqr = sqrt((1.9959528 * 1.9959528 * atmp * atmp * x * x) - (4.0 * a * reyn * reyn));
vref = 0.0;          /* Vref = 0.0 as it is not needed */
if(sqr < 0.0){
xx = -sqr;
  }

else{
xx = sqr;
  }

rho = (1.9959528 * atmp * x + xx)/(2.0 * a);
kvis = dvis / rho;
vel1 = vel = reyn * kvis / chtd;
press = vel * vel *rho /(22.297799*22.297799);
reyn1 = reyn;
reyn2 = 0.0;
vel2 = 0.0;
if( vel < 0.0){
sign = '-';
 }
```

```
else{
sign = '+';
  }

ave = (press + 0.0014)/0.0999;      /* using pressure transducer calibration
                                                    equation */

  }

outportb(CONTROL,0x0);              /* Switching of the stepper motor */
clrscr();

                                                    /* Outputs */

if(cho == 1)
chno = 0;
                                                    /* Output to the screen */
printf("\n\t\t\t Output Data");
printf("\n\t\t\t ***********\n");
printf("\n\t        Input Ch.no      = %1d",chno);
printf("\n\t        Voltage          = %6.5f V\n",ave);

printf("\n\t PHY.PROP AIR:     Pressure = %1c%7.5f inch H2O",sign,press);
printf("\n\t Density = %9.7f Kg/m3   Temp    = %5.2f deg C",rho,temp);
printf("\n\t K.vis  = %9.7f m2/sec  Dyn.vis = %9.7f N-sec/m2\n",kvis,dvis);

printf("\n\t DUCT:    Diameter        = %5.2f inches",duct);
printf("\n\t        Re.no           = %8.2f",reyn1);

if((cho == 2) && (vch == 2)){
delay(0);
sound(500);
delay(5000);
nosound();
printf("\n\t   Desired Average Velocity  = %7.3f m/sec",vref);
       }
printf("\n\t   Actual  Average Velocity  = %1c%7.3f m/sec\n",sign,vel1);

if(cho != 1){
printf("\n\t TEST SEC:  Char.length     = %5.2f inches",dyn);
printf("\n\t          Re.no           = %8.2f",reyn2);
if(vch == 2){
printf("\n\t   Desired Average Velocity  = %7.3f m/sec",vtest);
  }
printf("\n\t   Actual  Average Velocity  = %1c%7.3f m/sec",sign,vel2);
                }

fprintf(ofp,"\n\t\t\t Output Data");
fprintf(ofp,"\n\t\t\t ***********\n");
fprintf(ofp,"\n\t        Input Ch.no      = %1d",chno);
fprintf(ofp,"\n\t        Voltage          = %6.5f V\n",ave);

fprintf(ofp,"\n\t PHY.PROP AIR:     Pressure = %1c%7.5f inch H2O",sign,press);
```

```
fprintf(ofp,"\n\t Density = %9.7f Kg/m3   Temp    = %5.2f deg C",rho,temp);
fprintf(ofp,"\n\t K.vis  = %9.7f m2/sec  Dyn.vis = %9.7f N-sec/m2\n",kvis,dvis);

fprintf(ofp,"\n\t DUCT:    Diameter       = %5.2f inches",duct);
fprintf(ofp,"\n\t          Re.no          = %8.2f",reyn1);

if((cho == 2) && (vch == 2)){
fprintf(ofp,"\n\t          Des.Vel        = %7.3f m/sec",vref);
        }
fprintf(ofp,"\n\t          Act.Vel        = %1c%7.3f m/sec\n",sign,vel1);

if(cho != 1){
fprintf(ofp,"\n\t TEST SEC: Char.length     = %5.2f inches",dyn);
fprintf(ofp,"\n\t          Re.no          = %8.2f",reyn2);
if(vch == 2){
fprintf(ofp,"\n\t          Des.Vel        = %7.3f m/sec",vtest);
   }
fprintf(ofp,"\n\t          Act.Vel        = %1c%7.3f m/sec",sign,vel2);
                }

printf("\n\n\n\n\n To continue ->1");
printf("\n       Stop ->2 and <RETURN>");
scanf("%d",&in);
}

clrscr();
printf("\n\n\n\n\n\n\n\n\n\n\n\n\n\n\n");
printf("\n\t\t        Good day !");
printf("\n\n\n\n\n\n\n\n\n\n");

}
```

```
/* Function for the A/D conversion */

float rd_ad(chno)

int chno;
{
int i,lowbyte,hibyte;
float da,dat,data,su = 0.0;

for(i=0;i<1000;++i){
outportb(STATUS,chno);
outportb(ADHI,0);
while(inportb(STATUS) >= 128);
lowbyte = inportb(BASADR);
hibyte  = inportb(ADHI);
da = hibyte * 16 + lowbyte / 16;
dat = da * 10/4096;
data = dat - 5.0;
```

```
su = su + data;
delay(10);
  }

return(su);

 }
```

APPENDIX B

VELOCITY PROFILES

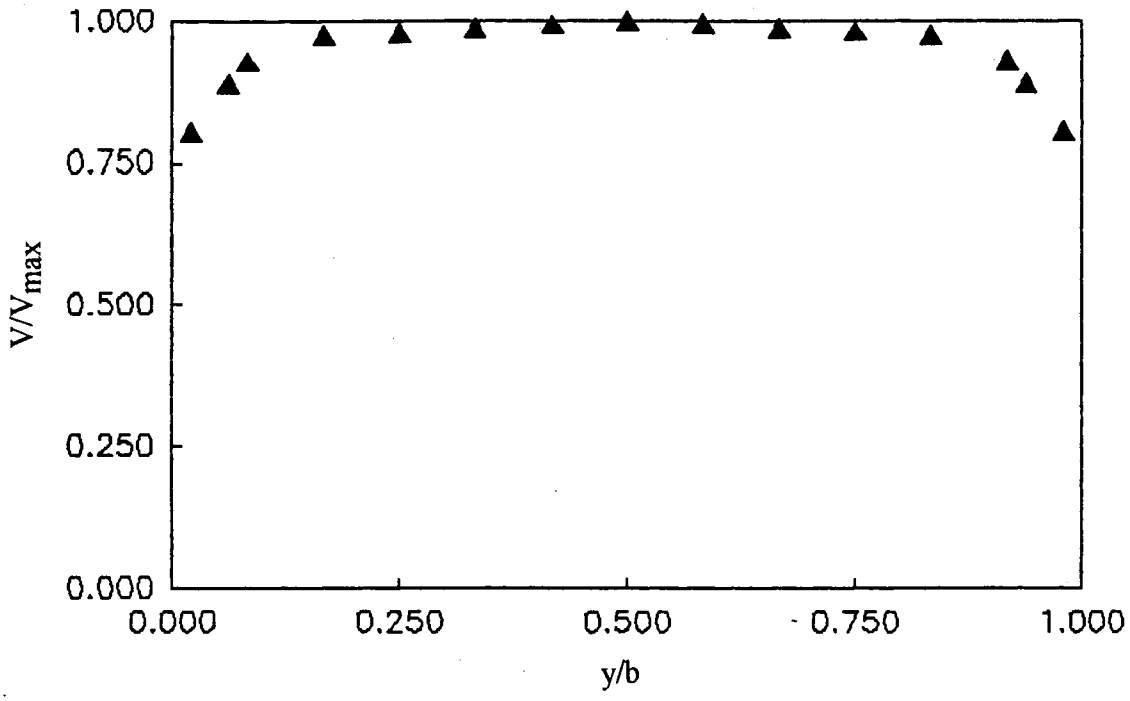

Figure B.1. Duct Velocity Profile (Low Flow Rate)

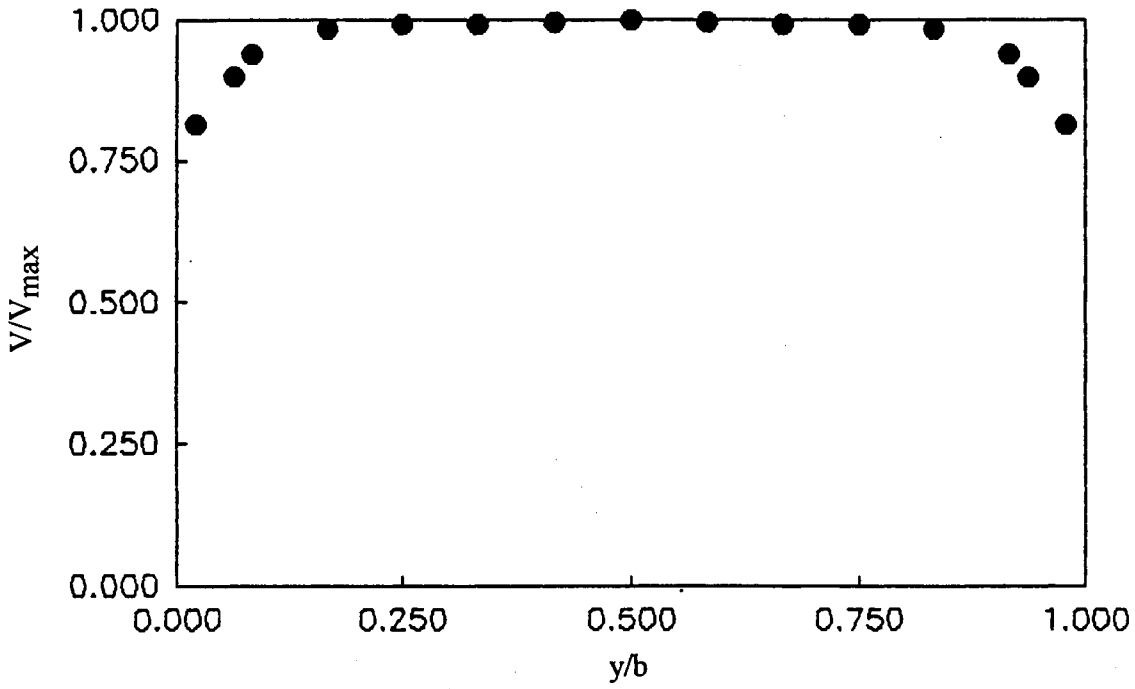

Figure B.2. Duct Velocity Profile (Medium Flow Rate)

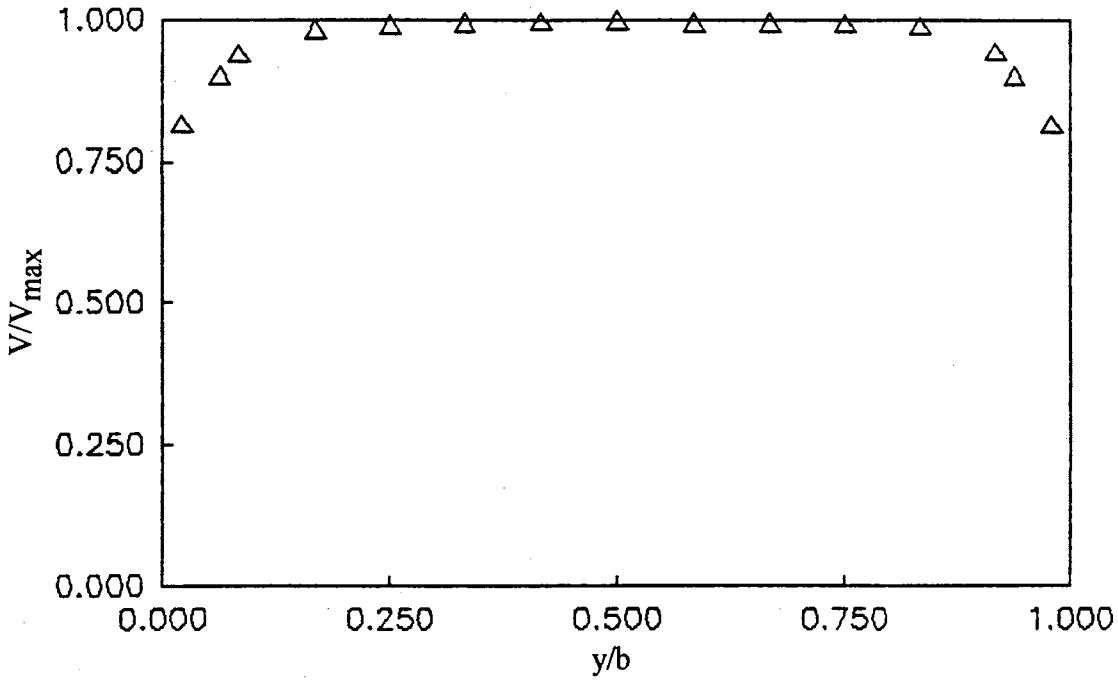

Figure B.3. Duct Velocity Profile (High Flow Rate)

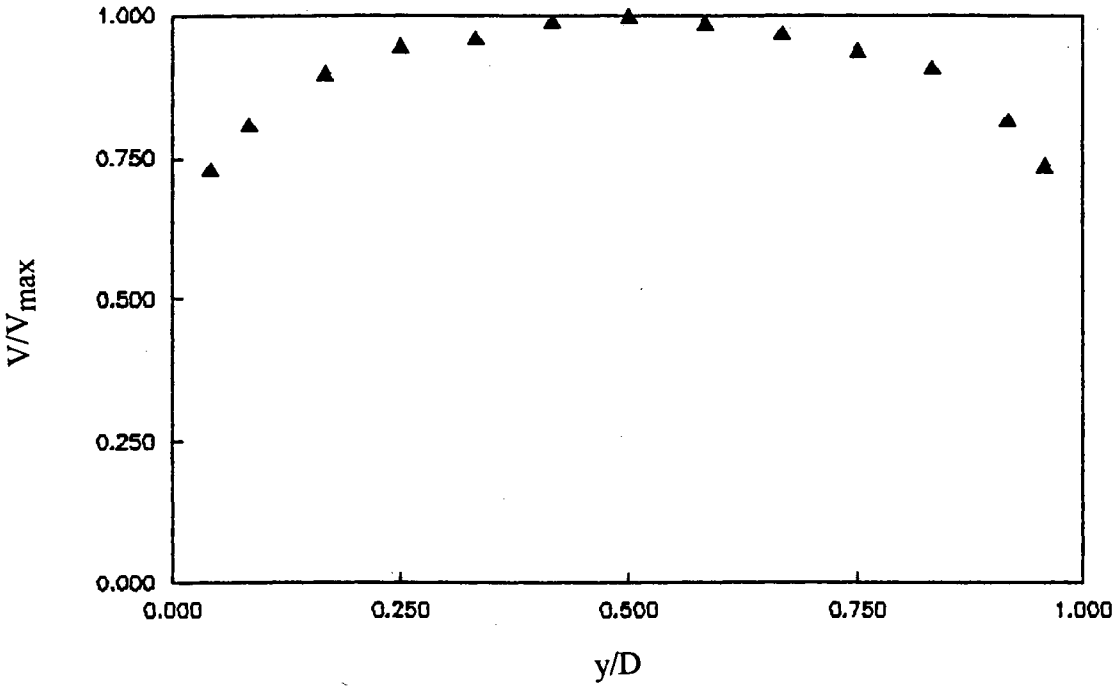

Figure B.4. Velocity Profile at the Left of Rectangular Channel (Low Flow Rate)

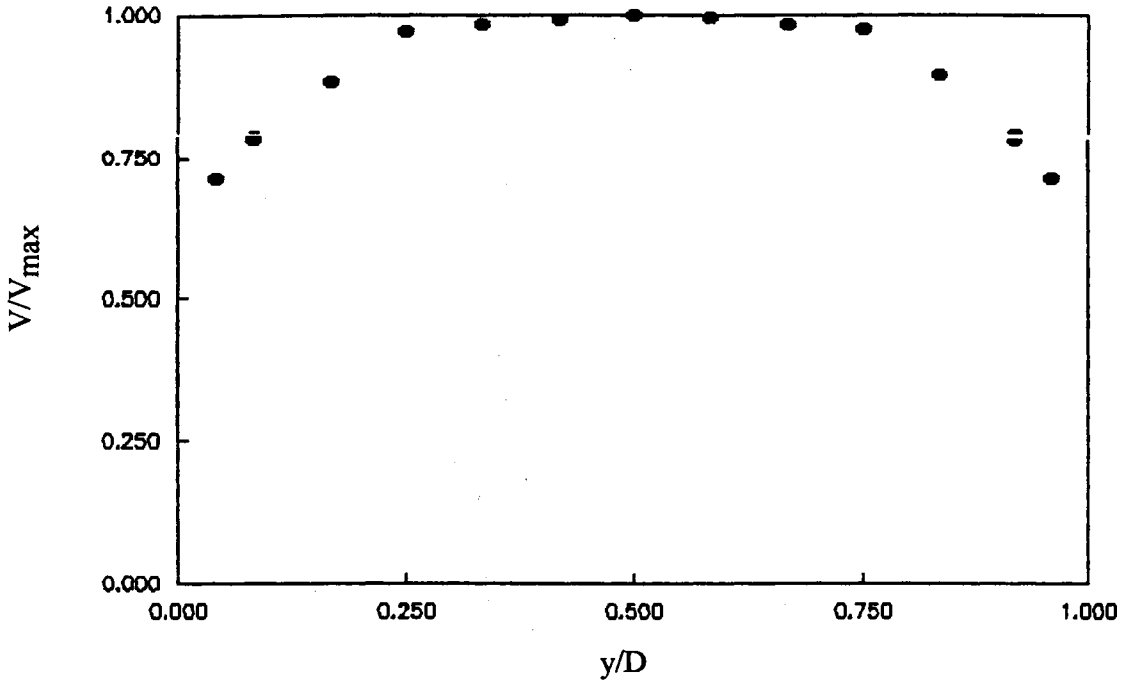

Figure B.5. Velocity Profile at the Center of Rectangular Channel (Low Flow Rate)

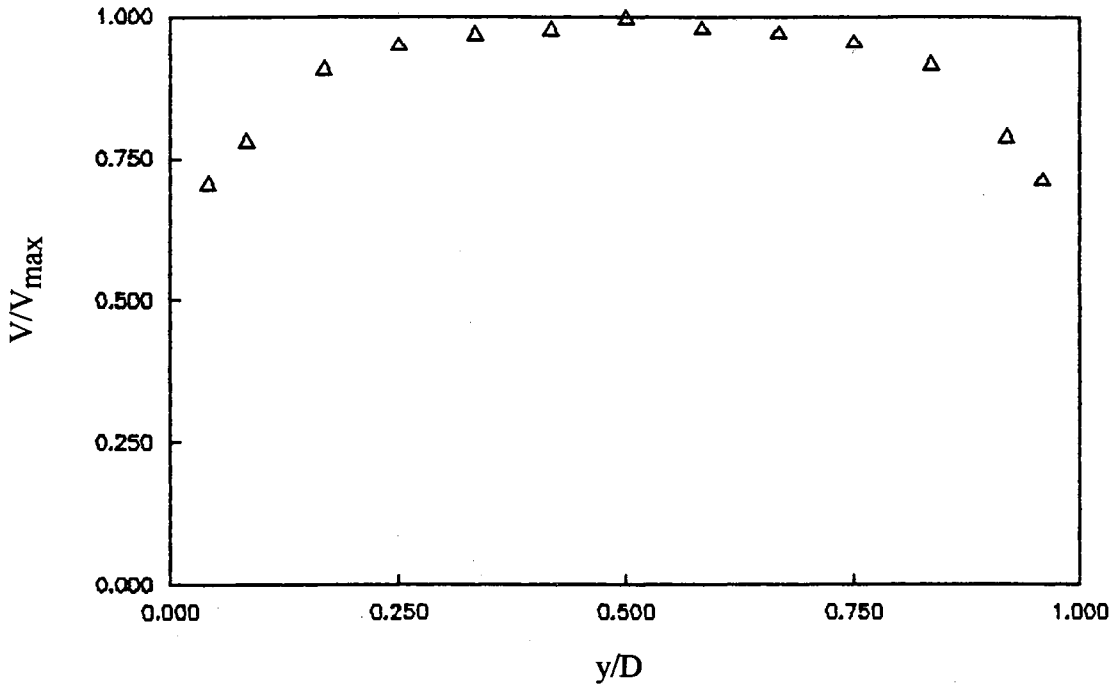

Figure B.6. Velocity Profile at the Right of Rectangular Channel (Low Flow Rate)

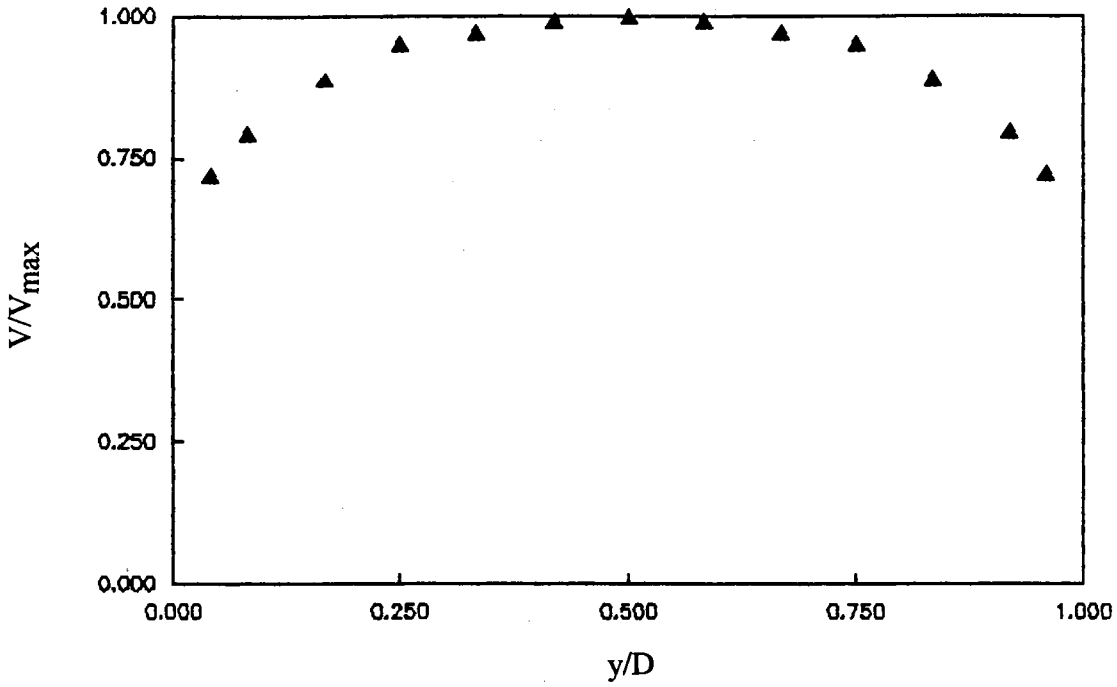

Figure B.7. Velocity Profile at the Left of Rectangular Channel (Medium Flow Rate)

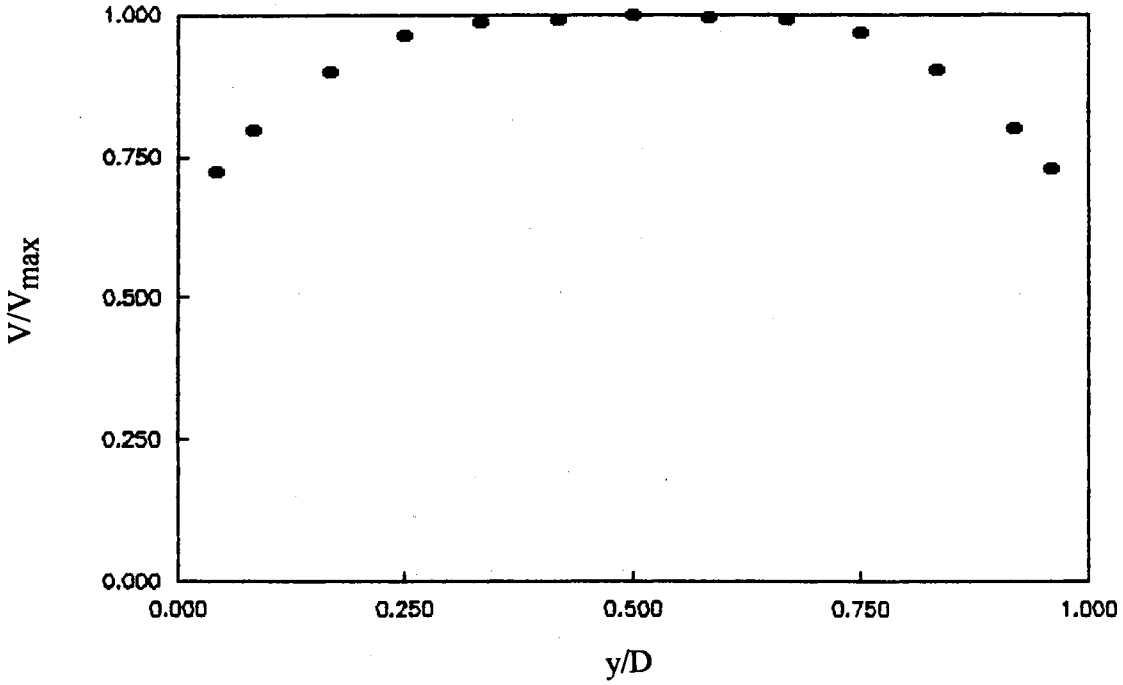

Figure B.8. Velocity Profile at the Center of Rectangular Channel (Medium Flow Rate)

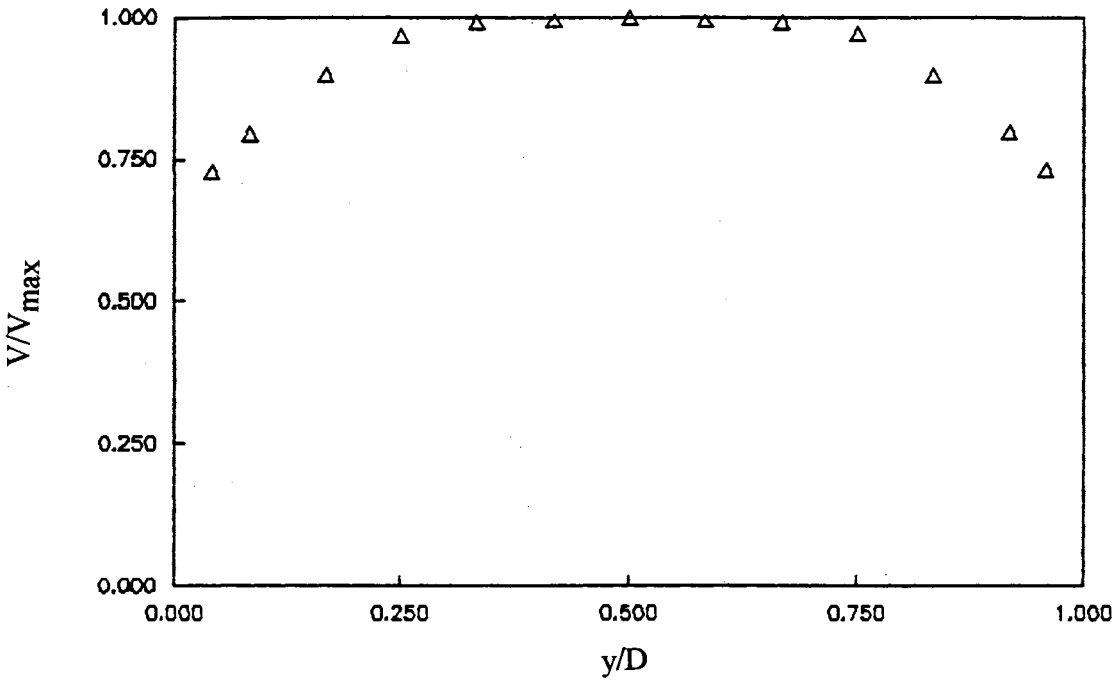

Figure B.9. Velocity Profile at the Right of Rectangular Channel (Medium Flow Rate)

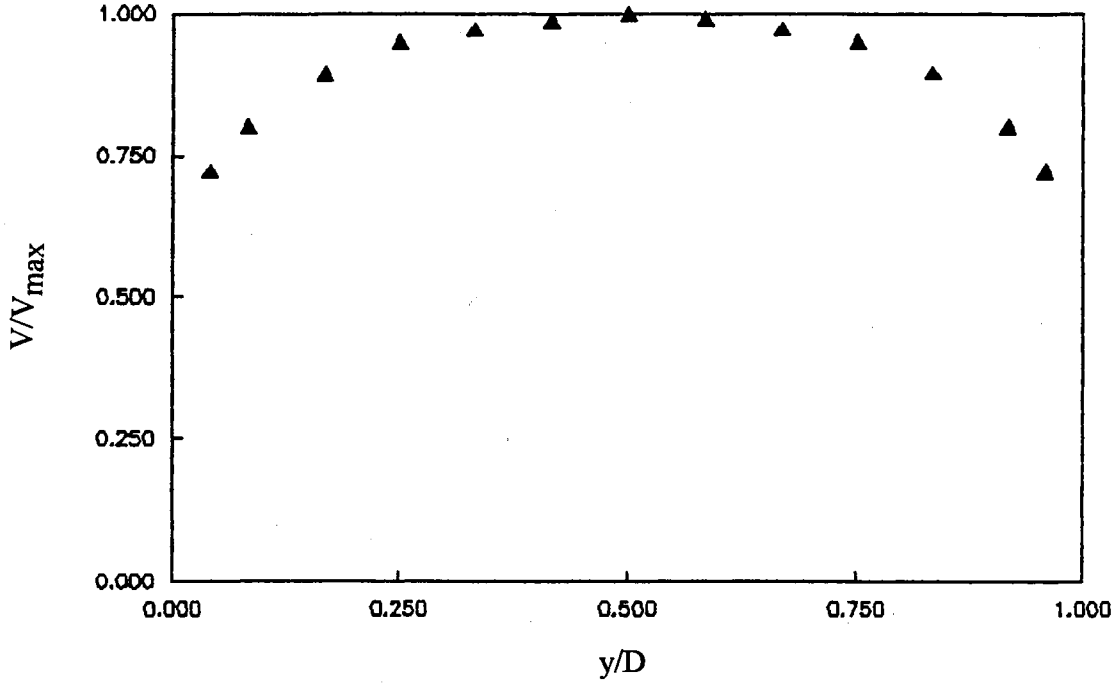

Figure B.10 Velocity Profile at the Left of Rectangular Channel (High Flow Rate)

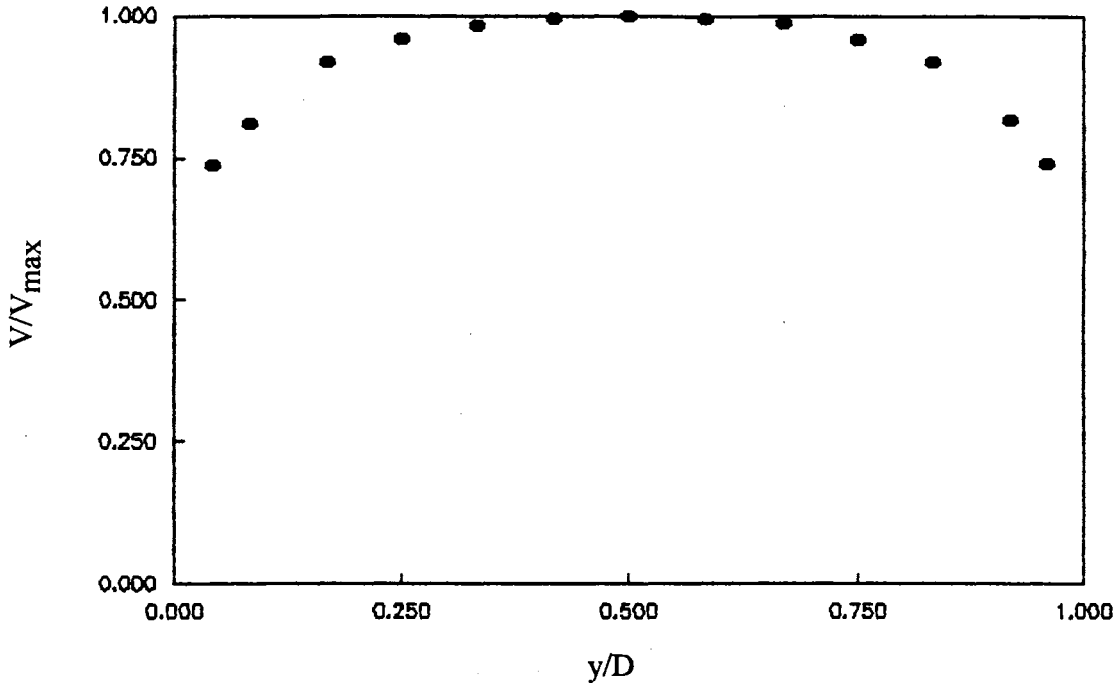

Figure B.11. Velocity Profile at the Center of Rectangular Channel (High Flow Rate)

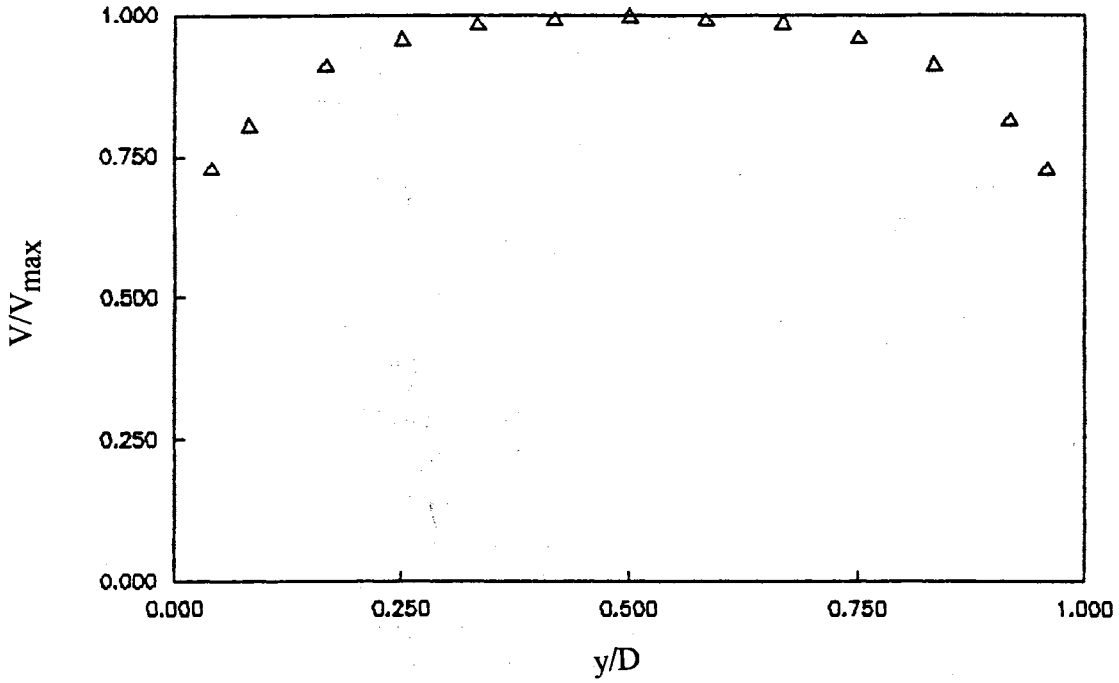

Figure B.12. Velocity Profile at the Right of Rectangular Channel (High Flow Rate)

APPENDIX C

UNCERTAINTY ANALYSIS

Estimates of Uncertainty in Duct Center Velocity (V_d)

$$V_d = 32.7153 \sqrt{\frac{(\Delta P) T_\infty}{P_{atm}}}$$

where ΔP is the differential pressure measured by pressure transducer in inches of water, and P_{atm} is the barometric pressure in mm Hg.

$\Delta P \pm \delta_{\Delta P}$, $T_\infty \pm \delta T_\infty$, $P_{atm} \pm \delta P_{atm}$, and $V_d \pm \delta V_d$ give the individual uncertainties.

$$\frac{\delta \Delta P}{\Delta P} = 0.3\% = 0.003$$

$$\frac{\delta T_\infty}{T_\infty} = \frac{0.5\ K}{293\ K} = 1.71 \times 10^{-3}$$

$$\frac{\delta P_{atm}}{P_{atm}} = \frac{1\ mm\ Hg}{730\ m\ Hg} = 1.37 \times 10^{-3}$$

$$\pm \delta V_d = \pm \left[\left(\frac{\partial V_d}{\partial \Delta P} \delta \Delta P \right)^2 + \left(\frac{\partial V_d}{\partial T_\infty} \delta T_\infty \right)^2 + \left(\frac{\partial V_d}{\partial P_{atm}} \partial P_{atm} \right)^2 \right]^{1/2} \pm 0.05$$

The term ± 0.05 should be added to uncertainty of V_d, since it was incorporated in program VELAIR to exit the program when V_d was within ± 0.05 m/sec of the desired duct center velocity.

$$\pm \frac{\delta V_d}{V_d} = \pm \left[\left(\frac{1}{2} \frac{\delta \Delta P}{\Delta P} \right)^2 + \left(\frac{1}{2} \frac{\delta T_\infty}{T_\infty} \right)^2 + \left(\frac{1}{2} \frac{\delta P_{atm}}{P_{atm}} \right)^2 \right]^{1/2} \pm \frac{0.05}{V_d}$$

$$= \pm 1.86 \times 10^{-3} \pm \frac{0.05}{V_d}$$

Estimates of Uncertainty in Channel Average Velocity

From Eq. (3.3):

$$(\overline{V}_{ch}) = \frac{C}{D} V_d$$

where C is the overall correction factor with uncertainty interval of $\delta C = \pm 0.008$, and D is the channel height in cm with uncertainty interval of $\delta D = \pm 0.025$ cm.

$$\frac{\delta C}{C} = \frac{0.008}{6.599} = 1.21 \times 10^{-3}$$

$$\frac{\delta D}{D} = \frac{0.025}{D}$$

$$\pm \delta \overline{V}_{ch} = \pm \left[\left(\frac{\partial \overline{V}_{ch}}{\partial C} \delta C \right)^2 + \left(\frac{\partial \overline{V}_{ch}}{\partial D} \delta D \right)^2 + \left(\frac{\partial \overline{V}_{ch}}{\partial V_d} \delta V_d \right)^2 \right]^{1/2}$$

Dividing by $(\overline{V}_{ch})$ to nondimensionalize:

$$\pm \frac{\delta \overline{V}_{ch}}{V_{ch}} = \pm \left[\left(\frac{\delta C}{C} \right)^2 + \left(\frac{\delta D}{D} \right)^2 + \left(\frac{\delta V_d}{V_d} \right)^2 \right]^{1/2}$$

$$= \pm \left[\left(1.21 \times 10^{-3} \right)^2 + \left(\frac{0.025}{D} \right)^2 + \left(1.86 \times 10^{-3} + \frac{0.05}{V_d} \right)^2 \right]^{1/2}$$

Substitute for V_d in terms of $(\overline{V}_{ch})$ with the use of Eq. (3.3) and rearrange:

$$\pm \frac{\delta \overline{V}_{ch}}{\overline{V}_{ch}} = \pm \left[1.464 \times 10^{-6} + \frac{6.25 \times 10^{-4}}{D^2} + \left(1.86 \times 10^{-3} + \frac{0.33}{\overline{V}_{ch} D} \right)^2 \right]^{1/2}$$

The above equation gives the nondimensionalized uncertainty for channel average velocity for different channel heights and channel average velocity. It is an inverse function of D and $(\overline{V}_{ch})$. The worst case was for minimum $(\overline{V}_{ch})$ and minimum D, i.e., for $(\overline{V}_{ch})$ = 2m/sec and D = 1.905 cm, the maximum percentage of uncertainty for $(\overline{V}_{ch})$ was ± 8.9%. The best case was when $(\overline{V}_{ch})$ and D were maximum, i.e., for D = 7.62 cm and $(\overline{V}_{ch})$ = 10 m/sec, the minimum percentage of uncertainty for $(\overline{V}_{ch})$ was ± 0.71%.

Estimates of Uncertainty in Heat Transfer Coefficient (h)

Using Eqs. (3.4), (3.5), (3.6), and (3.7) and rearranging:

$$h = \frac{1}{A_c}\left[\frac{Q_t}{\Delta T} - \frac{1}{110.5} - \frac{1.109 \times 10^{-11} T_c^4}{\Delta T}\right]$$

where $\Delta T = T_c - T_\infty$

$\delta T_c = \pm 0.5°C$, $\delta T_\infty = \pm 0.5°C$, and $\delta\Delta T$ are the uncertainty intervals for T_c, T_∞, and ΔT, respectively.

Then:

$$\pm \delta\Delta T = \pm\left[\left(\frac{\partial \Delta T}{\partial T_c}\delta T_c\right)^2 + \left(\frac{\partial \Delta T}{\partial T_\infty}\delta T_\infty\right)^2\right]^{1/2}$$

$$= \pm\left[(\delta T_c)^2 + (\delta T_\infty)^2\right]^{1/2} = \left[(0.5°C)^2 + (0.5°C)^2\right]^{1/2} = 0.707°C$$

$\delta Q_t = \pm 0.01\, Q_t$ and δh are the uncertainty intervals for Q_t and h, respectively. Then:

$$\pm \delta h = \pm\left[\left(\frac{\delta h}{\partial Q_t}\delta Q_t\right)^2 + \left(\frac{\partial h}{\partial \Delta T}\delta\Delta T\right)^2 + \left(\frac{\partial h}{\partial T_c}\delta T_c\right)^2\right]^{1/2}$$

$$= \pm\frac{1}{A_c \Delta T}\left[(0.01 Q_t)^2 + \left(\frac{-0.707 Q_t + 7.842 \times 10^{-12} T_c^4}{\Delta T}\right)^2 + \left(2.218 \times 10^{-11} T_c^3\right)^2\right]^{1/2}$$

Dividing by $h = \dfrac{Q_c}{A_c \Delta T}$ to nondimensionalize:

$$\pm\frac{\delta h}{h} = \pm\left[\left(0.01\frac{Q_t}{Q_c}\right)^2 + \left(-\frac{0.707}{(T_c - T_\infty)}\cdot\frac{Q_t}{Q_c} + \frac{7.842 \times 10^{-12} T_c^4}{Q_c (T_c - T_\infty)}\right)^2 + \left(\frac{2.218 \times 10^{-11} T_c^3}{Q_c}\right)^2\right]^{1/2}$$

The term Q_t/Q_c was almost close to unity, and did not have great effect on the percentage of uncertainty for h. The terms $\Delta T = T_c - T_\infty$, and Q_c were the more sensitive parameters and had great effects on $\delta h/h$. Since our experimental heat transfer data tabulated in Table IV, was collected for a fixed value of Q_t (4 Watts), the only effective

parameter on the value of $\delta h/h$ is the term $\Delta T = T_c - T_\infty$. Therefore, minimum percentage of uncertainty for the heat transfer coefficient corresponded to maximum $(T_c - T_\infty)$, while maximum of $\delta h/h$ corresponded to minimum $(T_c - T_\infty)$. Using the collected data in Table IV;

$\left(\frac{\delta h}{h}\right)_{min} = 2.1\%$ for the case: $D/t = 3$, $t/L = 0.5$, $r = 5$, $\overline{V}_{ch} = 1.74$ m/s

$\left(\frac{\delta h}{h}\right)_{max} = 8.6\%$ for the case: $D/t = 1.5$, $t/L = 1$, $r = 1$, $\overline{V}_{ch} = 10.07$ m/s

VITA

Masoud Arabzadeh

Candidate for the Degree of

Doctor of Philosophy

Thesis: EXPERIMENTAL STUDY OF GEOMETRIC EFFECTS AND CONDUCTION LOSS ON FORCED AIR-COOLING OF REGULAR IN-LINE ARRAY OF ELECTRONIC COMPONENTS

Major Field: Mechanical Engineering

Biographical:

Personal Data: Born in Lar, Iran, July 5, 1951, the son of Dr. Mahmood Arabzadeh and Mrs. Safieh Saadat.

Education: Graduated from Alborz High School, Tehran, Iran, May, 1970; received the Bachelor of Science Degree in Mechanical Engineering from Iran University of Science and Technology, Teheran, Iran, February 1976; received the Master of Science Degree in Engineering Systems from University of Tulsa, Tulsa, Oklahoma, December, 1979; completed requirements for the Doctor of Philosophy Degree at Oklahoma State University, December, 1993.

Professional Experience: Instructor of Physics, Chemistry, and Mathematics, Lar Technical School, Lar, Iran, November, 1970 to April, 1971; Graduate Teaching Assistant, Physics Department, University of Tulsa, August, 1979 to December, 1979; Design Engineer, National Iranian Oil Company (NIOC), April, 1980 to April, 1983; Contractual Expertise of Oil and Gas, Planning and Budget Organization (PBO), Tehran, Iran, May, 1983 to March, 1985; Graduate Research Assistant, School of General Engineering, Oklahoma State University, August, 1989 to December, 1989; Graduate Teaching Assistant, School of Mechanical and Aerospace Engineering, Oklahoma State University, January, 1990 to May, 1993; Coordinator of Academic Excellence Workshop for Minority Engineering Students, College of Engineering, Architecture, and Technology, August, 1992 to December, 1993.

Professional Organizations: Associate Member, American Society of Mechanical Engineers (ASME); American Institute of Aeronautics and Astronautics (AIAA).

Honors and Awards: Ranked first in the entrance test of academic year 1971-1972 in the field of Manufacturing Engineering (Machine Tool Design), Iran University of Science and Technology, received waive of tuition.